

KAUNAS UNIVERSITY OF TECHNOLOGY

ALFREDAS BRUNIUS

RESEARCH AND DEVELOPMENT OF
PIEZOELECTRIC COMPOSITE MATERIAL
FOR BIOMEDICAL APPLICATION

Doctoral dissertation
Technological Sciences, Mechanical Engineering (T 009)

2019, Kaunas

This doctoral dissertation was prepared at Kaunas University of Technology, Faculty of Mechanical Engineering and Design during the period of 2014–2018.

Scientific Supervisor:

Prof. Dr. Habil. Arvydas PALEVIČIUS (Kaunas University of Technology, Technological Sciences, Mechanical Engineering – T 009).

Scientific Advisor:

Assoc. Prof. Dr. Asta GUOBIENĖ (Kaunas University of Technology, Institute of material science, Technological Sciences, Material Engineering – T 008).

Doctoral dissertation has been published in:

<http://ktu.edu>

Editor:

Dovilė Dumbraskaitė (Publishing House “Technologija”)

© A. Brunius, 2019

ISBN 978-609-02-1591-3

The bibliographic information about the publication is available in the National Bibliographic Data Bank (NBDB) of the Martynas Mažvydas National Library of Lithuania.

KAUNO TECHNOLOGIJOS UNIVERSITETAS

ALFREDAS BRUNIUS

PJEZOELEKTRINĖS KOMPOZITINĖS
MEDŽIAGOS KŪRIMAS, TYRIMAS IR
TAIKYMAS BIOMEDICINOJE

Daktaro disertacija
Technologijos mokslai, mechanikos inžinerija (T 009)

2019, Kaunas

Disertacija rengta 2014-2018 metais Kauno technologijos universiteto Mechanikos inžinerijos ir dizaino fakultete.

Mokslinis vadovas:

Prof. habil. dr. Arvydas PALEVIČIUS (Kauno technologijos universitetas, technologijos mokslai, mechanikos inžinerija – T 009).

Mokslinis konsultantas:

Doc. dr. Asta GUOBIENĖ (Kauno technologijos universitetas, Medžiagų mokslo institutas, technologijos mokslai, medžiagų inžinerija – T 008).

Interneto svetainės, kurioje skelbiama disertacija, adresas:

<http://ktu.edu>

Redagavo:

Dovilė Dumbrauskaitė (Leidykla “Technologija”)

© A. Brunius, 2019

ISBN 978-609-02-1591-3

Leidinio bibliografinė informacija pateikiama Lietuvos nacionalinės Martyno Mažvydo bibliotekos Nacionalinės bibliografijos duomenų banke (NBDB).

CONTENT

ABBREVIATION	7
INTRODUCTION	9
1 LITERATURE ANALYSIS	13
1.1 Sensors and functional elements	13
1.2 Functional element materials	16
1.2.1 Piezoelectric materials	16
1.2.2 Shape memory materials	18
1.2.3 Electrostrictive materials	19
1.2.4 Magnetostrictive materials	19
1.2.5 Electro and magnetorheological fluids	20
1.2.6 Polyelectrolyte gels	21
1.2.7 Pyroelectric materials	21
1.2.8 Optoelectric/magneto materials	22
1.2.9 Superconducting materials	23
1.3 Functional elements for biosensors, medical sensing	24
1.3.1 Types of biosensors	24
1.3.2 Applications of biosensors in food industry	25
1.3.3 Application in medicine	26
1.3.4 Fluorescent biosensors	27
1.3.5 Application of biosensing for biodefence	27
1.3.6 Application in metabolic engineering	27
1.3.7 Biosensors in plant biology	28
1.4 Surface plasmon resonance sensors	29
1.5 A MEMS viscometric sensor for continuous glucose monitoring	29
1.6 Conclusion	31
2 METHODOLOGY	33
2.1 PZT synthesis	33
2.2 Screen-printing technique	34
2.3 Thermal embossing for imprinting the microstructure	35
2.4 Polarization	37
2.5 Analytical equipment for investigations	39
2.5.1 X-ray diffraction	40
2.5.2 X-ray spectroscopy	40
2.5.3 Fourier transform infrared spectroscopy	42
2.5.4 Scanning electron microscopy (SEM)	43
2.5.5 Atomic force microscopy (AFM)	45
2.6 Methods and equipment for analysing piezoelectric properties	46
2.6.1 An analysis of the direct piezoelectric effect	47

2.6.2	An analysis of reverse piezoelectric effect	49
2.7	Conclusion	51
3	INVESTIGATION OF CHEMICAL, MECHANICAL AND ELECTRICAL CHARACTERISTICS OF the FUNCTIONAL ELEMENT	52
3.1	An evaluation of functional element properties with various concentrations of PZT	53
3.1.1	Chemical compositions of PZT composite material	55
3.1.2	The evaluation of binding material	56
3.1.3	The formation and manufacturing of the functional element ...	58
3.1.4	Piezoelectric properties of PZT composite material with different concentrations of PZT	59
3.2	Natural frequency and first vibration mode analysis of a multilayer structure	61
3.3	The influence of layer thickness and pole alignment on the piezoelectric effect	63
3.3.1	Surface Morphology	65
3.3.2	Piezoelectric properties of PZT composite material with different layer thickness	66
3.4	Conclusion	68
4	PERSPECTIVE BIOMEDICAL APPLICATION	69
4.1	Biomedical application of periodical microstructures based on Surface plasmon resonance	69
4.2	Cantilever-type viscometric sensor	73
4.2.1	Phenomenological mathematical model for cantilever	74
4.2.2	Numerical analysis	76
4.2.3	Experimental application	78
4.3	Conclusion	79
	GENERAL CONCLUSION	80
	BIBLIOGRAPHY	81
	REFERENCES	83

ABBREVIATION

AC – alternating current
AFM – atomic force microscope
AFP – auto fluorescent protein
Ag – silver
Al – aluminum
AlN – aluminum nitride
AuCd – gold cadmium
BSE – backscattering electrons
CCD – charge-coupled device
CMOS – complementary metal oxide semiconductor
DC – direct current
EDS – energy dispersive spectrometer
EH – energy harvesting
ER – electrorheological
 F_{el} – elasticity force
FRET – forster resonance energy transfer
FTIR – fourier transform infrared spectrometer
GFP – green fluorescent protein
 HfO_2 – hafnium oxide
HPV – human papilloma virus
IL – interleukin
ITO – indium tin oxide
 La_2O_3 – lanthanum oxide
MEMS – micro electro mechanical system
MOCVD – metalorganic chemical vapor deposition
MOEMS – micro opto electro mechanical system
MR – magnetorheological
 Nb_2O_3 – niobium oxygen
NEMS – nano electro mechanical system
NiTi – nitinol
OEH – optoelectronic holography
 $Pb(CH_3COO)_2 \cdot 3H_2O$ – lead (II) acetate trihydrate
 $Pb(NO_3)_2$ – lead (II) acetate
PbO – lead oxide
PLZT – lead lanthanum zirconium titanate
PVB – polyvinyl butyral
PVC – polyvinyl chloride
PVDF – polyvinylidene fluoride
PZT – lead zirconium titanate
 R_a – arithmetic average of the roughness
RNA – ribonucleic acid
 R_q – root mean square surface roughness
RTD – resistance temperature detector
SE – secondary electrons

SEM – scanning electron microscope
SMA – shape memory alloy
SME – shape memory element
SMMs – shape memory materials
SPR – surface plasmon resonance
SQUID – superconducting quantum interference device
 T_{el} – elasticity torque
 T_g – glass transition temperature
 $Ti(C_4H_9O)_4$ – titanium butoxide
 TiO_2 – titanium dioxide
XRD – x-ray diffraction
 Z_{mean} – average height
ZnO – zinc oxide
 $Zr(C_4H_9O)_4$ – zirconium butoxide
 ZrO_2 – zirconium dioxide
 δ – the logarithmic decrement
 ξ – damping coefficient
 ω_d – damped natural frequency

INTRODUCTION

The evolution of micro electro mechanical systems (MEMS) started with silicon etching and polymer processing (Nathanson, Newell et al. 1967). In the last decades, sensors based on various sensing principles have been developed due to the growing interest in laser technologies, robotics, measurement and mostly in medical application. In order to create high quality MEMS and upgrade the production process it is necessary to improve the fabrication technology of microsystems including new and more effective materials. MEMS can be composed from several micro elements, but the main quality requirements of advanced systems are sensitivity, high resolution and reliability. Till nowadays, the intensive investments in MEMS and micro opto electro mechanical systems (MOEMS) achieved many successful projects of various micro elements that satisfy the requirements of produced systems.

Every microstructure fabrication material needs specific production technology. Therefore, effective materials and specific technologies have to be chosen according to such material properties as sensitivity, surface morphology, optical and mechanical properties to produce a microsystem. Lots of mechanical properties are known to be scale-dependent. Therefore, the properties of microscale (nanoscale) structures have to be investigated. Nowadays the traditional single materials are not able to perform the necessary functions and satisfy all requirements for producing high-tech microsystems. An innovative and interesting field of designing microsystems is related with the creation of novel active elements based on novel materials with exclusive properties, the so-called composite (nanocomposite) materials. Properties of composite materials can be adjusted to system requirements by changing the shape, thickness, imprinting various periodical microstructures.

This research encounters many problems including high sensitivity, accuracy of measurements and a huge number of analytes to monitor. The main motivation of this research is to create a composite material for an active element with a piezoelectric effect on a micrometric level for biomedical application. The major investigation in this thesis is the research experience and achieved knowledge about adaptive multifunction composite materials, their properties and synthesis process, periodical micro-structures imprint technology, the formation principles and application for biomedicine. The composite material and technological process were selected to be low cost so that the sensing element for the microsystem would be competitive in a market.

The experimental part of the dissertation thesis was funded by the “Development and analysis of new type micro resonator for micro electromechanical systems” (No. MIP–081/2015) grant from the Research Council of Lithuania and by the Lithuanian state studies foundation.

The aim of the dissertation

The aim of this thesis is to create and investigate an elastic PZT composite material which ensures the piezoelectric effect on the micro metric level of functional element for biomedical application.

The objectives

1. To analyze previous scientific publications related to piezoelectric materials and their usage for biomedical sensing.
2. To synthesize a piezoelectric composite material applying polymers and piezoelectric material nano particles.
3. To investigate the chemical, mechanical and electrical characteristics of the synthesized piezoelectric composite material.
4. To present an example of application of the synthesized piezoelectric composite material in biomedical sensing.

Methodology of research

Experimental and theoretical research methods of a novel composite material are applied in the study. Newly synthesized materials include piezoelectric ceramic Lead zirconium titanate (PZT) nanoparticles and polyvinyl butyral (PVB).

To evaluate the surface morphology, chemical, piezoelectric and mechanical properties of composite material, the following equipment was used: the Quanta 200 FEG scanning electron microscope (SEM), atomic force microscopes (AFM) NT-206 and JPK Nano Wizard 3, the electronic speckle pattern interferometry system PRISM, the QUANTAX energy dispersive X-Ray spectrometer (EDS) system Bruker XFlash 4030, the AGILENT 33220A function generator, the HQPower VPA3100MN voltage amplifier, the PICO 3424 oscilloscope, the LK-G82 series laser triangulation displacement sensor with an LK-G3001PV control block, custom made high voltage polarization equipment, the Vertex 70 Fourier transform infrared spectrometer.

The COMSOL Multiphysics programming environment was used for mathematical modeling. High voltage polarization equipment fabricated by the scientists from the Institute of Material Science (KTU).

Experimental research was performed at Kaunas University of Technology, Faculty of Mechanical Engineering and Design and at Institute of Material Science.

Scientific novelty

There have been a lot of investigations related to new materials and functional elements for sensing systems and various micro devices. Thus, lots of tasks still have to be solved or improved, such as sensitive gap, speed, accuracy of analytical measurements, optical response, surface morphology, longevity and other parameters which affects the work of systems.

The novelty of this work relates to the synthesis of composite materials with a piezoelectric effect on a micrometric level:

Ensuring the functionality of piezoelectric elements orientating the piezoelectric directional deformation by applying the polarization process.

Identified an effective layer thickness of the formed composite material which ensures an electrical signal while mechanical force is applied.

Created a piezoelectric material with elastic properties and the ability to form various geometric shapes and configurations.

Statements to defend

The synthesized lead zirconium titanate mixed with polyvinyl butyral polymer, when PZT concentration in the composite material is 80% ensures the piezoelectric effect on the micrometric level.

The polarization of a piezoelectric composite material improves the piezoelectric properties when compared to not polarized elements and enables directional deformations of the piezoelectric element.

The reaction of the created piezoelectric composite material to mechanical signal rises for the thinner layer.

Practical value of the research

Novel materials with an ability to operate on the micro metric level allows to create new type of sensors.

The created novel material with orientated directional deformation expands its usage for sensing technologies.

Generated electrical potential can be controlled by applying different layer thickness of composite material.

The elastic properties of created piezoelectric composite material allows to form various geometrical forms of functional elements for sensors.

Approval of dissertation

The experiments of this research were funded by the “Development and analysis of new type micro resonator for micro electromechanical systems” (No. MIP–081/2015) grant from the Research Council of Lithuania and by the Lithuanian state studies foundation. The results were presented in 3 conference proceedings and 4 articles in the ISI Web of science database with citation index.

The results of this dissertation thesis were presented at 3 scientific conferences:

“Novel piezoelectric effect, based material for periodical microstructure formation” *Mechanika 2015: proceedings of the 20th international scientific conference*, 23 - 24 April 2015.

“Development and analysis of new type micro resonator with electro-optic feedback” *Proceedings of SPIE: Optical modelling and design IV: Brussels, Belgium*, April 03, 2016.

“Influence of binding material of PZT coating on micro resonator’s electrical and mechanical properties” *Proceedings of SPIE: Smart sensors, actuators and MEMS VIII / Bellingham, WA. 2017*.

Structure of the dissertation

The dissertation contains an introduction, 4 chapters, general conclusions, a list of literature including 123 references and a list of published scientific publications. The dissertation is composed of 89 pages, 52 figures and 13 tables.

The introduction presents the problem of the thesis as well as the aim and objectives of the work. Moreover, the scientific novelty, defended statements and the practical value of research of thesis are presented.

The first chapter presents the analysis of literature and introduces materials for sensing elements and problems associated with their usage in practical application as well as the advantages and disadvantages of their properties. The analysis was performed with regards to the aim and objectives of the dissertation.

The second chapter presents the equipment and methods which were used to create, improve and investigate the PZT composite material.

The third chapter describes the PZT composite material formation and application by using the screen-printing technique. Surface morphology, chemical and piezoelectric properties are also analyzed. This chapter also describes the thermal imprint method and results. The chapter discusses methods and techniques for improving the properties of PZT composite material together with the influence of the binding material. Finally, the chapter outlines the natural frequency calculation together with first vibration mode arithmetical and mathematical modeling compared.

Chapter four describes prospective applications of the novel composite material. It presents the sensor's functional element overlaid with silver nanoparticles making the functional element aseptic. An example of an improved viscometric biosensor for glucose detection can also be found in this chapter.

The final chapter provides general conclusions of the dissertation, and the research finishes with references and author's scientific presentations and publications.

1 LITERATURE ANALYSIS

The development of sensing technologies can bring about advances in patient care through the identification of new labels of disease, rapid diagnoses and frequent or even continuous monitoring in the clinic or, ideally, at home. The enabling technology for this attractive progress ranges from molecular probes to complex measurement systems, including chemical sensors and biosensors, low power circuits, wireless transmission, and novel real-time signal processing (Dziąbowska, Czaczyk, Nidzworski, 2017). Latest technological evolution in biomedical sensing presents new advanced sensors with a wide application field and more features. Developing new biomedical sensors by using an advanced microfabrication technique, signal processing methods and employing new materials allows to create reliable, low cost and more accurate sensors. A wide selection of sensing elements has allowed to increase the range of measuring targets and detect more measurands. The miniaturization process in sensing and measuring systems allows to create combined micro systems, such as BioChemLab-on-a-Chip. The progress of miniaturizing sensing platforms has an important effect on medical diagnosis and care, makes prospective advances in biomedical sensing (Lin, Makarov, Schmidt, 2017; Cote, Lec, Pishko, 2003).

1.1 Sensors and functional elements

Usually a control system works with sensors and actuators. This type of system is called a mechatronic system. A basic mechatronic system consists of a sensor unit, an actuator and a controller unit. The sensing platform can be a single sensor or made with additional components like amplifiers, filters, converters or any other signal process component. The sensing unit sends a signal to the controller where a pre-programmed output control algorithm sends an output command to the actuator for further action.

The sensor can be described as a device that when affected with a physical agent (temperature, force, displacement, etc.), reacts and gives an output signal (electrical, mechanical, etc.). A sensor can be synonymously called a transducer, but transducers convert physical energy from one form to another while sensors respond to a change of specific physical effect. Sometimes sensors can be transducers if they respond to one form of physical phenomena at input and convert to another form of physical phenomena at output. Thermocouple is a good example of thermal energy being applied at input and converted to an electromotive force at output. Accordingly, a device like the thermocouple can be called a transducer or a sensor (Pawlak, 2006, Wang, Xu-dong, Wolfbeis, Otto, 2016; Anjanappa, Datta, Song, 2007).

Sensors can be classified according to different characteristics, such as their application field, specification, physical law, broad area of detection, etc. However, there are two main categories: active and passive sensors. Active sensors which require external power to operate can also be called parametric sensors (output is a function of a parameter, such as resistance). Passive sensors generate their own electric signal and do not require a power source; they can be described as self-generating sensors. Examples of this type of sensors are piezoelectric sensors, photodiode, thermocouples or magnetic microphones (Hnatushenko, Vasyliiev, 2016).

One of the most popular classifications is sensors' measurement objectives. Although this list is not comprehensive since it covers only the basic categories of sensors.

Linear/Rotational sensors include the linear/rotational variable differential transducer, hall effect sensor, electrical tachometer, optical encoder, gyroscope, capacitive transducer, strain gauge elements, magnetic pickup, interferometer.

Acceleration sensors are the piezoelectric accelerometer, seismic accelerometer.

Force, torque, pressure sensor are the ultrasonic stress sensor, piezoelectric load cells, dynamometers load cells, tactile sensor, strain gauge.

Flow sensors include the ultrasonic type, flow nozzle, pitot tube, venturi tubes, electromagnetic flow meter, turbine flow meter, rotameter.

Temperature sensors – thermistors, thermocouples, thermo transistors, RTD—resistance temperature detector, thermo-diodes, infrared thermography.

Proximity sensors – inductance, photoelectric, hall effect, eddy current, capacitance.

Light sensors – photodiodes, photoresistors, photo conductors, photo transistors, charge-coupled diode.

Smart material sensors – optical fiber (strain, level, force, temperature sensors), magnetostrictive (torque, force sensors), piezoelectric (accelerometer, strain, force sensors).

Micro and nano sensors – fiberscope, micro-ultrasonic, micro CCD image sensor, micro-tactile.

Rotational and linear position sensors are the fundamental ones of all measurements used in a typical mechatronics system. The position sensors produce an electrical output that is proportional to the displacement they experience (Hnatushenko, Vasylyev, 2016). Data from linear or rotary sensors can be used for acceleration measurement, since their output is directly proportional to the acceleration. The piezoelectric and the seismic mass type accelerometer are the two most commonly used ones. The piezoelectric accelerometer is compact and more suitable for high frequency applications. The mass type seismic accelerometer is based on the relative motion between the supporting structure and the mass. But there is a limitation in low and medium frequency application due to the natural seismic mass frequency (Mantjarvi et al., 2001; Khan, Raouf, Cheng, 2011). Force/torque sensors can be of various types, but the dominant are strain gauge dynamometer and the piezoelectric sensor. Strain gauge dynamometer sensors are limited because of the natural frequency and the piezoelectric sensors are especially suitable for dynamic loadings in a wide range of frequencies. Besides that, piezoelectric sensors are compact, submit high resolution over a wide range of measurement (Li and Chen, 1998). Flow sensors perform a rather complicated task. The analyzed fluid can be gas, liquid or a mixture of both. Moreover, the flow may be laminar or turbulent or even time-varying phenomena. The most popular are the plate restrict and venturi meter flow, identifying the flow rate by using the pressure difference. Besides these methods there is the pitot tube pressure probe sensing, rotameter, electromagnetic (non-contact sensing) and the ultrasonic non-contact sensing method. Non-contact sensing methods have an advantage because they can be used to sense corrosive fluids or liquids with abrasive particles (Lammerink et al., 1993; Pawlak, 2006). Lots of devices are

available for temperature sensing, but the most common are resistance temperature detectors, thermocouples and infrared types. Resistance temperature detectors are based on the phenomenon that temperature directly effects the resistance of a metal. They are most stable and linear over a wide range. One of the most universal devices for temperature sensing are thermocouples. Basically, thermocouples are made from two different metal cords joined together at the end by making a sensing junction. Temperature difference in thermocouples is between the reference junction and actual temperature expressed as a voltage potential. Thermocouples are low cost and have a wide range (reaches up to 1200°C). Infrared type sensors use radiation heat to sense the temperature from a distance at a specific point. Non-contact sensors can also be used to sense an area of vision to generate a thermal map of a surface (Reyes-Vera et al., 2017; Young et al, 2014; Pawlak, 2006). The hall effect, inductance, capacitance and photoelectric type devices can be used as proximity sensors. Hall effect sensors react when a current carrying conductor is exposed to a transverse magnetic field and the transverse proximity between the sensor and object is proportional to a voltage. Basically, inductance proximity sensors are made from a coil-wound and soft iron core rotated around. Such a sensor triggers voltage switch when a ferrous subject is in its proximity. Photoelectric sensors mainly have infrared light source and when a light beam is interrupted by a moving object it causes the voltage level change (Hyo Seung et al., 2016; Pawlak, 2006). Light sensors are often used in many controllable applications. Photodiodes, photoresistors, phototransistors are the most common types of light intensity sensors. Basically, photoresistors are made from cadmium sulphide the maximum resistance of which is in the dark and it decreases proportionally to light intensity. When balanced and interfaced with a circuit, the change in light intensity will show up as change in voltage. Such sensors are simple, reliable, and low cost used widely for measuring light intensity (Schembri et al, 2017; Lynch, Marchuk, Elwin, 2016; Rhind, Anjanappa, 1999).

The application of smart materials as sensors or functional elements for sensors is becoming more popular, particularly in specific sensing circumstances. The most attractive and popular are optic fiber, piezoelectric and magnetostrictive materials. Although, optic fiber is the most popular and is used to sense strain, force, liquid level or temperature with very high resolution. Smart materials are efficient for sensor production on large areas and they have found generous applications, such as vibration sensors, damage sensors, cure-monitoring sensors (Bogue, 2012).

Microsensors are basically the same sensors with a wide range of sensing application only miniaturized to micro sizes. Silicon micro processing technology has helped the development of many microsensors and continues to be one of the most active research and development topics in this area. Lots of micro sensing platforms found their application in biomedicine. For example, a fiberscope with a diameter 200 μm has been developed to inspect flaws inside tubes (Li et al, 2003). The progress in miniaturizing sensing systems has filled the development of nano-sensors. These are relatively new sensors that take one step further in the direction of miniaturization and are expected to open new areas for sensing applications (Bhushan, 1998; Li et al, 2003).

Smart materials show a lot of promise in the field of sensor production. Smart materials work in a wide range of parameters and one of the biggest advantages is that some of them self-generate energy and do not need external power. Therefore, it could be stated that smart materials are suitable for the production of MEMS, MEOMS or even NEMS. Many current and potential applications for MEMS/NEMS are not really practical because their mechanical properties have not been established on the micro level. Mechanical and structural aspects are highly important for a lasting stability of small structures. When producing miniaturized structures, it is very important to know the precise characterization of their mechanical properties at a microscale. A recent analysis showed that smart material properties are size-dependent (Bhushan, 2007; Li, 2003).

1.2 Functional element materials

Smart, adaptive and intelligent materials or structures are used as functional elements for mechatronic systems. The very first concepts of smart materials originated in the middle of 1980 along with the attempt to describe the newly developing research area. However, structures and materials need artificial intelligence through microprocessors, computers and control algorithms to achieve high intelligence. Therefore, smart materials, actuators, and sensors with control systems have redefined the structure concept from a traditional passive system to active or even adaptive multifunctional systems with the possibility for self-diagnosis, self-sensing and control ability (Gabbert, Tzou, 2001; Tzou, Lee, Arnold, 2004). Below, the dissertations reviews the following smart materials:

1.2.1 Piezoelectric materials

The Curie brothers (Pierre and Jacques) observed electric field generations on quartz crystals when subjected to mechanical forces in 1880. Piezoelectricity is an electric charge generated in certain materials when mechanical force is applied. Direct piezoelectric effect can be observed when a certain material responds to mechanical force and generates electrical potential. Respectively, reverse piezoelectric effect is when an electrical potential applied to a piezoelectric material induces mechanical stresses or strains. (Tzou, Lee, Arnold, 2004; Tzou, Natori, 2001). Mainly, direct piezoelectric effect is used in sensing platforms and reverse piezoelectric effect is used as a precise actuating platform. Depending on the design and configuration, reverse piezoelectric effect is used from nano to micro or even milli scale. Therefore, piezoelectricity is a first-order effect at low electric field that produces a strain proportional to the electric field and the direction of displacement dependent directly on the sign of the electric field (Safari, Akdogan, 2008). Many natural and synthetic materials exhibit piezoelectric properties, which can be classified into natural crystals, liquid crystals, non-crystalline materials and synthetic piezoelectric materials. Because synthetic materials (e.g., lead zirconium titanate and lead lanthanum zirconium titanate) and polymers (e.g., polyvinylidene fluoride) can be fabricated into arbitrary geometries and shapes, they are very popular in many sensor and actuator applications. Piezoelectric materials are widely used in aircraft structures, robot manipulators, vibration controls, high-precision devices, sensors/actuators, thin film

MEMS, health monitoring, displacement controllers, etc. (Tzou, Lee, Arnold, 2004; Duan, Wang, Quek, 2010).

For MEMS, zinc oxide, aluminum nitride and lead zirconium titanate are the most commonly used materials in the sensor industry. ZnO was one of the first piezoelectric materials used in commercial applications and is the most widely researched when it comes to MEMS fabrication studies (McKinstry, Muralt, 2004; Smith et al., 2012). Therefore, ZnO is widely available and reached a large degree of success in fabrication. ZnO processing benefits can be characterized to be less demanding vacuum conditions, good film quality, high sputtering rates, and ease of chemical etching. However, the piezoelectric coupling factor for ZnO is relatively high. Regardless, ZnO has such disadvantages as not very good compatibility with semiconductor technology where increased conductivity appears as well as some issues with temperature dependence.

On the other hand, AlN offers lots of advantages in these areas. It shows good stability under humidity and temperature variations, has a large resistivity, and is perfectly compatible with complementary metal–oxide–semiconductor processing. Furthermore, its high acoustic velocity makes it clearly useful for high-frequency applications like film bulk acoustic resonators, and its high-quality factor is useful in most resonator applications. In comparison with all named materials AlN has the lowest electromechanical coupling value, but it still relatively high when comparing to many thin film piezoelectrics. PZT is one of the most popular and widely used thin film alternatives because of its extremely high piezoelectric coupling. Moreover, PZT has more than an order of magnitude larger electromechanical coupling comparing to ZnO and AlN and is very suitable for applications where electromechanical coupling could be employed as energy harvesting devices. PZT electrical potential has attracted a lot of researches for an effective thin film processing technique. PZT can be applied by using radio frequency sputtering, screen printing, electron-beam evaporation, ion-beam deposition, epitaxial growth by radio frequency sputtering, magnetron sputtering, metalorganic chemical vapour deposition, laser ablation, jet deposition or sol gel methods (Sharma et al. 2015; Smith et al., 2012). All of these processes separate their applicability and processing requirements including such parameters as desired layer thickness or annealing temperature. These parameters may be very important since some applications have strict limits, especially for layer thickness, or have particular conditions for annealing temperatures. Radio frequency sputtering is usually the fabrication process of choice for thinner layer thicknesses. Its advantages include good step coverage, high quality surface topography with good grain boundaries, and general familiarity with sputtering within the MEMS processing. However, annealing in high temperatures can lead to cracking in the PZT layer, especially in small devices (Galassi et al, 2000; Smith et al., 2012; Xie, Wang, 2017).

There are five relevant development trends providing perspectives for further research: hard to soft, macro to nano, performance to reliability, homo to hetero, and single to multifunctional piezoelectric material applications (Uchino, 2017).

Piezoelectrics with a high-power factor and minimum energy loss are one of the popular research fields from the viewpoint of improving energy efficiency. However, the primary aim of analyzing converter application is to reduce hysteresis and increase

the mechanical quality factor by reinforcing resonance displacement. In smart materials, the methodology of universal loss characterization, piezoelectrics, and magnetostrictors, namely, by accurately measuring the mechanical quality factors for the resonance and for the antiresonance in the admittance/ impedance curve, can derive physical losses. Three groups of losses in piezoelectrics can be excluded: dielectric $\tan \delta$, elastic $\tan \phi$, and piezoelectric $\tan \theta$, each of which is further categorized as intensive and extensive losses (Xie, Wang, 2017; Uchino, 2017).

Taking into account the revival of the polymer era after 1980s according to their elastically soft superiority, nowadays lighter, thinner, elastic and mechanically flexible human interfaces are actual requirements for microsystems and various devices (Sharma et al. 2015). In the MEMS/NEMS area, piezoelectric-MEMS is one of the miniaturization targets for integrating the piezo actuators and piezo sensors in a micro-scale device, aiming at biomedical applications for maintaining the human health (Duan, Wang, Quek, 2010; Uchino, 2017). A recent research trend is also a homo to hetero structure transfer: stress gradient in a dielectric material exhibits piezoelectric equivalent sensing capability, while the electric field in a semi conductive piezoelectric is able to expose flex tensional deformation of the bimorph equivalent (Uchino, 2017).

One possibility to improve new features is coupling two effects. For example, piezoelectric PZT material (piezoelectric effect) can be coupled with a magnetostrictive Terfenol-D developing a magnetoelectric device. Like nuclear radiation, magnetic irradiation cannot be easily felt by humans. A simple and handy magnetic noise sensor can be developed for these environmental monitoring purposes. A high-voltage power transmission line is presented in **Fig. 1.1**, where a PZT disk is placed between Terfenol-D disks. When a magnetic field is applied, Terfenol expands and mechanically squeezes the PZT disk which generates equivalent electric charge. So basically, when monitoring electrical charge in the PZT disk, it is possible to detect a magnetic field (Uchino, 2017).

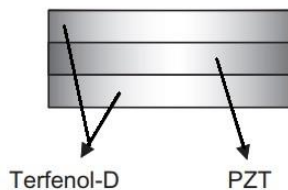


Fig. 1.1 Magnetic noise sensor consisting of a laminated composite of a PZT and two Terfenol-D disks

1.2.2 Shape memory materials

Shape memory materials are one of the main elements for a smart composite. Shape memory materials can be described by unusual features such as shape memory effect, high damping capacity and adaptive properties which appear in reversible phase transition, pseudo elasticity or big recoverable stroke. SMMs are able to respond to environmental changes by tuning technical parameters like shape, position, strain, damping, stiffness, friction, natural frequency and other dynamic or static

characteristics when effected with thermal, mechanical, electric stimulus or magnetic changes. Shape memory effect can be noticeable in a variety of ceramics, alloys, gels and polymers. SMMs have been analyzed and investigated from engineering and fundamental aspects and some of them have been used for commercial purpose till nowadays. Moreover, some of SMMs can be used for fabricating thin films, wires or fibers, porous bulks or particles and allowing them to be involved with other materials to form various hybrid composites (Wei, Sandström, Miyazaki, 1998; Boggs, 1993; Sun et al. 2014; Kong and Xiao, 2016). Shape memory effects can be classified into three different categories:

- One-way effect;
- Two-way effect;
- Pseudo-elasticity (super-elasticity).

1.2.3 Electrostrictive materials

Like piezoelectrics, electrostrictors belong to the ferroelectric category. Therefore, piezoelectricity is a first order effect and electrostriction is a second order effect, which means that the induced strain is proportional to the square of the applied electric field. Usually all dielectric materials have electrostriction, but the piezoelectric effect mostly dominant and electrostriction is very weak. However, when developing piezoelectric application, the second order smaller electrostrictive effect is mostly ignored in practice. Materials with high dielectric constant, like relaxor ferroelectrics, can expose high electrostrictive strains. Otherwise, like in piezoelectrics, polarization in relaxor ferroelectrics does not vanish at materials Curie temperature, but slowly decreases with temperature. Such an effect may be in wide temperature range permitting a mixture of paraelectric and pyroelectric phases related to a partially disordered distribution of cations in a relaxor ferroelectric. Therefore, relevant electrostriction, close to the nominal transition temperature, with minimal hysteresis is allowed when dielectric hysteresis in the transition region disappears before self-contained polarization. In nature where no electric manipulation of domains is required for dipoles' orientation and the material is stable, typical electrostrictors have strains in the order of 0.1% (Tzou, Lee, Arnold, 2004; Haertling, 1998, Pan, 2000; Auricchio, Sacco, 1997).

1.2.4 Magnetostrictive materials

Magnetostrictive material is a functional material which is able to convert energy from magnetic into mechanical. Magnetostrictive materials attract a lot of attention from the industry and research because of the advantages of the materials especially in giant magnetostrictive materials. A large magnetomechanical coupling coefficient, large output stress, fast response, high Curie temperature and high energy density are the main advantages of magnetostrictive materials. Magnetostrictive materials also have various applications in many areas, such as active vibration damping system, micro-valves, high-precision linear motor, giant magnetostrictive micro-pumps, micro-positioning devices. In order to effectively control magnetostrictive material devices and predict undesirable responses under a variety of complex magneto-mechanical loadings it is necessary to thoroughly describe the

constitutive relation of magnetostrictive material (Buschow, Boer, 2003; Zhang, Li, Zhou, 2017).

Magnetostriction is a second-order effect, when the applied magnetic field is proportional to the induced strain and this process is similar to electrostriction. However, the direction of applied magnetic field does not affect the caused strain and when the magnetic field is reversed deformation will be the same. The material can be used in sensing and actuator platform application because of its valuable ability to efficiently convert energy from mechanical to electrical and vice versa (Maetani et al. 2014; Kikuchi, 1968; Zhang, Li, Zhou, 2017).

1.2.5 Electro and magnetorheological fluids

The viscosity of electro and magnetorheological fluids can be controlled by their molecular structure and activated by applying external electric or magnetic fields. Active rheological fluids can be categorized into three groups: electrorheological, magnetorheological fluids, and ferrofluids. Basically, electrorheological and magnetorheological fluids include micro size particles in a carrier liquid and when external electric or magnetic field is applied, they develop a yield stress. A ferrofluids composition contains nano size particles that are dispersed in the oil and can be attracted when magnetic field is applied. The solid particles in the fluid align when a rheological fluid is exposed to an appropriate energy field and it causes the fluid's viscosity to decrease or increase. Viscosity is the rate of deformation of a fluid due to imposed shear stress. Normally, ER fluids behave like normal Newtonian fluids. ER fluids are colloidal suspensions that dramatically change properties when an appropriate electrical field is applied. Only a few milliseconds are required for an ER fluid to change yield stress and viscosity characteristics. ER fluids can change from a liquid to a solid structure almost instantly, which is highly advantageous in engineering applications (Guegan, Foulc, 2008; Tzou et al., 2004). There is one main difference between ER and MR fluids; i.e. applied proper energy field. For ER fluids, it is necessary to apply high voltage and low current electric field, while MR fluids respond to magnetic field which could operate on a battery generating high fluid shear stress. Therefore, ER fluids require high voltage for operation which leads to a need to pay attention to safety. Conversely, MR fluids react magnetically and do not need a high voltage and usually produce much higher shear stress when compared to ER fluids. There are more advantages of the MR fluids, such as high shear stresses at maximum applied field, they exhibit very low shear resistance at zero field, chemical inertness, fast response time, temperature stability and low hysteresis. ER/MR devices and systems can be divided into three basic modes (Bossis et al., 2002; Tzou et al., 2004).

- The first mode is the direct shear mode where one of the permanent magnets or electrodes moves and the fluid experiences a shearing effect.
- The second mode is the valve mode where the fluid is sandwiched between two stationary permanent magnets or electrodes resulting in an imposed flow field between the electrodes.
- The third mode is the squeeze film mode where the force and displacement of the fluid are parallel to the magnetic poles or electrodes.

ER/MR fluids include controllable applications of active vibration isolation, control, squeeze film damping devices, dampers, active vehicular shock absorbers, engine mounts, rotary active control damper, and so on (Wereley, Pang, 1998; Ying-Qing Guo, 2017).

1.2.6 Polyelectrolyte gels

Polyelectrolyte gels could be described as polymer chains with a charged polymer network with macro ions fixed on it and micro counter ions localized in the network frame. Polyelectrolyte gels have an ability to absorb a large amount of water (in some cases up to 2000 times of polymer weight) within its network structure and does not dissolve in water. Depending on linear polyelectrolyte solutions, polyelectrolyte gels exhibit relevant unique electrical responses. For example, when through a pair of needle electrodes DC voltage is applied to a water-swollen polyelectrolyte gel, an iterative current oscillation occurs. In terms of the molecular level deformation, the changes of motion and shape of polyelectrolyte gels are similar to biological motion, such as muscle, flagellar and ciliary movement (Kwon H. J., Osada Y., Gong, 2006).

Depending on the imposed environmental conditions, such as pH, electrical fields, electrical charge, light ionic polymeric gels are polymeric solutions that possess the ability to alter their physical properties. Most ionic polymeric gels expand depending on various imposed environmental factors. Acting on the gel polymer forces can be differentiated into four groups:

- inertial effect;
- elasticity;
- electrophoretic/ionic interaction and ion pressure;
- polymer–liquid viscous interaction.

When an electric field is applied through the solution emerging the gel depending on salt concentrations, pH and electric field strength, ionic polymers consisting gels appearing deformations (Rahalkar, Muthukumar, 2017; Hong, Zhao, Suo, 2010).

1.2.7 Pyroelectric materials

Pyroelectricity is defined as an instantaneous polarization of crystals in response to a temperature differential. Charges formed on the ends of the pyroelectric crystals due to thermal effects cause an inhomogeneous change of the temperature of pyroelectric materials. Only 10 groups are specified as pyroelectric while there are 20 piezoelectric groups from 32 groups of crystals. All crystal groups are described by polarization due to mechanical strain, therefore, pyroelectric materials are a subgroup of the piezoelectrics. Five main pyroelectric materials are mostly used: ceramic materials based on lead zirconate, lithium tantalate, triglycine sulfate, polyvinylidene difluoride and strontium barium niobate (Srinivasan, 1984; Tzou et al., 2004).

Two categories of pyroelectricity can be noted: tensorial and vectorial. When a crystal is heated uniformly and the generation of small charges appears at the ends of certain axes, it is tensorial pyroelectricity. Theoretically, tensorial pyroelectricity is applicable to all crystal structures besides cubic and is concerned with the quadrupole

moments in crystals. Therefore, vectorial pyroelectricity may be described as the change of negative and positive polarization charges with temperature on specific portions of crystals belonging to specific classes. Pyroelectric devices can be directly applied to measurements related to temperature or for infrared detection. For example, pyroelectric materials could be applied for: x-ray generation, measurement of thermal parameters, the testing of reflectivity, infrared CCD camera, vehicle monitoring, integrated circuit monitoring, electrostatic attraction and so on (Tzou et al., 2004; Bowen et al, 2014; Alply et al., 2014).

1.2.8 Optoelectric/magneto materials

Optoelectric/magneto materials can be grouped into three groups:

- Photostrictive materials;
- Magneto-optical materials;
- Photo-ferroelectric materials.

Photostrictive materials can be used as sensors or actuators, while magneto-optical and photo-ferroelectric materials can be used as storage devices, therefore, magneto-optical materials are often used in optical systems to manipulate and control light orientations.

Photostriction (or opto-piezoelectricity) is a photo-deformation process that includes two fundamental opto-electromechanical effects: the photovoltaic effect and the converse piezoelectric effect. When photostrictive materials are used in an actuator system, such a system is usually produced of two-layer photosensitive materials connected at opposite polarity by making a bimorph configuration where their planar spontaneous polarities are opposite to each other. It is noteworthy that the bonding layer has impenetrable light transmission and perfectly binds the surfaces and the viscoelastic effect can be ignored. Therefore, when the material is illuminated, the top layer absorbs it and light does not penetrate into the bottom layer. When the surface illuminated with uniform high-energy light, absorbed energy induces a current due to the photovoltaic effect and the direction of the current is opposite to the direction of polarization (Tzou et al., 2004; Haertling, 1987; Nadarajah A. and Sheldon, 2017).

The magneto-optical effect is noticeable in ferromagnetic materials. In the ferromagnetic state and with the spin orbit coupling existing in combination with the net spin polarization, magneto-optical effect is produced. Electric dipole matrix elements and optical selection rules that are managed by the spin orbit interaction couples the spin components of the electron wavefunctions to the spatial components (Bader S.D., Erskine, 1994). One of the relatively simple samples of the magneto optical effect is a magneto optical memory device. The Curie point for a basic magnetic medium is close to room temperature and such a medium has a low coercivity. Temperature at which the magnetic field of a material can be permanently altered can be described as the Curie point. Even so, regular magnetic media effected with external magnetic field can be erased. Though, optical and magneto-optical data storage have relatively high Curie points and despite how strong a magnetic field is applied to permanently stored data, it does not affect any data unless it is heated above the Curie point temperature. For data storage on a magneto-optical disc, it is necessary to point a laser beam to the recording layer in a DC manner by raising the temperature

of the irradiated spot and applying a modulated magnetic field across the recording layer at the same time (Kimel, Kirilyuk, Rasing, 2007).

Photo-ferroelectric materials mainly have been used for information storage. When a light impulse is applied to a material it becomes relatively polarized. To reorient or reverse ferroelectric domains in the exposed regions, the combination of a positive bias voltage and light exposure has to be applied. It effects only the exposed regions. Depolarization and light scattering produced when light is transmitted through a polycrystalline ceramic plate and encounters refractive index mismatches at grain and domain boundaries (Jianqiao et al., 2018).

1.2.9 Superconducting materials

The phenomenon of superconductivity has not lost its fascination ever since its discovery in 1911, when it was observed that the resistance of mercury wire vanished as the temperature approached absolute zero. This phenomenon led into a new age of superconductivity. Electrical resistance in metallic conductors arises within the lattice structure at room temperature due to material impurities, defects, and ion vibrations. Therefore, in some materials resistance decreases due to the vibrating ions when temperature is lowered. Material comes into a superconductive state in most nonmagnetic elements, compounds, and alloys when temperature decreases below a certain value of critical temperature. In a superconductor material, resistance disappears due to ion vibration when the temperature comes below the critical temperature (Tzou et al., 2004; Guo, Langlois, Goddard, 1988; Rahman A., Rahaman Z., Samsuddoha, 2015).

However, superconductivity is not only the disappearance of resistance. In 1933, Meisner effect was discovered which states that as opposed to a merely perfect conductor, superconductivity is a true thermodynamical state. Superconductivity has been established as common low-temperature instability of most metallic systems according to the progress of cooling technique which gave access to lower and lower temperatures. The zero-entropy postulate of thermodynamics for this limit points to its nature as a macroscopic quantum state, as the apparent T approaches 0 K state of metals (Hott, Kleiner, Wolf, Zwicky, 2004).

Superconductors can be classified into three different groups. The first group (type 1) has two very different states. The state of the material is determined by a combination of temperature and external magnetic field. If the magnetic field is very weak and the temperature is very low, the material is in the superconducting state. The second group (type 2) of superconductor materials remains superconducting to a much higher temperature than the first group or they can be in a mixed state. When external magnetic field is greater than the first critical field but lesser than the second at a given critical temperature, the state of the materials resides between the normal state and the purely superconductive. Filaments existing in the normal state or the solid consists of thin cores in the mixed state. The surrounding material is in the superconductive state, while the cores stay in the normal state. Magnetic flux through each core is produced when current flows around each core in the superconductive material. Superconductors of the third group (type 3) are the high-temperature variety. These superconductors in terms of molecular weight do appear as though the heavier

the compound is, the higher its critical temperature and primarily derived from metal oxides (ceramics) (Tzou et al., 2004; Scanlan, Malozemoff, Larbalestier, 2004; Larbalestier et al, 2001).

1.3 Functional elements for biosensors, medical sensing

Biosensors are the same sensors which convert a biological response into an electrical signal. Basically, biosensors could be called transducers which can be used for interpreting biochemical or biophysical property of a medium. Therefore, this type of sensors is unique and different from other types of sensors due to the possibilities with biological or organic recognition elements which allows the detection of particular biological molecules in the medium (Wang J, 2006). A new era of advancement in science came with the development of biosensors. The phenomenon of biosensing withholds set techniques of interaction among biological molecules for the production of an accessible detection signal. Such device that enables sensing of these molecular interactions is called a biosensor. It is an interdisciplinary technology that involves the collaborative efforts of engineering, microbiology, physics, chemistry, biology, biotechnology and so on (Hinze, 1994; Ibraheem, Campbell, 2010).

Due to their exclusive properties' biosensors are widely analyzed in various scientific disciplines. In medicine, biosensors can be widely adapted for precise detection of pathogens, tumors, toxins, glucose level in blood evaluation, etc. Biosensors are based on fluorescent production and encoded by genes are very important to scientists who analyze and study complex chemical processes happening in cells. Such a type of biosensors is suitable for targeting specific locations in the cell or it may be expressed in an organism specific cell. Through these biosensors, it is possible to achieve long-term incorporation of any specific substance into the host cells (Palmer A.E., 2011). Biosensors could be easily adopted in the food industry for detecting food contamination, for checking the growth of bacteria or fungus in fresh food or detection of gasses released from spoiled food (Situ, 2010). Biosensors are also very helpful for environmental security, since they are able to detect pollution in the air or the presence of any pathogens, heavy metals, etc. (Tamayo, 2001). Even in the military, biosensors can be used for defense systems for biological attack detection, such as the intentional use of biological entities like Ebola, Bacillus anthracis, hepatitis C viruses, etc. They can detect any harmful biological materials that would otherwise remain undetectable and cause death (Edelstein, 2000).

1.3.1 Types of biosensors

Biosensors based on enzymes were first introduced in 1967 by Hicks and Updike. Immobilization methods, such as covalent bonding, ionic bonding or adsorption of enzymes by van der Waals forced the creation of enzymes used for biosensors. Amino oxidases, peroxidases, polyphenol oxidases and oxidoreductases are enzymes usually used for biosensing (Akyilmaz, Yorganci, Asav, 2010).

In 1975, first reports about cell-based or microbe-based biosensors appeared. An inhibitor or a substrate can be an analyte of interest for these processes. Tissue-based biosensors are formed from animal and plant sources. One of the first tissue-

based sensors was developed for the determination of amino acid arginine. Using microsomes, chloroplasts, membranes and mitochondria an organelle-based biosensor was developed. Even despite its high stability, the detection time of such type of biosensors was too long and the specificity was reduced (Rechnitz, 1978; Akyilmaz, Yorganci, Asav, 2010).

Biosensors for immune sensing (immunosensors) were developed on the basis that antibodies specifically bind to pathogens or toxins, or interact with components of the host's immune system.

In the DNA, biosensors' interaction exists because of the formation between the two nucleic acid strands of stable hydrogen bonds. Such a biosensor has a specific property that single-strand nucleic acid molecule is able to identify and bind to its complementary strand in a sample (Wang, 1998).

The development of genetically-encoded biosensors begins from green fluorescent protein and following auto fluorescent protein variants. Genetically-encoded biosensors are user-friendly, easy to manipulate, engineer and transfer into cells. Another example is a single chain FRET biosensor, which develop from two AFPs and when they approach each other fluorescence resonance energy transfers between them. Based on AFPs lifetime, ratio or intensity various methods may be chosen to regulate the changes in Forster resonance energy transfer signals. Employing synthetic chemistry followed by enzymatic labelling with synthetic fluorophores peptide and protein biosensors can be easily manufactured. Such a biosensor is readily utilized to control target activity and constitute attractive alternatives because of their independence of genetically-encoded AFPs. Therefore, they have an added superiority of being possible to increase signal-to-noise ratio and sensitivity of response through the introduction of chemical quenchers and photoactivatable groups (Mehrotra 2016; Lippincott-Schwartz, Patterson, 2003; Wu et al., 2011).

Magnetic biosensors are mini sensors which are able to detect magnetic microparticles or even nanoparticles using the magnetoresistance effect in microfluidic channels (Scognamiglio, Arduini, Palleschi, Rea, 2014).

Optical biosensors basically consist of a light source, optical components, a sensing head with a photodetector. Optical components generate a specific light beam and beelines this light to the modified sensing head (Leatherbarrow, Edwards, 1999).

Piezoelectric biosensors are mainly of two types: the quartz crystal microbalance and the surface acoustic wave device. The measurements are based on the mass changes of the crystal structure by effecting the resonance frequency of a piezoelectric crystal.

1.3.2 Applications of biosensors in food industry

For food analysis, traditional techniques such as spectroscopy or chemical analysis have drawbacks because of their expensive and time-consuming analysis. Nowadays the food industry requires alternative food monitoring and authentication techniques and equipment, which are inexpensive, fast responding or able to monitor in real time. Therefore, biosensors satisfy all the necessary requirements and can be easily adapted in the food industry for various analyses (Scognamiglio, Arduini,

Palleschi, Rea, 2014). For example, cobalt phthalocyanine-based enzymatic biosensors could be employed to monitor beer ageing.

Using biosensors *Escherichia coli* or pathogens in food can be effectively detected. Potentiometric alternating biosensing systems are very effective for *Escherichia coli* detection; the system measures pH variation caused by ammonia. Using peptone water for vegetable wash provides a liquid phase and bacterial cells are separated from food items (Torun, Boyaci, Temur, Tamer, 2012). Biosensors are very effective for the creamery industry, where enzyme-based biosensor is integrated into flow cell. Enzymes were immobilized on electrodes by engulfment in a photo-cross-linkable polymer. The automated flow-based biosensor could quantify the three organophosphate pesticides in milk (Mehrotra 2016; Mishra, Dominguez, Bhand, Munoz, Marty, 2012; Yan et al. 2014).

Biosensors are effectively used for detecting general toxicity or specific toxic metals due to their ability to respond with only the precarious metal ion fractions. Such pesticides as organophosphates and carbamic insecticide species is a serious threat to the environment. Most effective, high-speed agri-food, sensitive and environmental monitoring have been proved to be immunosensors. Biosensors based on acetylcholinesterase and butyryl cholinesterase can effectively detect chlorpyrifos methyl, carbaryl, aldicarb, paraoxon, etc. Biosensors with screen-printed electrodes using oxon or similar have supremacy in detecting pesticides in orange juice or wine and bacteria-based bioassays help to identify and measure arsenic (Mehrotra 2016; Suprun et al. 2005; Backer et al. 2013).

1.3.3 Application in medicine

Biosensor application in medicine is becoming more popular and their adaptation is growing rapidly. For example, biosensors for glucose monitoring are widely used in clinics for precise control of diabetes mellitus over blood glucose level (Rea, Polticelli, Antonacci, 2009). Infectious diseases are effectively diagnosed by employing biosensors in the medical field. A wide field in medicine still needs effective detecting techniques and is still under study. For example, urinary tract infection diagnosis along with pathogen identification and anti-microbial susceptibility is under intensive investigation. Another important area is the identification of end-stage heart failure patients, who are prone to adverse outcomes during early phase of left ventricular assisted device implantation. To analyze the interaction between recombinant human interleukin with the corresponding monoclonal antibody, hafnium oxide-based biosensors are studied for early cytokine detection after device implantation. The most relevant task in medicine nowadays is heart failure for more than a million people suffering from it. Fluorometric, and enzyme-linked immunosorbent assay and immunoaffinity column assay are the main techniques for detecting cardiovascular diseases. Biosensors with a particular biomarker of interest and established on electric measurement can be employed for biochemical molecular recognition for desired selectivity. Biosensors are becoming more and more employed for various detections in biomedicine: immunosensor array for clinical immunophenotyping of acute leukemias, the effect of oxazaborolidines on immobilized fructosyltransferase in dental diseases, microfluidic impedance assay for

controlling endothelin-induced cardiac hypertrophy, biochip for a quick and accurate detection of multiple cancer markers and neurochemical detection by diamond microneedle electrodes, quantitative measurement of cardiac markers in undiluted serum, histone deacetylase inhibitor assay from resonance energy transfer, etc. (Mehrotra 2016; Lee, Zine, Baraket, 2012; Chen, Liu, Kaneko, McIntyre, 2010; Ooi et al. 2006).

1.3.4 Fluorescent biosensors

Fluorescent biosensors can be described as imaging agents and they are able to discover drugs or even cancer. They are able to affect and regulate enzymes at the cellular level. Biosensors which are able to transfer genetically encoded fluorescence resonance energy and those based on green fluorescent protein are very important in biosensing technologies. Fluorescent probes are mounted on a small staging through a receptor. A specific target or analyte is detected by the receptor and transduces a fluorescent signal which is immediately detected and measured. Moreover, fluorescent biosensors are able to investigate protein biomarkers, ions, metabolites with a high sensitivity or even able to detect a target in a complex solution. They are effectively used for intravital imaging and image-guided surgery, response to treatment/therapeutics, for monitoring disease progression, sensing cancer and metastasis, viral infection, inflammatory diseases, cardiovascular and neurodegenerative diseases, examining indications of arthritis. Fluorescent biosensors are able to detect biomarkers in molecular and clinical diagnostics, are suited for drug discovery programs where drugs are identified with high content screening approaches, high throughput, optimization of leads and for post-screening analysis of hits. It is a very important tool for clinical validation of therapeutic potential and pre-clinical evaluation, pharmacokinetics and biodistribution of candidate drugs. And finally, such a biosensor is able to probe gene expression, conformation and protein localization in such fields like signal transduction, apoptosis and cell cycle, transcription (Mehrotra 2016; Mizutani et al. 2010; Wang, Nakata, Hamachi, 2009).

1.3.5 Application of biosensing for biodefence

Biosensors are successfully employed for a military purpose to detect biological attacks. The main task of such a biosensor is to selectively and sensitively detect organisms posing threats, toxins, bacteria and viruses or any other biowarfare agents in real time. Various techniques for military biosensing were used on purpose to recognize the chemical markers of biowarfare agents. Some biosensors work using a molecular technique, antibody-based detection, but nucleic acid-based sensing platforms are more sensitive. Such a sensor is not only more sensitive but also provides gene-based specificity without utilizing amplification steps to attain detection sensitivity to the required levels (Mehrotra 2016; Woolston, Edgar, Stephanopoulos, 2013).

1.3.6 Application in metabolic engineering

Metabolic engineering greatly aided the production of many chemicals, such as drug intermediates, pharmaceutical molecules, biofuels or fine chemicals. The

production of many chemicals was enabled by metabolic engineering using low-cost and readily available raw materials. To improve and optimize these processes, effective biosynthetic pathways have to be built and the optimization of product titers and yields, right choice of a microbial host, discovery of all the necessary pathway genes and correct construction of the pathway in the host is especially important for practical application and inexpensive products. Lately, metabolite biosensors have become the most powerful tool in metabolic engineering. Enzymes, transcription factors, riboswitches are natural sensors which are able to sense a wide variety of metabolites in each living cell and responds by properly maintaining cells functions. Employing synthetic biology and due to inexpensive gene synthesis, metabolic engineering research acceleration is expected. Genetically encoded biosensors can be applied to actuate the needed metabolic engineering function in synthetic circuits to dynamically respond to metabolites. Various biosensor classification methods exist in metabolic engineering. There are two main application areas: determining dynamic regulation network for biosynthetic pathways and monitoring and inspecting the production of aimed products or significant intermediates in developed cells. Biosensors can be sorted in to groups according to the source of the signal detected by the cellular biosensors: biosensors for extracellular chemicals, biosensors for environmental signals, biosensors for intracellular chemicals and metabolites. Moreover, various types of biosensors can be named based on their manufacturing base: whole-cell biosensors, RNA-based biosensors, transcription factor-based biosensors, protein activity-based biosensors, etc. Likewise, biosensors can be classified according to their aim: to dynamically control metabolic fluxes, to sense desirable products in selective conditions, to target high-producing strains by high-throughput screening and others (Zhang, Keasling 2011; Mehrotra 2016; Berens, Suess, 2015; Becker, Beer, Freitag, Kuck, 2015; Bermejo et al. 2011).

1.3.7 Biosensors in plant biology

Traditional methods are not able to exhaustively analyze information regarding the location and dynamics of enzyme substrates, receptors and transporters. Only cellular and subcellular localization, and the measure of ion and metabolite levels could be precisely analyzed by applying spectroscopy methods. However, wider information can be successfully obtained by using biosensors. For a dynamic process measurement under physiological circumstances, tactics are supposed to be devised to visualize the actual process, for instance, metabolite conversion one into another or the triggering of signaling events. Such a visualization can be done with dynamically responding sensors. The lab of Roger Tsien was one of the firsts to develop a prototype of protein sensors which were able to measure caspase activity and control calcium levels in live cells. The following sensors were based on FRET of green fluorescent protein with two spectral variants. The application of biosensors in a living organism involves great temporal resolution using cameleon sensor imaging of calcium oscillations. Moreover, biosensors can be utilized to identify the lacking components pertinent to metabolism, regulation, or analyte transportation. Sucrose detection FRET sensor which is responsible for the identification of proteins performs a transport step in phloem loading-sucrose outflow from the mesophyll. FRET sucrose

sensors with fluorimeter-based assays successfully recognize sugar transporters that can proceed immediately after glucose effect of starved yeast cells. Parallel assays identify genes that affect cytosolic or vacuolar pH in yeast, and justify that it is possible to apply biosensors in genetic screens provided that imaging technologies of suitable productivity are available (Mehrotra 2016; Jones, Grossmann, Danielson 2013; Okumoto, 2012).

1.4 Surface plasmon resonance sensors

Surface plasmon resonance is a phenomenon when a light interface between positive and negative permeability materials is stimulated by an incident and the resonant oscillation of conduction electrons occurs. SPR sensing is in great demand for producing high sensitivity sensors due to its highly improved local electromagnetic field reactive to the surrounding environment. SPR-based sensors have a wide application possibility, such a food safety, environmental monitoring, biomolecular interaction analysis or medical analysis. various new materials including metal oxides are increasingly used for improving SPR sensors. Prism-based SPR sensors are complicated to use in MOMES or in situ analysis, fiber optic SPR sensors are more appropriate for this purpose and have a lot of promising features. For example, ITO is predominantly used as a transparent conductor due to its characteristics of low electrical resistivity, great transmissivity of visible light and wide band gap semiconductor. Furthermore, ITO films are more advanced comparing to silver and gold films and have no participation of inter band transition and agglomeration problems. Unfortunately, the spectral range in most metal-based optic fiber SPR sensors is in a limited visible spectrum, which limits the measurement range and sensing utilization. (Lixia et al. 2017).

SPR sensors have a lot of advantages and are perfectly suited for real-time analysis interplay in chemistry or biology analysis; it is also able to thoroughly detect binding reaction processes of target molecules. Surface sensitivity can be significantly increased by surface plasmon resonance (Bedford, Spadavecchia, Pradier, Gu, 2012). SPR sensors are making meaningful progress in technologies and application. New and combined production techniques and various configurations are developed to improve and eliminate the shortcomings for detecting smaller molecular weight chemical and biological analysis under various extreme circumstances (Singh, 2016).

1.5 A MEMS viscometric sensor for continuous glucose monitoring

Fig. 1.2 shows a viscometric microsensors and **Fig. 1.4** presents the principle scheme view of the whole sensing system for glucose detection in liquid. A functional sensing element is based on a cantilever and located inside a microchamber. The base of the cantilever is made of polymer thin film and fixed at one end to the substrate. At the free end of the cantilever thin film stripes made from permalloy are allocated. To avoid the ripple of the cantilever due to internal stress discrepancy between metal and polymer thin films, it is covered with a polymer layer. The cantilever is placed in a microchamber which is covered with a polymer membrane and filled with dextran and Con A solution. The membrane is semi-permeable which allows to infiltrate glucose into the microchamber, but it does not permeate dextran or Con A. When a magnetic

field is applied to a system, it effects the permalloy strips and the cantilever periodically vibrates. Glucose permeates in and out of the microchamber and changes the viscosity of the solution. Different solution viscosity affects the characteristics of the cantilever vibration and different parameters can be measured depending on glucose concentration (Zhao et al., 2007).

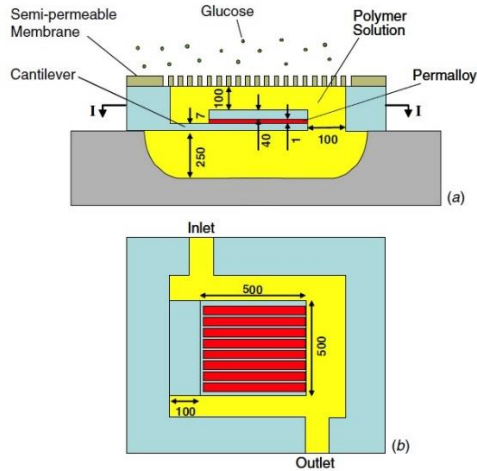


Fig. 1.2 Schematic of the MEMS viscometric glucose sensor: (a) cross-sectional view and (b) top view of the microchamber looking down from the cross-section I–I shown in (a). Dimensions shown (in micrometers) are those of the microfabricated prototype devices (Zhao et al., 2007)

Glucose attraction in a sensing system principle is presented in **Fig. 1.3**. The solution used for sensing includes dextran, glucose and Con A. Con A is a protein which specifically attracts glucose up to four units each. Con A attracts dextran molecules and glucose molecules, and they compete with each other which will bind to the Con A. However, when glucose molecules enter the microchamber through the semi-permeable membrane they crosslink the Con A which results in partial de-crosslinking of the dextran and Con A complex. Moreover, when Con A is banded with dextran, the solution is highly viscous (gel-like), but when Con A is conjuncted with glucose molecules, the viscosity of the solution decreases. This process is reversible and such sensor can be used for long-term monitoring. Therefore, when the concentration of glucose decreases outside of the microchamber and glucose molecules stop entering through the membrane, the glucose and Con A conjunction will separate, glucose molecules will unbind and dextran crosslinking will restore hence increasing the viscosity. When the concentration of glucose outside and inside of the chamber are collated the equilibrium of Con A and glucose is reached (Zhao et al., 2007).

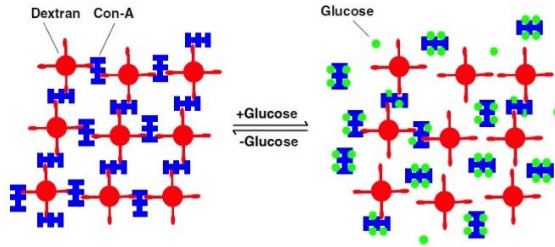


Fig. 1.3 A schematic illustration of the gravitation glucose sensing principle

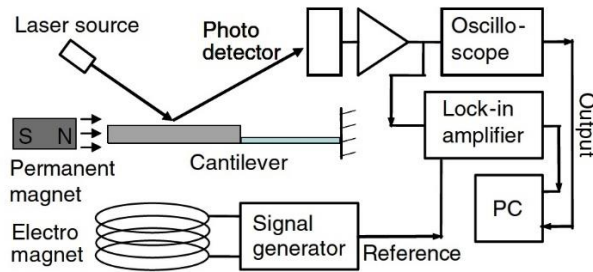


Fig. 1.4 A scheme of the viscometric sensor (Zhao et al., 2007)

Therefore, the hypodermis of glucose concentration position is when the viscosity of the solution reaches the equilibrium position. In whole this process the semi-permeable membrane bandwidth of glucose does not influence the equilibrium functionality. Moreover, the accuracy of glucose concentration viscosity and measurement accuracy will not be affected by additional partial barrier layers on the semi-permeable membrane. The microchamber contains a cantilever surrounded with a sensing solution which vibrates and detects viscosity thus describing the glucose concentration in a solution. To activate the device, it has to be placed in a magnetic field which could, for example, be generated with solenoid. Permalloy strips on a cantilever exposed with magnetic field generate torque. The generated torque has a magnitude of $T = MVH$. M is magnetization on the permalloy strips over long, V is permalloy volume and H is magnetic field element vertical to the surface of the cantilever. Cantilever bending is caused by torque which is directed through the cantilever width; the cantilever vibrates when time-dependent torque is generated by the time-dependent magnetic field. The viscosity of the solution is directly influenced by hydrodynamic damping or inertia of the cantilever, which allows to measure the viscosity of the sensing solution (Zhao et al., 2007).

1.6 Conclusion

The review of scientific literature presented various sensing elements, materials and sensing platforms with different options. However, there is not enough information about elastic functional materials with a piezoelectric effect, especially on the micro metric level. Piezoelectric materials can be used in a wide range of sensing by adapting them to specific conditions. Piezoelectric ceramics is a very

important material because of its high piezoelectric effect although it has some disadvantages, like cracking, complicated production on the micro level, and longevity. Those problems could be solved by creating a composite material with piezoelectric ceramic. Thus, the aim of this dissertation is to create and investigate a piezoelectric composite material which ensures the piezoelectric effect on a micro metric level of functional elements for biomedical application.

2 METHODOLOGY

2.1 PZT synthesis

PZT is the most frequently used piezoelectric ceramic till nowadays. The main advantages of piezoelectric ceramics over other materials is low-cost manufacturing, they are chemically inert and physically strong. Moreover, they can be easily adapted for various specific purposes. PZT ceramics have a very high electromechanical coupling factor and are very popular as ultrasonic actuators or transducers. Nowadays, PZT thin films are extensively researched for MEMS and usage with semi-conductor circuitry. PZT ceramic is revered because it has an even greater sensitivity and higher operating temperature than other piezo ceramics (Losego, Maria, 2010).

The variation of dielectric constant with temperature for different Zr/Ti content is presented in **Fig. 2.1 a**. It is seen that the transition temperature decreases as the content of Zr increases in the PZT ceramic. PZT ceramics with Zr/Ti ratio of 52/48 exhibited the most promising dielectric properties. The dielectric loss remained invariant with the variation of Zr/Ti ratio **Fig. 2.1 b** shows how polarization influences the electrical field for various Zr/Ti ratios. The 52/48 Zr/Ti ratio showed the widest electrical field from all analyzed ratios. For further experiments it is expedient to use PZT 52/48 ratio (Losego, Maria, 2010).

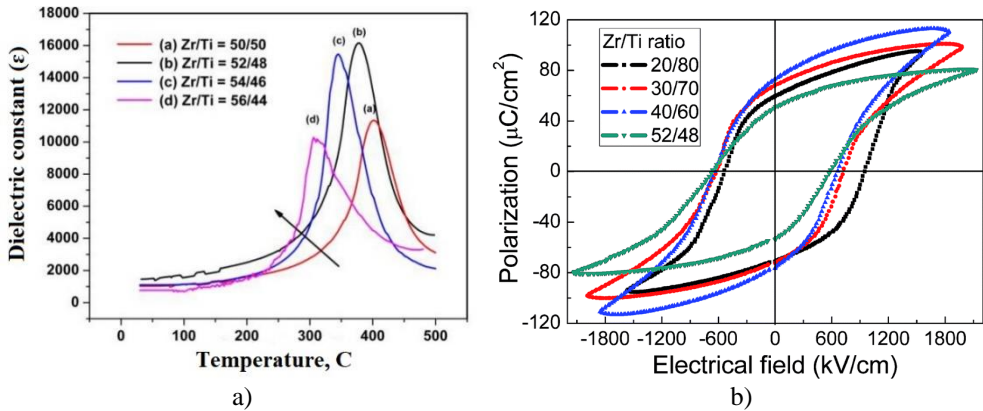


Fig. 2.1 A comparison of PZT with different Zr/Ti ratio a) dielectric constant from temperature, b) polarization from electrical field (Losego, Maria, 2010)

The mixed oxide technique is the most common and easy way to obtain piezoelectric ceramic, it is also known as the conventional ceramic technique. An oxalic acid/water-based synthesis of powders for lead zirconate titanate [$\text{Pb}(\text{Zr}_x, \text{Ti}_{1-x})\text{O}_3$] with $x = 0.52$ —also known as PZT (52/48)—was chosen. Before mixing the oxides, the required quantity of precursors was calculated **Table 1**.

Table 1 Precursor weight data

Precursor	Atomic mass	Moles	Required mass
Pb (Zr _{0.52} , Ti _{0.48}) O ₃	325.58g	1	325.58 g
Pb (CH ₃ COO) ₂ 3H ₂ O	379.2 g	1	379.2 g
Ti (C ₄ H ₉ O) ₄	339.88 g	0.48	163.14 g
Zr (C ₄ H ₉ O) ₄ (80%)	383.2 g	0.52	199.26 g (249g 80% solution)
C ₂ H ₂ O ₄ 2H ₂ O	126 g	3	378 g

To synthesize 325.58 g (which is the sum of PZT molar mass) it is necessary to mix precursors in the amounts calculated and presented in **Table 2**. In order to use the precursors economically, 10 g of PZT was synthesized.

Table 2 Precursors' mass calculation for PZT synthesis

PZT	Pb (CH ₃ COO) ₂ 3H ₂ O	Pb (NO ₃) ₂	Ti (C ₄ H ₉ O) ₄	Zr (C ₄ H ₉ O) ₄ (80%)	C ₂ H ₂ O ₄ 2H ₂ O
325.58 g	379.2 g	268.86 g	163.15 g	249 g	378 g
10 g	11.65 g	8.26 g	5.1 g	7.65 g	11.61 g

To synthesize a PZT (52/48) ceramic, lead (II) acetate [Pb (NO₃)₂] instead of lead (II) acetate trihydrate [Pb (CH₃COO)₂ 3H₂O] were used as precursors in appropriate proportions, as well as titanium butoxide [Ti(C₄H₉O)₄] and zirconium butoxide [Zr(C₄H₉O)₄]. In the mixing process, oxalic acid, acetic acid, ammonia solution and deionized water were used as support reagents. Firstly, 8.26g of lead (II) acetate [Pb (NO₃)₂] was poured into 100 mL of deionized water; then acetic acid was added and the solution was heated to 50°C and mixed to dissolve. Twelve grams of oxalic acid [C₂H₂O₄ 2H₂O] was dissolved in 500 mL of deionized water, followed by titanium butoxide [Ti(C₄H₉O)₄] (5.1 g) and zirconium butoxide [Zr(C₄H₉O)₄] (7.65 g) at a concentration of 80%. Afterwards, both solutions of titanium butoxide and zirconium butoxide were mixed with the lead acetate solution. To finalize and reach an acidic pH 9–10, the solution was alkalized with 25% ammonia solution and mixed for an hour. The sediments of the solution were filtered in a vacuuming environment and washed with acetone and water during filtering. Then the filtering material was dried at 100°C for 1 hour and in room temperature for 12 hours. The final calcination was performed at 1000°C for 9 hours. Finally, the mixed PZT material was milled to nano powder. To create a novel PZT composite material, the milled nano powder has to be mixed with a polymer.

2.2 Screen-printing technique

For covering the substrate with a novel PZT composite material screen-printing technique was chosen. The screen-printing technique allows to control the thickness of the covering layer and form any shape of the printed layer. The biggest advantage of this method is the possibility to form equal layer thickness over the printed area. Various layer thickness can be achieved by using different screen mesh. To form a specific shape of the screen-printed layer, the screen mesh has to be prepared in advance. The mesh has to be covered with a special paste leaving open only the area

with the preferred shape. To form a layer of material, screen mesh has to be fixed over the substrate and the distance between substrate and screen mesh has to be 1 mm higher than the printing layer (formed layer thickness plus 1 mm). The screen-printing technique is employed when printing paste is applied on a squeegee and moved across the screen to fill the open mesh apertures with mixed paste. For impeccable layer formation, the screen mesh has to unstick from the formed layer for perfect layer shape and even layer surface after the squeegee moves across (Horvath et al., 2014, Suikkola et al., 2016). Three different types of polyester monofilament screen mesh were used in the experiments: 32/70, 48/70, 140/34. were copper foil with a thickness of 50 μm was used in the substrate. Characteristics of the screen mesh are presented in **Table 3**.

Table 3 The properties of screen mesh and layer thickness

Screen mesh type	Mesh opening, μm	Thread, μm	Open area, %	Mesh thickness, μm	Theoretical ink volume, cm^3/m^2
32/70	245	70	60.5	108	65
48/70	130	70	42.3	107	46
140/34	30	34	22	52	11

Screen-printing method **Fig. 2.2** is mostly used with ink or other kind of paint, which has to be liquid. To screen-print a novel PZT composite material it is supposed to be liquid and to achieve it, a polymer was mixed with benzyl alcohol then PZT nano powder was added and mixed for 5 minutes until viscous solid mass. The viscosity of the prepared mass can be controlled with the quantity of benzyl alcohol. After mixed and screen-printed chemical composition, it needs to be heated to dry it and vapor benzyl alcohol. Finally, PZT composite material printed on a substrate with the consistency of PZT nanoparticles and polymer in chosen proportions was created by using the screen-printing method (Horvath et al., 2014).

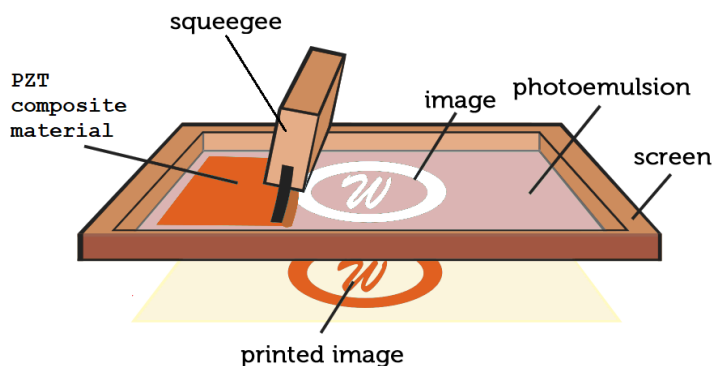


Fig. 2.2 The principle scheme of screen-printing (Horvath et al., 2014)

2.3 Thermal embossing for imprinting the microstructure

Thermal embossing is a process which takes place when a specimen is heated to polymer melting temperature range and pressed with a heated mould into the

specimen forming the surface structure. Due to its simple set-up and relatively short implement time, this technology has attracted users in micro and nano replication processes. The thermal embossing technique can be used to replicate various features with the dimensions from several nanometres to hundreds of micrometres. The process can also be characterized by a capability to replicate various materials, low shear stress and short flow distance. The main disadvantage of thermal embossing is a relatively long cycle time which could take up to 60 minutes depending on the design of the mould and the replicated material. A schematic graphic of thermal embossing is given in **Fig.2.3** (Worgull, 2009).

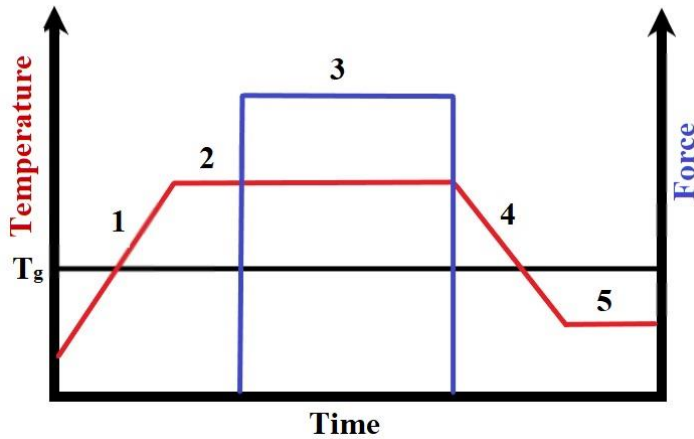


Fig.2.3 Typical thermal embossing process flow

1. Temperature ramp up;
 2. Temperature above T_g ;
 3. Imprinting force;
 4. Cooling down below T_g for dismantling;
 5. Dismantling temperature;
- T_g – glass transition temperature of polymer to be imprinted.

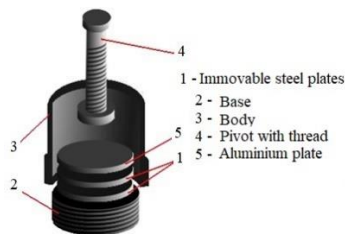


Fig. 2.4 Thermal embossing equipment

A typical thermal embossing cycle incorporates the following steps: a) micro mould prepared and fitted onto the machine **Fig.2.4** and a specimen is inserted and fixed; b) specimen and mould are heated to the embossing temperature (imprinting PZT composite material heated to 100°C); c) mould is pressed into the specimen (for PZT, at 5 atm. pressure); d) depending on the material holding time can be from few

seconds to few minutes (for PZT, held for 10 seconds); e) specimen and the mould are cooled down to the demoulding temperature which is glass transition temperature; f) the mould and specimen are separated by moving them away from each other. Thermal embossing can be used for a wide variety of materials in comparison with other replication technologies. Even so, the most appropriate embossing materials are polymers. The technique of thermal embossing can be found in the production area for optical devices, such as lenses, mirrors, compact discs, optical benches and switches. Also, this technology is used to produce micro fluidic devices, such as valves, pressure sensors or flow sensors. Also, this technology is suitable for fabricating electrical devices, like sensors, switches and combined devices. **Fig. 2.5** schematically presents the process for imprinting a microstructure.

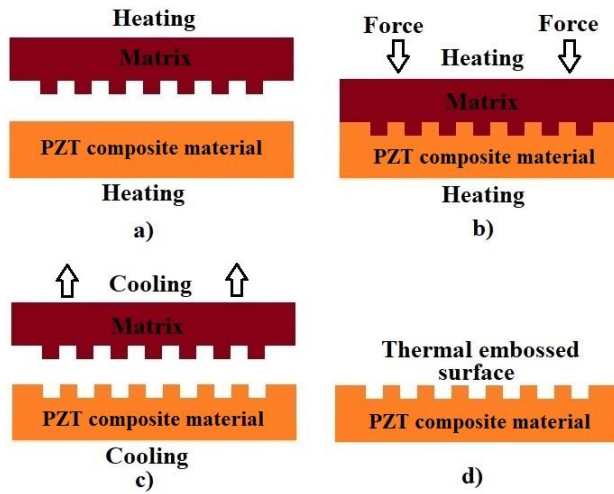


Fig. 2.5 Thermal embossing process for imprinting a microstructure

A specimen with screen-printed PZT composite material and mould are placed together and fixed in the metallic shell between plates **Fig. 2.5a**. The mould and specimen are heated and the mould is pressed in to the PZT composite material specimen **Fig. 2.5b**, after holding under pressure it is cooled down below glass transition temperature and the mould is separated from the specimen **Fig. 2.5c**. A well-defined periodical microstructure has been obtained **Fig. 2.5d**.

2.4 Polarization

Polarization (poling) could be described as a behaviour of materials which is present when an external electric field is applied. There are four different mechanisms of polarization:

- Electronic or atom polarization – when an electrical field displaces the centre of charge of the electrons with respect to the nucleus and causes a dipole moment.

- Ionic polarization – appears in ionic materials. Upon the application of an electric field to such materials, anions and cations get displaced in opposite directions distributing the rise to a net dipole moment.
- Interface or space charge polarization – limited movement of charges is present in this mechanism following in alignment charge dipoles under applied field. This mostly occurs at the grain boundaries.
- Dipolar or orientation polarization – this is the orientation of molecular dipoles in the direction of applied field. If an electrical field is not applied, molecular dipoles are randomly distributed due to thermal randomization.

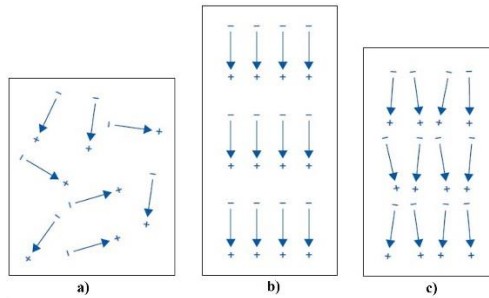
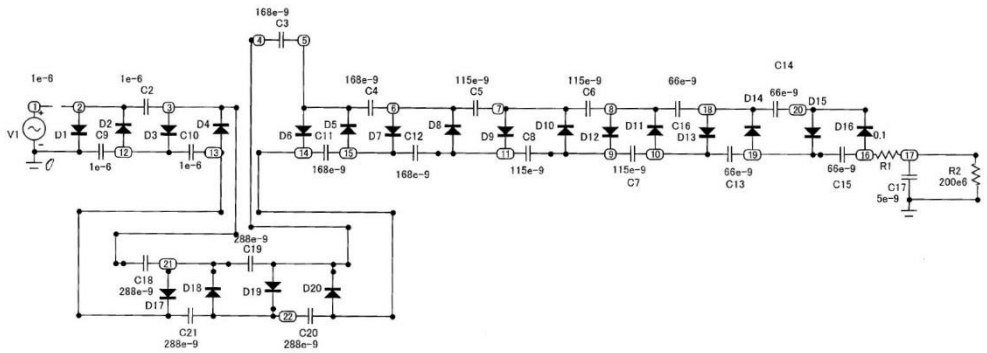


Fig. 2.6 Schematic polarization process: a) unpolarized; b) during polarization; c) polarized

Polarization appears when there is a concentration of charge at an interface between two materials or in a region between two materials because of an external field. This can appear when there are two electrodes connected to a material or when the sample is in an area between two contacts in a charge region. This type of electric polarization is unique because it effects not only positive and negative charges (ionic and covalent bonded structure) but free charges as well. Therefore, the charge balance of the dielectric material amorphous properties will appear effected by the electric field. However, mobile charges will migrate in the dielectric material instead of maintaining charge neutrality and cause polarization.

During polarization the specimen is placed in a high electric field that orients all the dipoles in the direction of the field. After the electric field is switched off, most of dipoles keep their orientation and do not come back to their initial orientation as a result of pinning effect which happens in the crystalline lattice of micro defects. Schematically this process presented in **Fig.2.6**. It is important that such a material can be depolarized if it is affected by a high electric field oriented opposite to the polarized direction or affected by higher temperature than the Curie temperature of the material (Ugwu, Limbi, Onyekachi, Sambo, 2016).



2.7 Fig. High voltage generator scheme

Polarization was accomplished with custom-made equipment. A high voltage generator was designed schematically **Fig. 2.7** and parameters able to generate up to 5 kV voltage were calculated. The equipment was produced together with a specimen holder **Fig. 2.8**. An element with PZT composite material was fitted in a custom-made holder between negative and positive poles. After all the equipment was connected the high voltage generator was set to 5 kV voltage and held under electric field for 30 minutes.

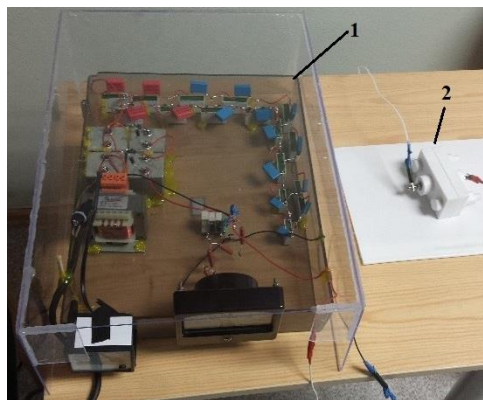


Fig. 2.8 Polarization set. 1 – high voltage generator, 2 – specimen holder

2.5 Analytical equipment for investigations

To evaluate the properties of the composite material, different analytical equipment and methods were used. To evaluate successful synthesis of PZT, x-ray diffraction was performed. Further x-ray spectroscopy was used to investigate the chemical composition of the PZT composite material and FTIR analysis was used to confirm that PZT ceramic nanoparticles did not affect the chemical structure of PVB. Scanning electron microscopy and Atomic force microscopy were applied to measure and analyze the surface morphology and elastic properties of the composite material. Specifications, working parameters and a description of all used techniques are provided below.

2.5.1 X-ray diffraction

X-ray diffraction analysis was performed to confirm successful PZT synthesis using x-ray diffractometer D8 Discover from Bruker **Fig. 2.9**. XRD is an effective non-destructive analytical technique which is able to describe crystalline materials, analyze such structural parameters as crystallinity, crystal defects, average grain size and strain. It also describes preferred crystal orientations, phases and structures. XRD-generated peaks show every set of lattice plane in a specimen of X-rays scattered at specific angles by indirect interference of a monochromatic beam. The allocation of atoms within the lattice is described by peak intensities. Therefore, an XRD template is a fingerprint of a given material of recurrent atomic arrangements. In the last decades, XRD has been employed in various fields, such as forensic science, pharmaceuticals, glass manufacturing, microelectronics, geological applications, corrosion analysis (Bunaciu, Udriștioiu, Aboul-Enein, 2015).

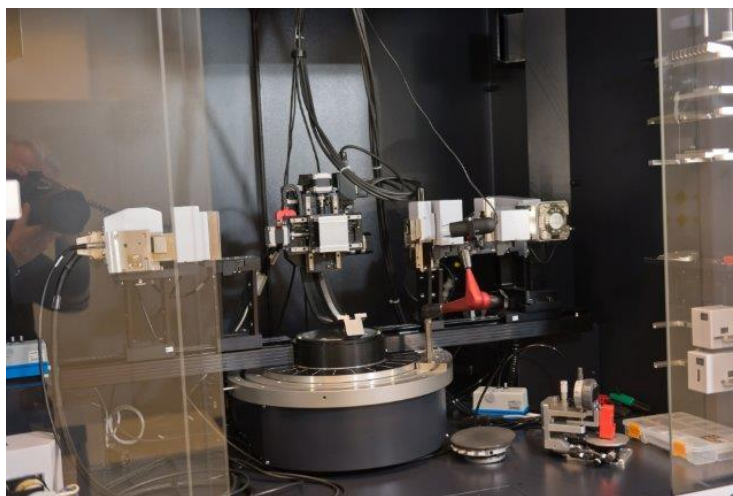


Fig. 2.9 X-ray diffractometer

2.5.2 X-ray spectroscopy

The possibilities of X-ray spectroscopy for chemical analysis were tested at the very first stage of its invention. Energy dispersive x-ray spectroscopy (EDS, EDX) is an analytical technique used for sample analysis and characterization. Energy dispersive x-ray spectroscopy has a detector which evaluates the comparative abundance of their energy versus emitted x-rays. A charge impulse which is proportional to the energy of the x-ray generated when the incident x-ray hits the detector. Even after the charge impulse is converted into a voltage impulse it remains proportional to the x-ray energy. Impulses are sorted by voltage with a multichannel analyser and then the energy from voltage measurement for each incident x-ray is sent to a computer for further data evaluation. The elemental composition of the sampled volume is determined by evaluating spectrum of x-ray energy versus counts.

The x-ray spectrometry analytical method allows a quick analysis in comparison with wet chemical methods. It is possible to analyse all elements from 92 Uranium to

22 Titanium, and under specific conditions, even down to 11 Sodium. Most of the elements can be detected in as low as 0.001 percent concentration. EDS analysis is a non-destructive method and widely applied in solving a lot of chemical problems (Goldstein et al. 2003).

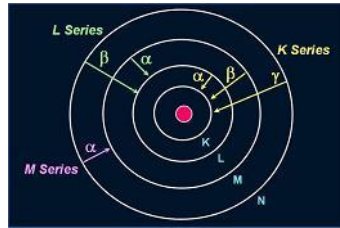


Fig. 2.10 X-ray characteristic lines

The names of x-ray lines depend on the layer in which primary cavity appears and the layer from which electron fills that cavity **Fig. 2.10**. For example, if a cavity appears in the K series layer and the filling electron drops from the neighboring L series layer that shows that a $K\alpha$ x-ray is emitted, but if the electron drops from the M series layer which is two layers away, then the emitted x-ray is $K\beta$. The same logic applies with other layers; if an electron is ejected from the L layer and that vacancy is filled with an electron from the M layer then the emitted x-ray will be $L\alpha$. Within a given layer there may occur electrons whose energy in the orbit differs due to attaching. However, the $K\alpha$ x-ray actually consist of $K\alpha_1$ and $K\alpha_2$ peaks. They are near to each other and not solvable in this system, so the $K\alpha_1$ and $K\alpha_2$ duplet is considered to be $K\alpha$ x-ray at the energy in a middle of two individual units their intensity respective to the weight average. The most expected transition occurs when a K layer vacancy is produced and electron transition is L to K, because these are neighboring layers. Therefore, $K\alpha$ radiation compared to $K\beta$ radiation is more intense and it follows that $K\alpha$ radiation is of lower energy than $K\alpha$ radiation. It means that energy difference between K and M layers is greater than the energy difference between K and L layers. Energy differences between neighboring layers become smaller progressing outwards from the nucleus. It means that the energy for electron emission between neighboring outer layers is smaller than that released to the transition of inner layers. For example, $K\alpha$ radiation is higher than $L\alpha$ radiation, which in turn is higher than $M\alpha$ radiation. The minimum quantity of energy which is the obligatory energy of a particular inner layer electron must contain for atom ionization the ionizing radiation and it is specific characteristic energy for each atom's electron. K layer electrons have bigger binding energy comparing to L shell electron because the K layer is closer to the nucleus and bound more tightly. Therefore, if there is enough energy to excite K x-ray then the L and M x-rays are excited too, but only if these shells and one shell above them are occupied. Additionally, if the incident beam produces $K\alpha$ x-rays then $K\beta$ radiation should be generated as well (Goldstein et al. 2003). The following common can be used for peak identification:

- $K\alpha$: $K\beta=10:1$;
- $L\alpha$: $L\beta_1: L\beta_2: L\gamma = 10:7:2:1$;
- $M\alpha$: $M\beta = 10:6$;

It follows that if there $K\alpha$ x-rays is identified in the spectra then $K\beta$ x-rays should be approximately one tenth of $K\alpha$ x-rays. For x-ray emission bigger beam energy is necessary for ionization which is termed the critical ionization energy. In practice, the factor for critical ionization energy is 1.5 to 3 which is called overvoltage (Goldstein et al. 2003).

2.5.3 Fourier transform infrared spectroscopy

Fourier transform splits any function into a sum of sinusoidal basic functions. Each of these basic functions is a complicated exponential of various frequency. Consequently, Fourier transform presents a unique way of viewing any function as a sum of ordinary sinusoids.

Fourier transform infrared (FTIR) spectrometers **Fig. 2.11** are widely used in polymer science, pharmaceutical industry, food analysis, etc. In addition, a chemical reaction mechanism and unstable substances can be investigated since FTIR spectrometers can hyphenate to chromatography. Full infrared spectra are 12800–10 cm^{-1} and can be divided into three different areas:

- 12800–4000 cm^{-1} near infrared region;
- 4000–200 cm^{-1} mid infrared region;
- 1000–50 cm^{-1} far infrared region

Infrared light was discovered back in the 19th century, and since then researchers have determined different ways to employ it. The infrared spectrum can be described as a molecular vibrational spectrum. Infrared absorption spectroscopy method which identifies the structures of molecules with the molecule's characteristics of infrared radiation absorption. When a specimen is exposed to infrared radiation, it changes the dipole moment of molecules by absorbing radiation at a specific wavelength. Therefore, the molecules of the specimen transfer from ground state to excite state due to the level of vibrational energy. The vibrational energy gap identifies the frequency of the absorption peak. The number of vibrational freedoms of the molecule is connected to the absorption peak number. The intensity of the absorption peaks depends on the ability of the transition of energy levels and change of dipole moment. There are several exceptions when molecules are not infrared-active, such as O_2 , N_2 , and Cl_2 (homonuclear diatomic molecules) due to zero dipole change in the vibration of these molecules. One of the biggest advantages of infrared absorption spectroscopy is that it is able to analyse liquid, gas and solid samples. Most frequently used region for FTIR spectroscopy is 4000–400 cm^{-1} because the absorption radiation in this region exists for most inorganic ions and organic compounds (Wang et al. 2017).



Fig. 2.11 Fourier transform infrared spectrometer Vertex 70

Considering the generations of infrared spectrometers, FTIR spectrometers would be the third generation. Fourier transform infrared spectrometers have several specific advantages:

- The signal-to-noise ratio is considerably higher than in spectrometers of the previous generation.
- The accuracy of wavenumber is in the range of $0.01 \pm \text{cm}^{-1}$, which is much greater than any previous generation of infrared spectrometers.
- Short scan time of any frequencies (approximately 1 second).
- High resolution ($0.1\text{--}0.005 \text{ cm}^{-1}$).
- Stray light interference is reduced.

Due to all these advantages dispersive infrared spectrometers were replaced with FTIR spectrometers (Wang et al. 2017).

2.5.4 Scanning electron microscopy (SEM)

Scanning electron microscope (SEM) Quanta 200 FEG was used to analyze designed composite material structure and chemical composition during experiments **Fig. 2.12**. It also has an integrated energy dispersive X-ray spectrometer (EDS) detector X-flash 4030 from Bruker. The energy of 133 eV (at Mn K) is achieved with a 30 mm^2 area solid-state flow detector at 100000 cps and cooled with Peltier cell. The scanning electron microscope is mostly used for analyzing topographies of specimens at very high amplification. Using the SEM, the beam of electrons is focused on the specimen and is transferring energy to the spot. These bombarding electrons can be attributed to primary electrons, dislodge (secondary) electrons from the specimen. Secondary electrons are magnetized and collected by positively set grid (detector) and converted into a signal. To convert the signal into an SEM image the electron beam is moved across the area, amplified and translated into topography images. The energy of primary electrons establishes the quantity of secondary electrons and the radiance of secondary electrons from the specimen depends directly on primary electron energy increases until a particular limit is reached. Beyond this point, secondary electrons decrease while primary energy increases, because primary beam is activating electrons deep in the sample. Usually electrons from such depth

recombine before emission. To generate the useful information received from the SEM analysis three different processes can be used:

- Images from backscattering electrons (BSE).
- Images generated from emitted secondary electrons (SE).
- Images generated from elemental X-ray mapping.

The difference between BSE and SE is that their emitting energy and produced mechanisms are different. “Inelastic” or “elastic” dissipate occurs when a high energy primary electron interacts with an atom. Elastic dissipate is caused by the interaction with an atomic nucleus and inelastic dissipate is the result of primary electron interaction with an atomic electron. Higher energy electrons in the elastic dissipate are those which have been dissipated without the loss of kinetic energy from the atom nucleus. A primary electron can lose some of its energy to inelastic dissipate before collision appears. Generally, BSE is considered to occur when energy is higher than 50 eV of emitted electron and most of BSE energy can be comparable to the primary beam. Backscattering depends on the atomic number of materials, a higher atomic number gives higher probability for backscattering. Therefore, BSE can indicate multiple phases of a mixture structure of different materials (Goldsmith, Miller, 2009).



Fig. 2.12 Scanning electron microscope Quanta 200 FEG

Most SE read by SEM are generated only a few nanometers deep in the material surface. During inelastic collision, some amount of energy is transmitted from one electron to another. If the transfer of energy is not high enough, the emitted electron is not be able to leave through the surface of the material, but the emitted electron will exit the solid if the energy transfer is sufficiently high. Secondary electrons are electrons which are emitted with energy less than 50 eV (Reimer, 1998).

EDS analysis is very useful for identifying materials and their composition, estimating their relative concentrations on the specimen surface. Interaction between a primary electron beam and the specimen can cause a core electron to be emitted

from the atom can be described as elemental x-ray characteristic. X-ray characteristic or Auger electron can be emitted when an excited atom loosens from its ground position. Using an energy dispersive spectrometer, the emitted x-ray signals can be separated by their energies. Primary electrons can penetrate long distance into a solid material before losing sufficient energy through inelastic collisions. That means that a smaller primary beam will generate x-ray emission from a larger volume around the focused beam (Reimer, 1998).

2.5.5 Atomic force microscopy (AFM)

An atomic force microscope JPK Nano Wizard 3 **Fig. 2.13** was used to investigate the surface morphology. Force or potential energy between the specimen and cantilever-type tiny probe is measured where the cantilever provides a force actuator and a force sensor. To measure the topographic height, the cantilever has to be pressed to the specimen. There are various methods for obtaining measurements: tunneling current measurement, optical deflection technique, piezo resistive and fiber interferometry methods. For measuring forces between atoms, tip and the specimen have to be located as close as 0.1–100 nm and those forces can be classified into repulsive and attractive. The repulsive forces can be described as very short-range forces and have inverse power law with a high level distance dependence. For attractive forces, electrostatic and chemical forces together with van derWaals interaction are included. Chemical forces can be described by different theoretical models like Morse, Stilling–Weber or Tersoff potentials. Typically for a solid bulk the interatomic force has a constant in the range of 10–100 N/m. To obtain high resolution images of atomic arrangements, short-range force complicity is used. Working with a non-magnetic tip and equalizing electrostatic potential between the sample and tip, electrostatic, meniscus and magnetic forces can be eliminated. Long range forces can be decreased by working in the dynamic mode and choosing correct a oscillation amplitude of the cantilever (Ando, 2018).

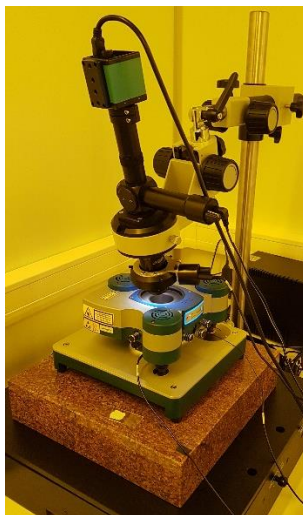


Fig. 2.13 Atomic force microscope JPK Nano Wizard 3

There are three main modes of operation with the Atomic force microscope: tapping, contact and non-contact mode. AFM operation modes can be divided into two groups: static, where the contact mode is applied, and dynamic, where non-contact and intermitted contact modes are used (Dufrene et al. 2017).

In the static mode applying contact to the surface, an image signal is received when long and short-range forces are added and the overall force is deterrent. The tip of the cantilever is dragged over the substrate and the force is estimated from detected cantilever bending variations. Afterwards, those signals are transferred to draw image which presents a topographic view of the scanned surface $z(x, y)$. In the static mode there is a risk of deformation for either the tip or the sample regarding collision. In the dynamic mode the cantilever vibrates at resonant frequency with external excitation and mounted on the actuator. Large and maximum orders for the amplitude of the vibrating energy are stored by the system. Amplitude, phase and frequency characterize the resonance of the cantilever. These three exponents and their variations with regards to the interaction force can be measured and force can be evaluated from the registered data. It is difficult to obtain atomic resolution in ambient conditions using the dynamic mode. The system allows a flexible switch between recorded parameters for surface map modeling to get more detailed results. Using amplitude modulation, the phase of the cantilever or amplitude of vibration is controlled by a feedback signal when output frequency is fixed. To estimate the distance between the tip and sample, a numerical alteration of the amplitude or phase is recorded and calculated (Dufrene et al. 2017).

Atomic force microscopy has another very important feature called force spectroscopy. A graph generated from the recorded data and function of the tip and sample range indicating force extent. Any kind of interaction forces involved can be an interpretation of force versus distance curves. Single atoms of different types can be indirectly discriminated using spectroscopic analysis. It can be concluded that interaction value differs from weak to strong for various species (Dufrene et al. 2017).

Spectrometric data for the static mode is collected by moving the sample in z direction back and forth while cantilever deflection is observed. Hysteresis loops shows assigned to jump to contact and jump of contact phenomena. A spectroscopic field has advantages with the AFM non-contact mode. Stable force measurements, low thermal noise and increased sensitivity are essential for improved quality of measurements; low temperature is also recommended for experiments. DC forces are preferred to be recorded for frequency shift measurements, because they ensure low noise and high accuracy. In other words, vertical and lateral thermal drift and large noises can impede the accuracy of spectrometric measurements (Radmacher, Tillmann, Fritz, Gaub, 1992).

Main morphology parameters: Z_{mean} – average height, R_a – arithmetic average surface roughness, R_q – root mean square surface roughness.

2.6 Methods and equipment for analysing piezoelectric properties

To evaluate the piezoelectric properties, it is necessary to conduct energy harvesting experiments for direct piezoelectric effect applying periodical excitation experiments and single impulse experiments. For reverse piezoelectric effect

electronic speckle pattern interferometry system PRISM was employed. Specifications, working parameters and a description of all used techniques is provided below.

2.6.1 An analysis of the direct piezoelectric effect

The term of energy harvesting (EH) indicates energy generation from such sources as temperature change, air flow or vibration. An energy harvesting phenomenon allows converting environment energy can be used as self-sufficient energy supply for small electric devices, such as sensors or transmitters. Piezoelectric elements convert kinetic energy (vibrations or shocks) into electric energy which can be measured as voltage on the electrodes of the piezoelectric element. Using the right electronics, this effect can be used to create a self-sufficient energy supply system. The advantages of such a system include the replacement or replenishment of the batteries and a minimization of maintenance expense. The main application of EH systems is for independent sensor networks which consist of wireless sensors attached on various surfaces, such as the human body, vehicles, buildings or any other surface in order to inspect the physical conditions. In order to use energy harvesting from the environment, it is preferable to record vibrations with frequencies of up to 200 Hz, because this frequency is dominant in daily life. As excitation force vibrates the energy harvester, mechanical energy is converted to electrical energy by the piezoelectric element. The generated piezoelectric current and voltage are alternating, a diode rectifier is required to convert it into direct current (DC) power supply. Regulation circuit is required because of the large amplitude of generated power and frequency oscillation. The regulated chain produces constant voltage output (Maiwa, 2016).

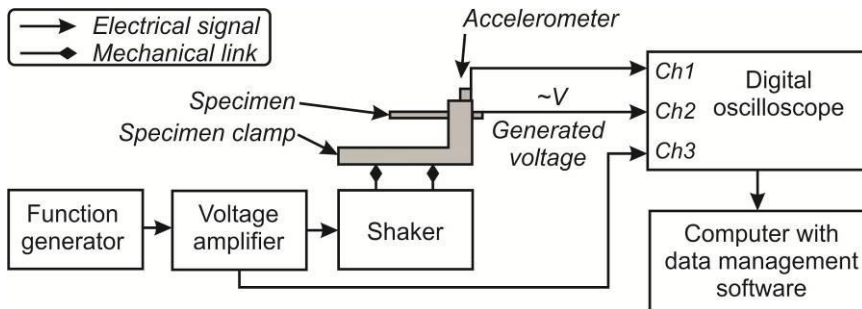


Fig. 2.14 An experimental setup scheme used to measure energy harvesting

The piezoelectric properties were measured using the scheme presented in **Fig. 2.14**. The experimental setup was composed of a piezoelectric element, excitation and measurement systems with a connected data analysis system. The excitation system is mainly an electromagnetic shaker which excites the specimen fixed in a custom-build terminal made of acrylic glass. A harmonic excitation signal is transferred to the electromagnetic shaker and controlled by a function generator AGILENT 33220A through a voltage amplifier HQPower VPA3100MN. To measure the acceleration a single axis miniature accelerometer KD-35 was attached at the top of the clamp which works at a 5Hz to 5kHz frequency and has a sensitivity of 50 mV/g±2%. The

experimental data from accelerometer, specimen and voltage amplifier were collected using a 4-channel oscilloscope (analogous to a digital converter) PICO 3424 and forwarded to a computer. Data were converted to a graph with the Pico-scope 6 software.

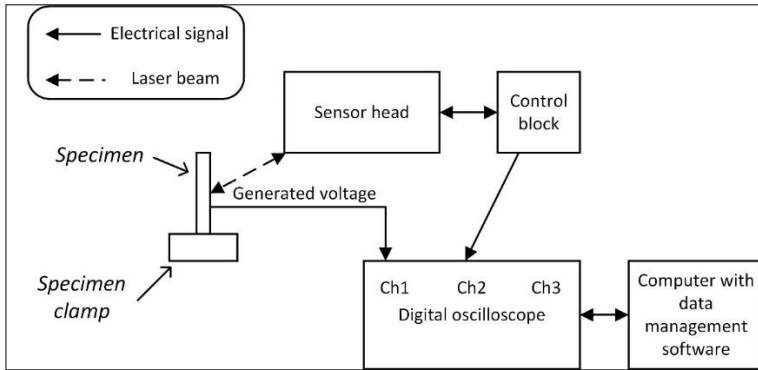


Fig. 2.15 The experimental setup scheme for a single-hit piezoelectric effect measurement

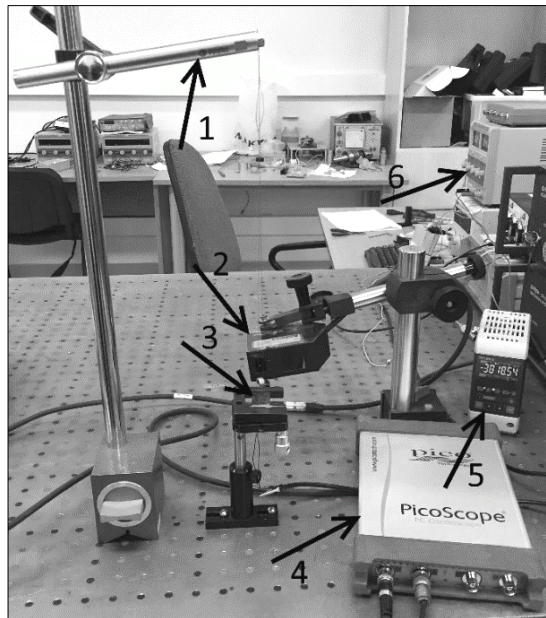


Fig. 2.16 The experimental setup consists of: (1) mathematical pendulum; (2) LK-G82 sensor head; (3) specimen; (4) PicoScope oscilloscope; (5) LK-G3001P control block; and (6) power supply block.

Further investigation was performed by analysing the piezoelectric effect using single-hits excitation. For this experiment, the equipment was reassembled and the shaker was replaced with a mathematical pendulum and an LK-G3000-series laser triangular displacement sensor (sensor head LK-G82, control block LK-G3001P) was added **Fig. 2.16**. A schematic view of experimental setup is presented in **Fig. 2.15**.

Table 4 Specifications of sensor head LK-G82 from Keyence

Reference distance	80 mm (Diffuse reflection), 75.2 mm (Specular reflection)
Measuring range	± 15 mm (Diffuse reflection), ± 14 mm (Specular reflection)
Light source	Red semiconductor laser (655 nm)
Spot diameter	Approx. $\varnothing 70$ μm
Repeatability	0.2 μm
Operating temperature range	0 to 50 $^{\circ}\text{C}$
Operating ambient humidity	35 to 85% RH
Vibration	10 to 55 Hz, double amplitude 1.5 mm
Weight	Approx. 380 g

The experimental setup was projected as a mathematical pendulum which produces a single impulse to the consolidate specimen when indicated. The response of vibrations was scanned with an accuracy of 0.2 μm using a LK-G3000-series laser triangular displacement sensor (Keyence, IL, USA). Specifications of sensor head LK-G82 are presented in **Table 4** and the specifications of control block LK-G3001PV are presented in **Table 5**. The measured data was collected with a PicoScope oscilloscope system (with data reading velocity 5 Gs/s).

Table 5 Specifications of control block LK-G3001PV from Keyence

Type	PNP
Minimum display unit	0.01 μm
Refresh rate	10 times/sec
Analog output voltage	± 10 V x 2 outputs, output impedance: 100 Ω
Analog current output	4 to 20 mA x 2 outputs, maximum load resistance: 350 Ω
Operating temperature range	0 to 50 $^{\circ}\text{C}$
Operating ambient humidity	35 to 85% RH
Weight	Approx. 480 g

2.6.2 An analysis of reverse piezoelectric effect

An electronic speckle pattern interferometry system PRISM **Fig. 2.17** with measurement sensitivity < 20 nm and measurement range > 100 μm was used to evaluate the electrical excitation response of the investigated specimen.

This experimental setup analyzes reverse piezoelectric effect. This is a very effective measurement method which allows to measure vibrations and deformations with minimal sample preparation and with no contact with the specimen. The PRISM setup can be also described as a high-speed holographic technique, equipped with a computer and software. The laser beam directed to the object is an object beam; the beam directed to the camera is the reference beam **Fig. 2.18**.

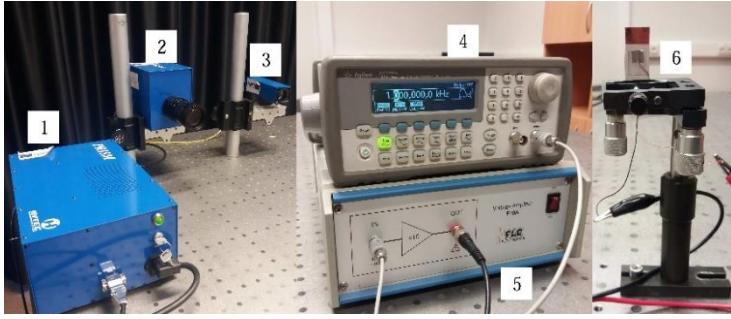


Fig. 2.17 Electronic speckle pattern interferometry system PRISM: 1 – block; 2 – video head; 3 – illumination head; 4 – generator; 5 – amplifier; 6 – specimen with PZT composite material

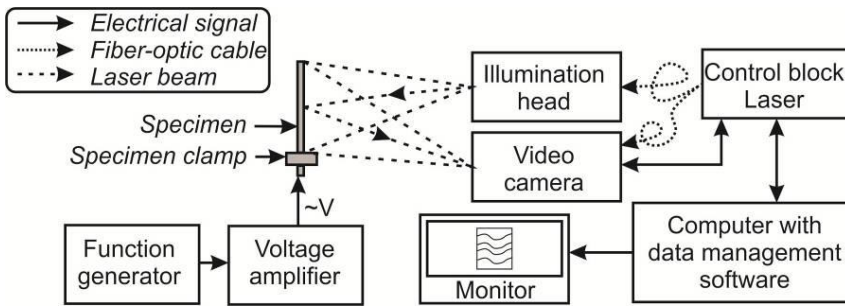


Fig. 2.18 The schematic PRISM experimental set-up

Dissipated laser light from the object is collected with the camera lens and the images subjected to the sensors of the CCD cameras. The image of the object overlaps when the reference ray is pointed directly to the camera. Shape changes appear between a reference and a stressed state of the object and fringes could occur on the monitor. Electrical excitation of the analyzed specimen can be evaluated from the received data.

Optoelectronic holography (OEH) technique can be applied to various fields of non-destructive testing of objects. Recent technology is non-invasive, has no contact with the specimen and is able to provide quantitative and qualitative information on the shape and deformations of the specimen various conditions and loads. The universality of optoelectronic holograph raised with technological advances in coherent light sources, calculation, detector technologies and imaging. Those technical properties allow to use the OEH methodology in a micrometric setup to analyze MEMS structure and investigate materials used for their fabrication.

One of OEH methods used to accomplish form measurement examinations of a sample consist of gaining and processing 2 sets $I(x, y)$ and $I'(x, y)$ of phase-stepped intensity models measured before and after. The first set of phase-stepped intensity patterns is described by (Furlong, Pryputniewicz, 2003; Ragulskis, Ostasevicius, Palevicius, 2002):

$$I_n(x, y) = I_B(x, y) + I_M(x, y) \cos[\Delta\Phi(x, y) + \theta_n] \quad (2.1)$$

where

$$I_B(x, y) = I_0(x, y) + I_r(x, y) \quad (2.2)$$

is the background irradiance and

$$I_M(x, y) = 2\sqrt{I_0(x, y) * I_r(x, y)} \quad (2.3)$$

is the modulation irradiance. In equations 2.1–2.3, $I_0(x, y)$ – object and $I_r(x, y)$ – reference beams irradiances, $\Delta\Phi(x, y) = \Phi_0(x, y) - \Phi_r(x, y)$, with $\Phi_0(x, y)$ expressed a random phase due to light scattering from the object of interest and $\Phi_r(x, y)$ expressed a uniform phase θ_n from a smooth reference beam wave front, θ_n is the conciliatory n phase step, with a rate received during calibration following the phase stepping algorithm that is realized, (x, y) characterize Cartesian coordinates of the image. The second set of phase-stepped intensity patterns is described by (Furlong, Pryputniewicz, 2003; Ragulskis, Ostasevicius, Palevicius, 2002):

$$I'_n(x, y) = I_B(x, y) + I_M(x, y)\cos[\Delta\Phi(x, y) + \Delta\gamma(x, y) + \theta_n] \quad (2.4)$$

In equation 2.4, $\Delta\gamma(x, y)$ is the transform in optical phase which appears between the value related to specimen deformation and acquisition of two sets of phase-stepped strength patterns. With the optoelectronic holography, the two sets of phase-stepped intensity patterns are processed to data and display modes. Secondary interference patterns $Q_D(x, y)$ of the display mode are generated, displayed at video rates and modulated at cosinusoidal function of the form (Furlong, Pryputniewicz, 2003; Ragulskis, Ostasevicius, Palevicius, 2002):

$$Q_D(x, y) = 4I_M(x, y) \cos\left[\frac{\Delta\gamma(x, y)}{2}\right] = \{[I_1(x, y) - I_3(x, y) + I'_1(x, y) - I'_3(x, y)]^2 + [I_2(x, y) - I_4(x, y) + I'_2(x, y) - I'_4(x, y)]^2\}^{1/2} \quad (2.5)$$

which introduces a video image with 8-bit resolution acquired after performing four phase steps: $\theta_n = (0), (\pi/2), (\pi), (3\pi/2)$. The screen mode is applied for adjusting the experimental parameters for accurate optoelectronic holography investigation in real time (Ragulskis, Ostasevicius, Palevicius, 2002).

Using optoelectronic holography technique, it is possible to reach high measurement resolution for the characterization of shape or deformation of MEMS devices.

2.7 Conclusion

Effective technological equipment and materials for composite material creation, thin layer and periodical microstructure formation and analytical equipment for properties evaluation were chosen. The choice of materials depended on their properties and price. A low-cost, effective and simple screen-printing technique was selected. For periodical microstructure imprinting, the thermal embossing technique was chosen. Experimental results were analysed with various analytical equipment for chemical, mechanical, surface morphology and piezoelectric properties of composite material. Consequently, the creation of novel composite material and its application technique is low cost, not complicated, precise, effective and requires only specific knowledge.

3 INVESTIGATION OF CHEMICAL, MECHANICAL AND ELECTRICAL CHARACTERISTICS OF THE FUNCTIONAL ELEMENT

In order to create a novel PZT composite material, PZT powder was synthesized and its chemical composition properties were confirmed. One of the most effective methods is energy distribution analysis performed with a dispersive X-ray diffraction spectrometer (XRD). The XRD pattern of synthesized PZT powder after final calcination process is presented in **Fig.3.1**.

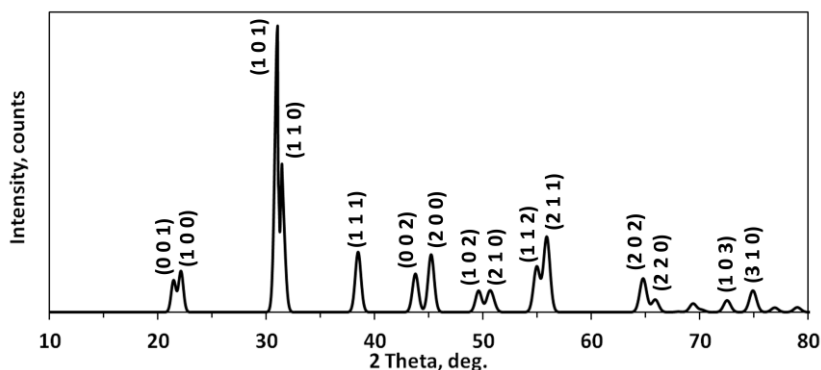


Fig.3.1 X-ray diffraction (XRD) pattern of lead zirconate titanate powder

The PZT ceramics formed in a characterized tetragonal structure ($\alpha = \beta = \gamma = 90$ deg. $a = b = 4.006 \text{ \AA}$, $c = 4.128 \text{ \AA}$), with a spot fraction of $P=4 \text{ mm}$ (non-central symmetric) and the crystallographic plane orientations: $(3\ 1\ 0)$, $(1\ 0\ 3)$, $(2\ 2\ 0)$, $(2\ 0\ 2)$, $(2\ 1\ 1)$, $(1\ 1\ 2)$, $(2\ 1\ 0)$, $(1\ 0\ 2)$, $(2\ 0\ 0)$, $(0\ 0\ 2)$, $(1\ 1\ 1)$, $(1\ 1\ 0)$, $(1\ 0\ 1)$, $(1\ 0\ 0)$, $(0\ 0\ 1)$. The XRD pattern of the PZT powder corresponds to $\text{Pb}(\text{Zr}_{0.52}\text{Ti}_{0.48})\text{O}_3$ with R_f factor of 0.31.

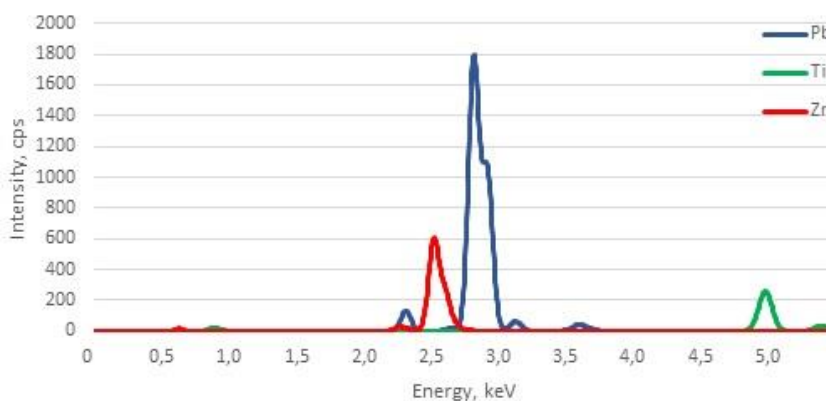


Fig. 3.2 Energy dispersive spectrum of PZT powder

The energy dispersive spectrum (EDS) shows the expected elements peaks in a specific location which characterize PZT elements (Pb, Ti, and Zr). Lead showed the intensity of up to 1797 cps at the 2.8 keV while Zirconium reached 610 cps at the 2.55

keV; Titanium intensity was 250 cps at the 4.9 keV energy. Energy dispersive spectrum is presented in **Fig. 3.2**.

3.1 An evaluation of functional element properties with various concentrations of PZT

Three different PZT concentrations of 40%, 60% and 80% were chosen for further investigation of surface morphology and chemical properties.

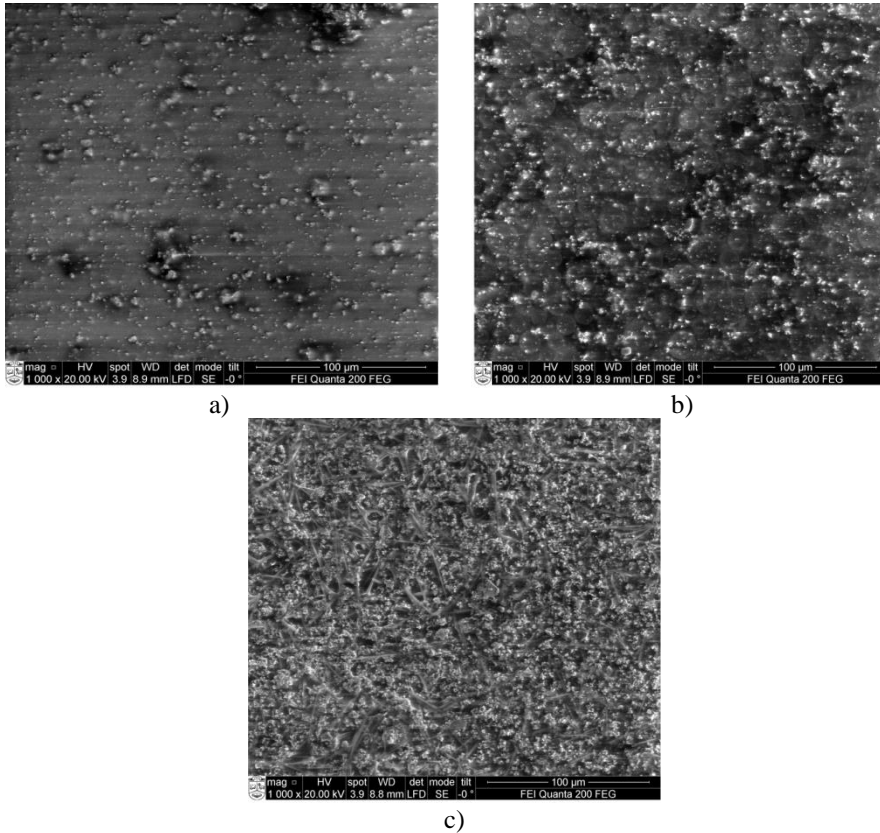


Fig. 3.3 A scanning electron microscope view of PZT composite material with the concentration of: a) 40%, b) 60% and c) 80%.

Surface morphology of three different specimens was investigated using a scanning electron microscope **Fig. 3.3** and atomic force microscopy **Table 6**. When analyzing the samples, different granular structures were observed: the surface of the specimen with 40% of PZT was relatively smooth with 5–15 µm diameter concentrated grains on the top **Fig.3.3a**, the specimen with 60% of PZT presented denser islands on the surface **Fig. 3.3b**. Upon increasing the concentration of PZT to 80%, the surface of the sample became more granular with grain size below 4 µm **Fig. 3.3c**. PZT powder mixed with polyvinyl butyral might be the cause of dissimilar shape, nucleation and gain in the solution, therefore forming groups of smaller grains. Island structures were formed in samples with 40% and 60% of PZT where smaller

grains surround larger ones. It is also noticed that high density is achieved in the specimen with 80% of PZT concentration, despite several pinholes **Fig. 3.3c**.

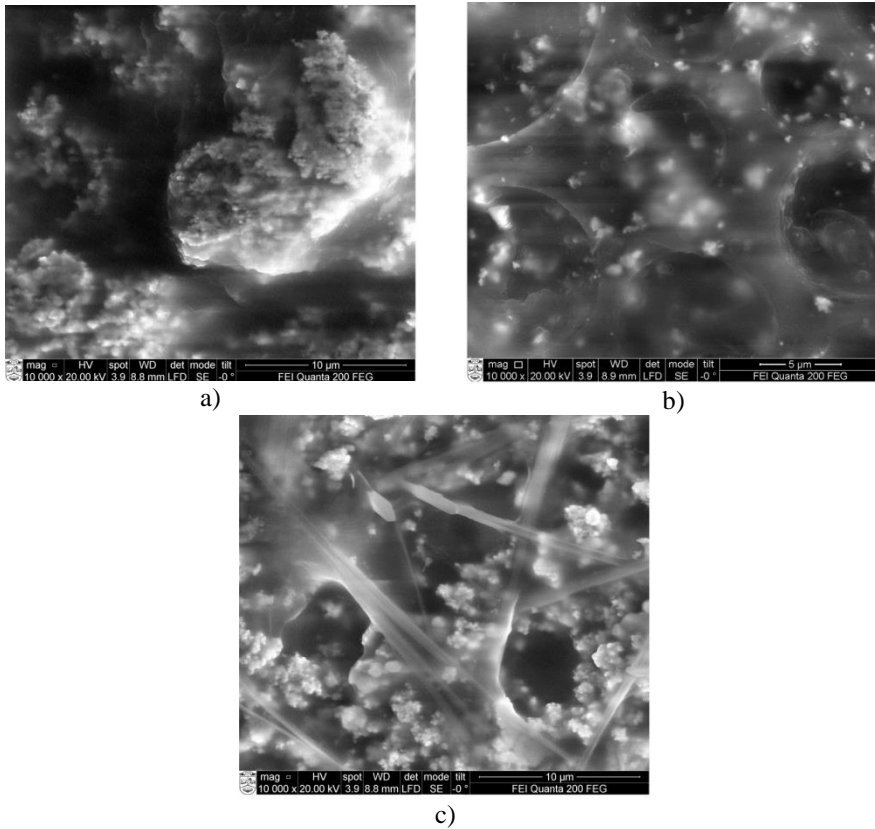
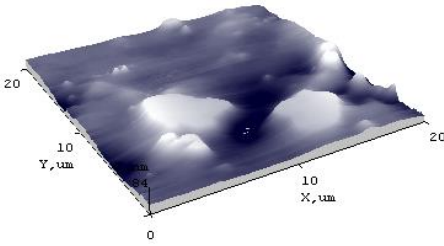
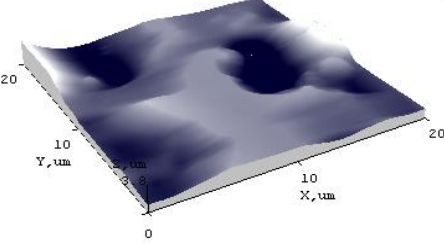
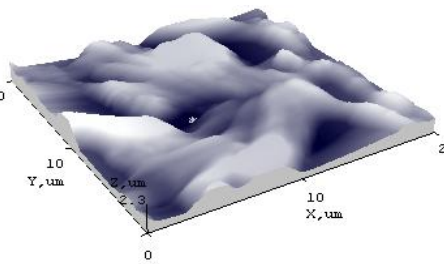


Fig. 3.4 Images of SEM of PZT composite material with concentrations of: (a) 40%; (b) 60%; (c) 80%.

More accurate scanning electron microscope views with a scale of 5–10 micrometers are presented in **Fig. 3.4**. The specimen with 40% concentration of PZT **Fig. 3.4a** consists of about a 10 µm size structure, while the sample with 60% concentration of PZT has a net structure with formed cavities **Fig. 3.4 b**. A higher concentration of PZT leads to a granular structure with net joints and empty cavities of about 7 µm in diameter **Fig. 3.4c**.

The results are presented in **Table 6**. The concentration of PZT has a direct impact on surface morphology. The surface with a bigger PZT concentration obtained a more even layer.

Table 6 AFM measurements of PZT composite layers with different concentrations

<p>40% PZT</p> <p>$Z_{mean} = 32.5 \text{ nm}$</p> <p>$R_a = 8.89 \text{ nm}$</p> <p>$R_q = 12.31 \text{ nm}$</p>	
<p>60% PZT</p> <p>$Z_{mean} = 1559.89 \text{ nm}$</p> <p>$R_a = 424.22 \text{ nm}$</p> <p>$R_q = 562.66 \text{ nm}$</p>	
<p>80% PZT</p> <p>$Z_{mean} = 1073.63 \text{ nm}$</p> <p>$R_a = 360.97 \text{ nm}$</p> <p>$R_q = 436.77 \text{ nm}$</p>	

3.1.1 Chemical compositions of PZT composite material

The chemical compositions of PZT composite material were investigated with an energy-dispersive (ED) spectrometer; pulse height analysis is employed. Electrical charge is produced when ionization is caused by incident X-ray photons. The ED spectrum is introduced where X-ray energy in channels 1.5 to 5 keV is represented in the x-axis and the counts per second per electron-volt are up to 700 cps/eV given in y-axis. Only the main elements of PZT were investigated in the specimens: Lead, Zirconium and Titanium. Titanium K_{β} X-ray emission spectroscopy (XPS) peak is specified at 4.94 keV. For Zr, L_{α} X-ray intensity ratio peak is at 2.05 keV and Pb peak is at 2.35 keV **Fig. 3.5**.

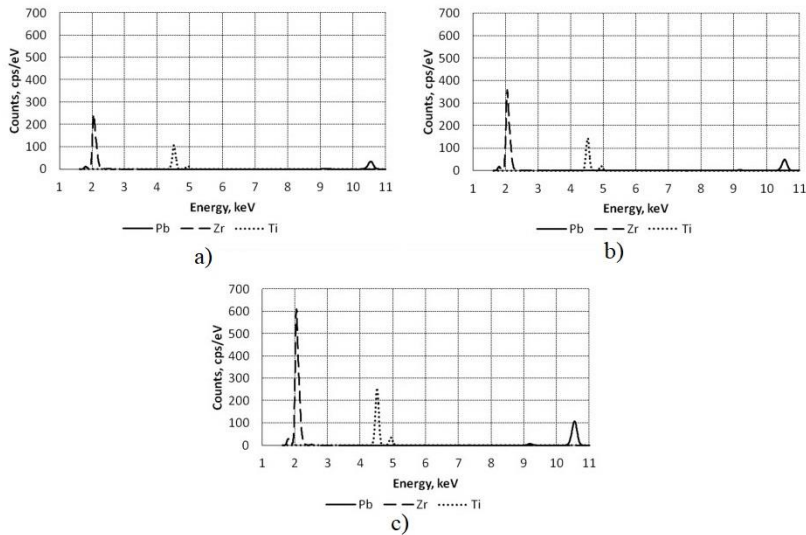


Fig. 3.5 ED spectrum showing peaks of Pb, Zr and Ti in the PZT composite material with concentration of: (a) 40%; (b) 60% and (c) 80%.

Energy dispersive spectrum values of Pb, Zr and Ti of the investigated specimens (with PZT concentrations: 40%, 60% and 80%) for more precise comparison are presented in **Table 7**.

Table 7 EDS peak values of Pb, Zr and Ti of PZT composite materials

Concentration	Pb 10.5515 keV	Zr 2.04236 keV	Ti 4.50486 keV
40%	34.49	244.44	107.73
60%	48.62	359.21	143.94
80%	108.05	609.85	256.81

Energy dispersive spectroscopy characterizes each element by its specific peak position, which corresponds to the conversion in the electron. EDS analysis indicates that Pb, Zr and Ti concentrations directly connected to PZT concentration and increases proportionally. K and L peaks for Zr and Ti are respectively dominant and the Pb spectrum is more combined, but the dominant peak is indicated at 2.35 keV.

3.1.2 The evaluation of binding material

PZT composite material with concentration of 80% is used for further experiments, since it reached the best results in previous experiments. When producing micro sensors, materials must be tested under various conditions and satisfy the necessary requirements. The binding material comprises 20% of the composition which directly impacts adhesion and deformation and it is the main mechanism causing friction. Additionally, adhesion influences the degree of deformation of the structure's roughness at contact and is overwhelmed by the grand portion of the interacting forces between the surface atoms of both of the contacts. Surface morphology analysis was done with an AFM which allows to evaluate the properties

of PZT coating. Profiles and 3D views including surface roughness data are presented in **Fig. 3.6**.

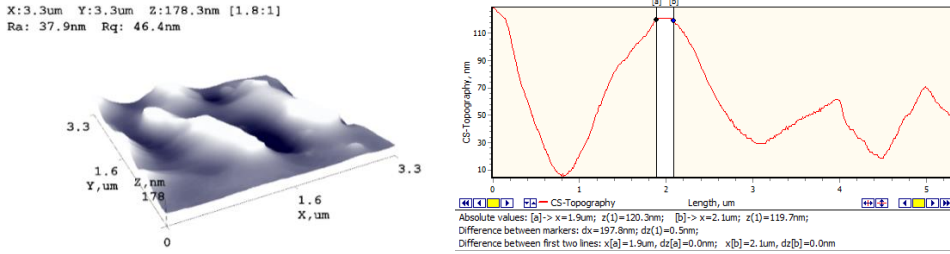


Fig. 3.6 Surface morphology (left) and profile view (right) of the specimen with PVB binding material.

An analysis of AFM surface morphology shows that surface roughness was R_q determined 46.4 nm. AFM analysis also identifies the size of PZT nanoparticles which are 177 ± 10 nm.

Fourier transform infrared spectroscopy (FTIR) analysis was performed to determine the chemical composition. Specimens of different thickness as well as poled and not poled elements were analyzed. As long as there was no significant difference between the thickness of the piezoelectric layer, PZT composite material of 60 μm thickness was chosen for further experiments. Electrical pole alignment did not affect the structure of polymers, and only poled specimens were used for further experiments as they showed higher results in experiments before. A typical FTIR absorbance spectrum at 4000–500 cm^{-1} of PZT composite material with PVB binding polymers was compared with the polymer FTIR absorbance spectrum **Fig. 3.8**. Chemical bonds in a molecule can be identified by their produced infrared absorption spectrum. Molecular structure of PVB binding material is presented in **Fig. 3.7**.

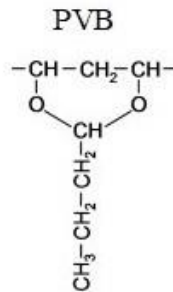


Fig. 3.7 The molecular structure of PVB binding materials

FTIR spectrum of PVB and PZT composite materials with PVB binding material and their characterized bonds are presented in **Fig. 3.8**. Aliphatic stretching of the C-H bond can be observed at 680 cm^{-1} and 1010 cm^{-1} absorption bands. The C-O-C stretching band showed absorption at 1150 cm^{-1} which is related to the butyral ring. C-H bonds of the C-H₂ group show bending absorption at 1280 cm^{-1} and two peaks, at 2880 cm^{-1} and 2980 cm^{-1} . A C-H Band of C-H₃ group can be observed at 1380 cm^{-1} . C-O absorption bond is noted at 1720 cm^{-1} band stretching vibrations. O-

H stretching bond appears between 3400 cm^{-1} and 3600 cm^{-1} with long absorption band which is characteristic to the PVB polymer.

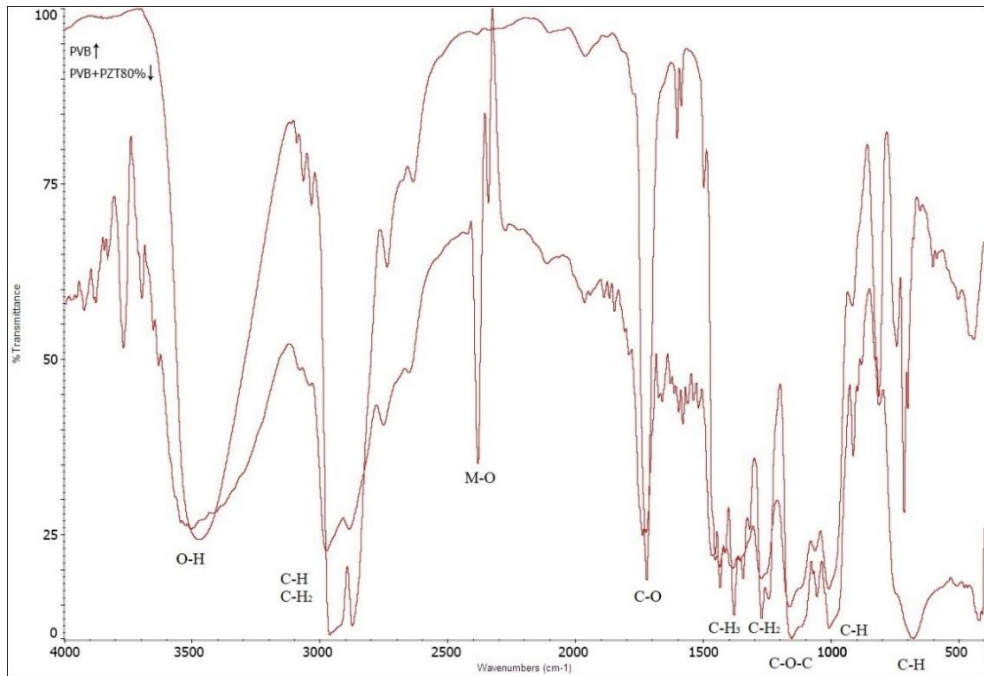


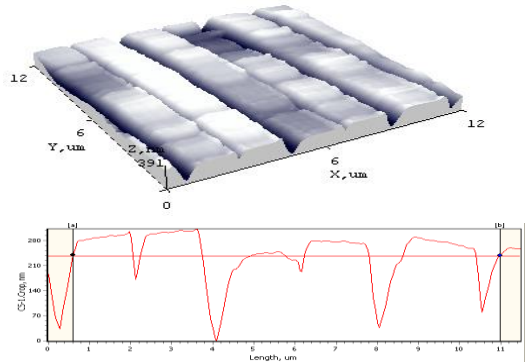
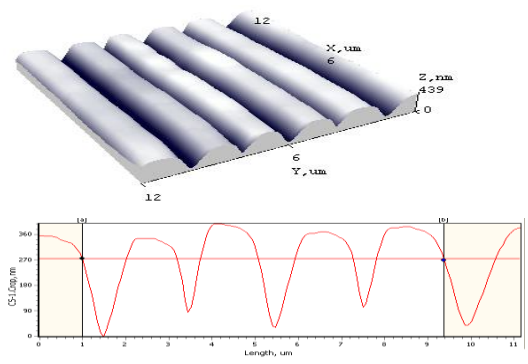
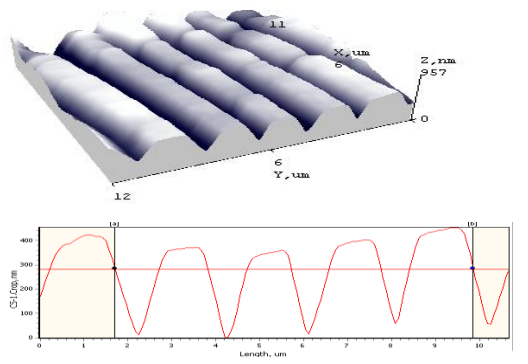
Fig. 3.8 A comparison of the FTIR absorbance spectra of the PVB polymer and the PZT composite material with the PVB binding material

Strong absorption at 2400 cm^{-1} in the FTIR spectrum of the PZT composite material with a binding material shows that an M-O bond is present, where M is a metal. It shows that besides binding material, Ti-O or Pb-O bond can be observed. FTIR spectroscopy analysis shows that PZT composite material does not change when PZT nano particles are mixed with the chemical composition of the polymer which means that the polymer does not change any chemical properties of the PZT besides elasticity.

3.1.3 The formation and manufacturing of the functional element

Hot embossing was used to replicate the diffraction grating. The formation was done on copper foil substrate with screen-printed PZT composite material. For the imprint, a trapezium-shaped nickel matrix was chosen as well as the period of $2\text{ }\mu\text{m}$. The formation process was accomplished with a pressure of 5 atmospheres held for 10 seconds at 100°C . After hot embossing, all three specimens were analyzed with an AFM and the results and AFM views with profile sections are presented in FTIR spectroscopy analysis shows that PZT composite material when PZT nano particles mixed with polymer chemical composition has not changed which means that polymer didn't change any PZT chemical properties besides elasticity **Table 8**. According to results presented in **Table 8**, the quality of the imprinted structure depends on the concentration of PZT; a more concentrated element leads to a better structure profile.

Table 8 Surface morphology parameters of thin film nanocomposites with PZT after hot embossing

<p>40% PZT</p> <p>$Z_{\text{mean}} = 240.7 \text{ nm}$</p> <p>Period = 2.06</p> <p>$R_a = 56.19 \text{ nm}$</p> <p>$R_q = 71.28 \text{ nm}$</p>	
<p>60% PZT</p> <p>$Z_{\text{mean}} = 276 \text{ nm}$</p> <p>Period = 2.1</p> <p>$R_a = 94.1 \text{ nm}$</p> <p>$R_q = 111.3 \text{ nm}$</p>	
<p>80% PZT</p> <p>$Z_{\text{mean}} = 286,6 \text{ nm}$</p> <p>Period = 2.03</p> <p>$R_a = 116.61 \text{ nm}$</p> <p>$R_q = 140.33 \text{ nm}$</p>	

3.1.4 Piezoelectric properties of PZT composite material with different concentrations of PZT

PZT composite material was screen-printed on cantilever-type specimens to investigate energy harvesting response to oscillation. All specimens were made the same size: length 20 mm, width – 5 mm and thickness of 0.1 mm. At the acceleration of 0.007g with a frequency of 52 Hz, the specimens generate different electrical

potential **Fig. 3.9**. The PZT element with 40% PZT generates up to 50 μV of electrical potential **Fig. 3.9a**, the PZT element with 60% concentration generates up to 40 μV of electrical potential **Fig. 3.9b**. The best result was generated by the PZT element with 80% of PZT concentration which generates up to 80 μV **Fig. 3.9c**. All of those results were pretreated with a 500 Hz low pass filter.

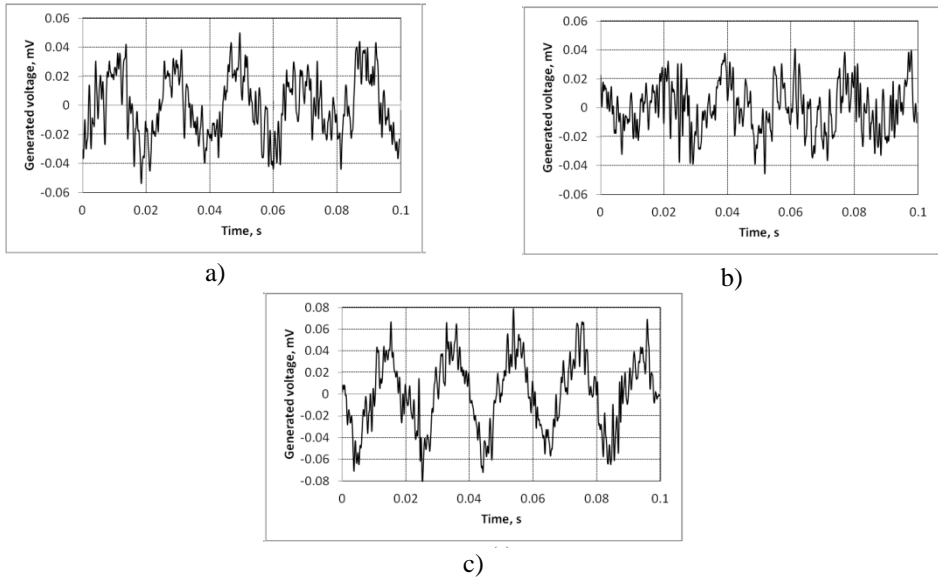


Fig. 3.9 The results of electrical potential generated by the designed elements with PZT: (a) 40%; (b) 60%, and (c) 80%.

According to the results presented in **Fig. 3.9**, when PZT composite material with 80% concentration generates up to 80 μV , low frequency vibrations are transformed into electricity. One of the advantages is that the PZT composite material can be applied to any uneven vibrating surface.

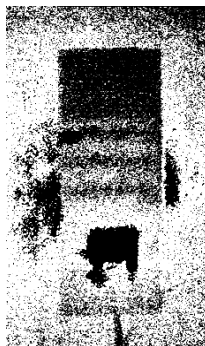


Fig. 3.10 A hologram of the cantilever-type piezoelectric element with PZT 80%

A PRISM experimental setup was used to examine the reverse piezoelectric effect of the designed cantilever-type element. Specimens with 40% and 60% concentration of PZT had no signs of ability to convert electrical potential into mechanical displacement. The specimen with 80% concentration of PZT was excited

by a sinusoidal function at a frequency of 52 Hz and amplitude of 5mV **Fig. 3.10**. At the first resonant frequency the element vibrates as a clamped–free cantilever resonator in its fundamental flexural mode. One of the main advantages of PT composite material is its ability to design a piezoelectric sensor at any size, thickness; it can be applied on any form of vibrating surface.

3.2 Natural frequency and first vibration mode analysis of a multilayer structure

To compare the theoretical and experimental models the natural frequency of the multilayer specimen had to be calculated. The calculation and experiments used a cantilever-type specimen with the length of 5 mm and width of 1.5 mm, the thickness of 0.1 mm was used. The experimental vibrational response graph has been registered using a PicoScope oscilloscope. Theoretical natural frequency was calculated with formulas 3.1, 3.2 and 3.3.

$$\omega_d = \omega_n \sqrt{1 - \xi^2} \quad (3.1)$$

where, ω_d – the damped natural frequency, ω_n – the natural frequency, ξ – the damping coefficient

$$\xi = \frac{1}{\sqrt{1 + \left(\frac{2\pi}{\delta}\right)^2}} \quad (3.2)$$

where, ξ – the damping ratio, δ – the logarithmic decrement

$$\delta = \frac{1}{n} \ln \frac{x(t)}{x(t+nT)} \quad (3.3)$$

where, δ – the logarithmic decrement, n – the number of subsequent periods, $x(t)$ – amplitude at time t , $x(t + nT)$ – amplitude at time $t + nT$, T – period.

The values of amplitudes were taken from the vibrational response graph of multilayer element to a single impulse **Fig. 3.11**.

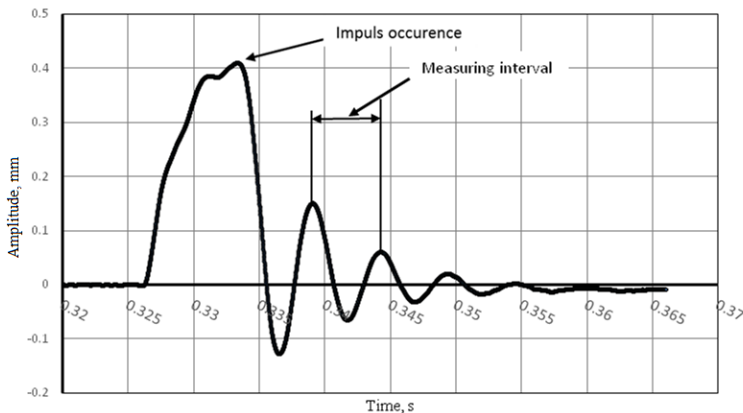


Fig. 3.11 Vibrational response of multilayer element to a single impulse.

A natural frequency of 186 Hz was calculated from the experimental results. Vibration amplitudes in the measuring interval were 150 μm and drop to 60 μm after

one period. The theoretical natural frequency was calculated using formulas presented above, with a result of 187 Hz.

The microcantilever (mass–spring) system for bending vibration schematically is presented in **Fig.3.12**. This configuration is described by the Timoshenko model.

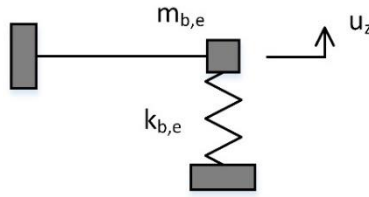


Fig. 3.12 The micro-cantilever bending vibration model

Considering the conditionally short beam, the shearing effect becomes more relevant and creates additional angular deformation. The relative resonant frequency of such a model can be found by means of stiffness and effective mass using formula (3.4).

$$\omega_{b,e}^{sh} = 11.832 \sqrt{\frac{EGI_y A(GAl^2 + 3\kappa EI_y)}{ml(140\kappa^2 E^2 I_y^2 + 77\kappa EGI_y A l^2 + 11G^2 A^2 l^4)}} \quad (3.4)$$

Where, E – modulus of elasticity, G – shear elastic moduli, I_y – inertia moment to y axis, A – cross-sectional area, κ – the coefficient accounting for the cross-sectional shape, which is equal to $5/6$ for a rectangular shape, l – the length of micro-cantilever.

The Timoshenko model allows to calculate the first mode of vibrations theoretically. Experimental results were compared with numerical calculations **Fig. 3.13** and it represents the first mode of vibrations of the modelled composition. The model of multilayer element gave similar results.

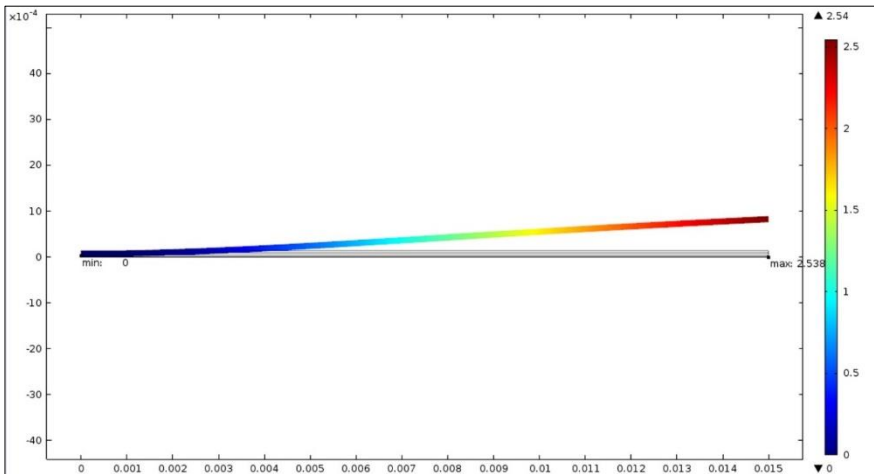
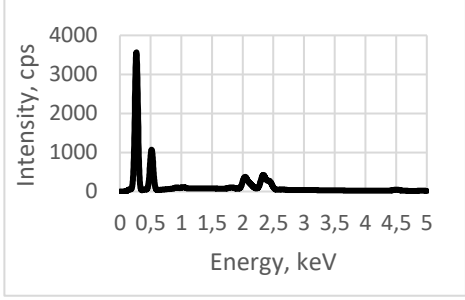
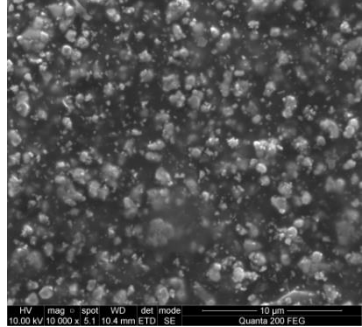
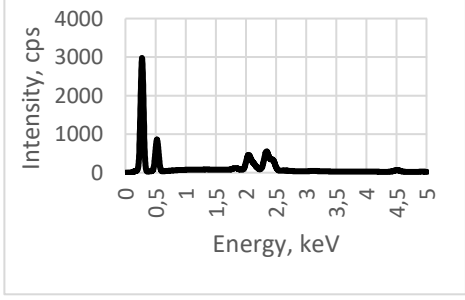
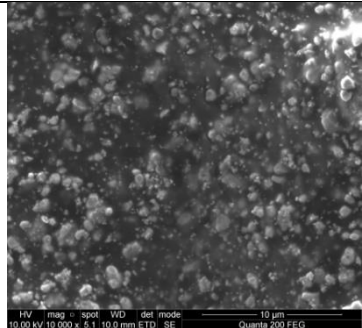
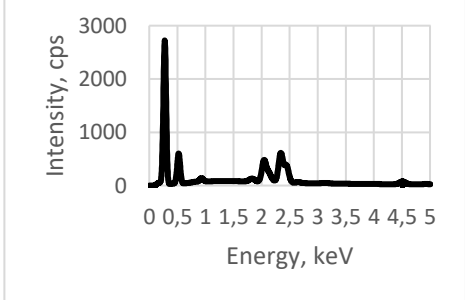
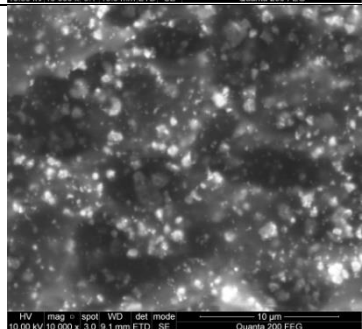


Fig. 3.13 First vibration form of multilayer element model in COMSOL Multiphysics environment

The first vibration mode in the COMSOL Multiphysics model was achieved at the natural frequency of 187.9 Hz. The difference between theoretical and experimental values was only 0.43%. Considering that experimental and theoretical natural frequencies are almost identical, it could be stated that Young's modulus of created PZT composite material of 3.9 GPa was defined correctly. According to Young's small modulus of created material, it is possible to use for micro-sensor creation which can be operated in low-frequency range allowing to increase their sensitivity. Comparing regular PZT material to a novel PZT composite material the first resonant frequency decreases by 2.3 times (from 439.4 Hz to 187.9 Hz).

3.3 The influence of layer thickness and pole alignment on the piezoelectric effect

Table 9 Energy dispersive spectrum of poled specimens and SEM views

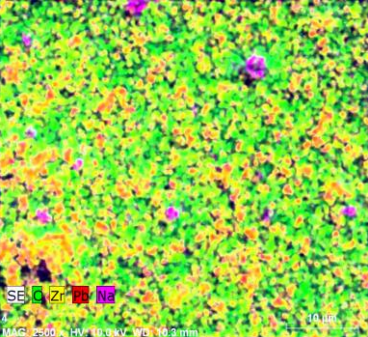

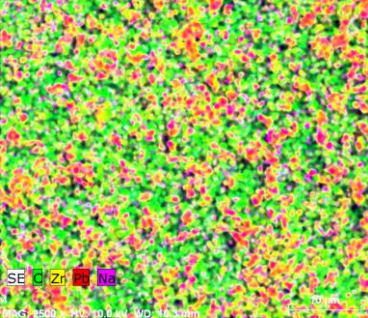

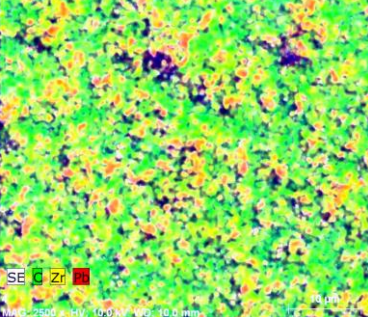
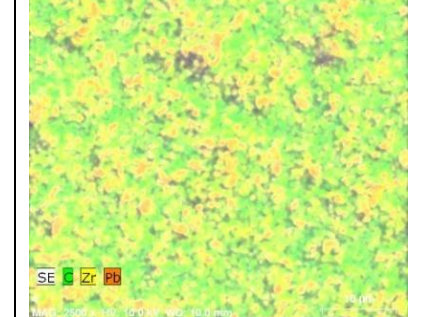
Functional element 1 Mesh type: 32/70 Layer thickness 70 μm		
Functional element 2 Mesh type: 48/70 Layer thickness 60 μm		
Functional element 3 Mesh type: 140/34 Layer thickness 25 μm		

This section investigated samples with 80% concentration of PZT composite material as it showed the best results before. The structure and chemical composition

of PZT composite material was investigated with an SEM integrated with an energy dispersive X-ray spectrometer detector. Six elements of three different thicknesses (two specimens of each thickness, poled and not poled) were analyzed. 100,000 cps was achieved with energy resolution of 133 eV with a 30 sq.mm area solid drift detector.

Measurements were between different quantum modes of the system with probability so that the system jumps between these modes. Results with the energy dispersive spectrums are presented only for the poled element **Table 9** since they were identical between poled and not poled specimens. The results confirm that PZT composite material is dominant in the composition of all specimens.

Table 10 Elemental mapping accomplished with SEM

Element 1 (mesh 32/70);		
Element 2 (mesh 48/70);		
Element 3 (mesh 140/34).		

Energy dispersive spectroscopy results demonstrate the same peak locations for all specimens and verify PZT composite material elements (Pb, Ti, Zr) in each sample. A comparing of EDS results for each specimen indicated that peak intensity depends

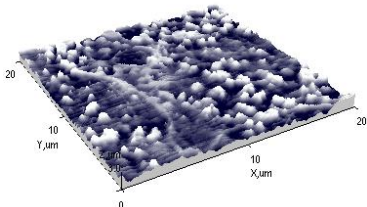
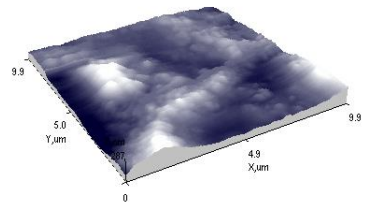
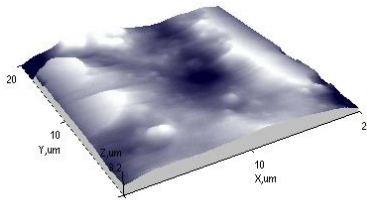
on layer thickness; the peaks for thicker PZT composite material are higher which proves a greater concentration of PZT. It could be influenced by the screen-printing mesh density and lead to better piezoelectric properties. SEM images in **Table 9** show that the surface of functional element 1 and 2 is smoother and granular with small grains of about 1 μm in diameter. The structure of functional element 3 is three-dimensional with periodic empty cavities with a diameter of around 7 μm .

The full structure of element mapping was identified in **Table 10**. Carbon and Zirconium are two main elements in the mapping structure and are good conductors which ensures high piezoelectric properties as functional elements in designed MEMS.

3.3.1 Surface Morphology

To evaluate the surface morphology of screen-printed elements the research used atomic force microscopy with three different screens. Results presented in **Table 11** show that the roughness of each element with a sufficiently smooth surface reached roughness of $R_q = 29 \text{ nm}$ for element 1. For elements 2 and 3 surface roughness was identified to be $R_q = 189 \text{ nm}$ and $R_q = 149 \text{ nm}$, respectively. The screen-printing method with different types off screen mesh allows to control not only the thickness of a layer but also its surface roughness.

Table 11 AFM values of surface morphology and Atomic force microscopy (AFM) 3D views

Layer thickness 70 μm Mesh type 32/70 $Z_{\text{mean}} = 54 \text{ nm}$ $R_a = 21 \pm 1 \text{ nm}$ $R_q = 29 \pm 1 \text{ nm}$	
Layer thickness 60 μm Mesh type 48/70 $Z_{\text{mean}} = 396 \text{ nm}$ $R_a = 156 \pm 0.5 \text{ nm}$ $R_q = 189 \pm 0.5 \text{ nm}$	
Layer thickness 25 μm Mesh type 140/34 $Z_{\text{mean}} = 457 \text{ nm}$ $R_a = 112 \pm 0.5 \text{ nm}$ $R_q = 149 \pm 0.5 \text{ nm}$	

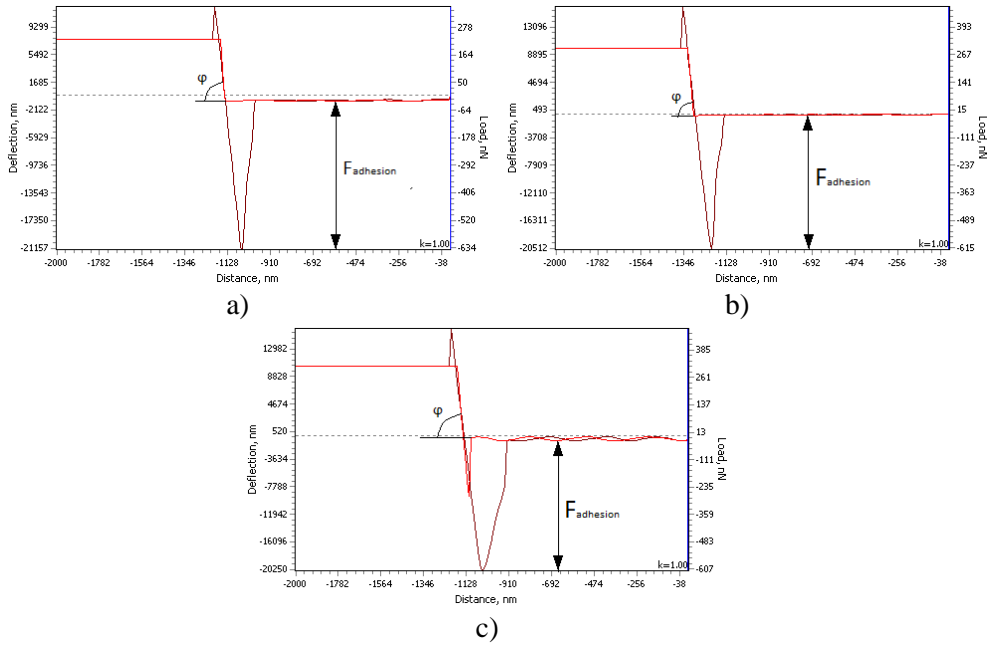


Fig. 3.14 AFM hysteresis with layer thickness of: a) 70 μm , b) 60 μm , c) 25 μm

Fig.3.14 presents graphs of hysteresis obtained with AFM. It presents adhesion force while surface stiffness could be calculated from angle φ . Those parameters are very important for selecting a proper operating mode. Surface stiffness can be calculated using the following equation:

$$k_s = \tan \varphi \quad (3.4)$$

Table 12 Hysteresis parameters

Layer thickness, μm	Adhesion force, nN	Surface stiffness, N/m
70	634	8.14
60	615	9.51
25	607	11.43

As presented in **Table 12**, adhesion force decreases for the thinner layer while surface stiffness does the opposite, i.e. increases for the thinner layer. Therefore, it could be stated that it is expedient to use a thicker layer of functional material for sensing platforms where analytes have to be attracted to the functional element. Also, surface stiffness is very important for selecting a proper working mode, especially in micro systems.

3.3.2 Piezoelectric properties of PZT composite material with different layer thickness

Six specimens with three different thicknesses and poled and not poled elements of each thickness were taken in order to investigate the piezoelectric properties. Results show that the process of pole alignment has much influence on the piezoelectric effect. All specimens were treated with an impulse force of 5 N and the

results for poled elements were more than 3 times better in comparison with the not poled elements. Poled elements generated from 1.4 mV to 3.42 mV of voltage **Fig. 3.15**. The results also showed the influence of layer thickness to the generated voltage since the thickest specimen generated 1.42 mV and the specimen with the thinnest layer generated up to 3.42 mV. The not poled element generated only from 0.2 mV to 1 mV voltage. These results prove the efficiency of pole alignment for any layer thickness.

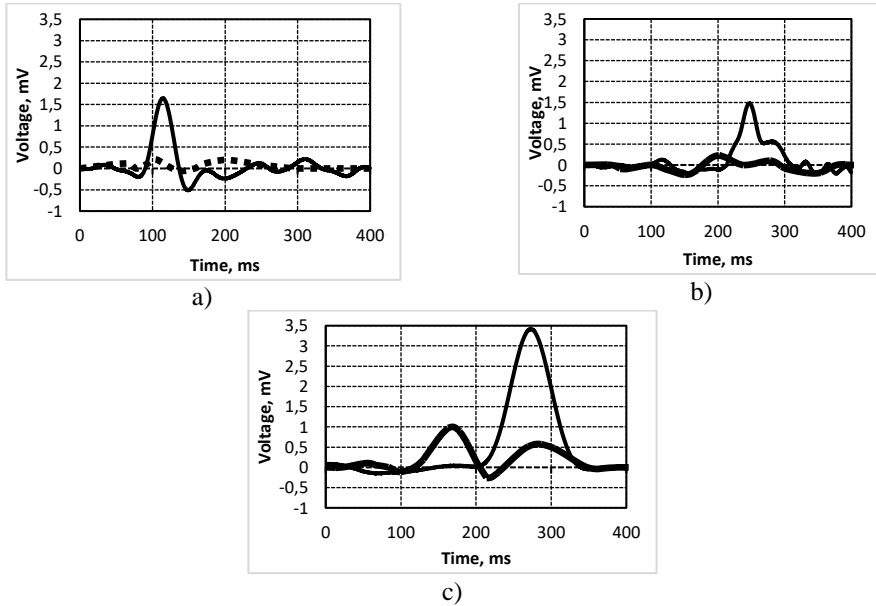


Fig. 3.15 A generated electrical potential diagram of elements with different thicknesses (—poled, - - - not poled): a) 70 μm layer, $\Delta = 1.428$ mV; b) 60 μm layer, $\Delta = 1.48$ mV; c) 25 μm layer, $\Delta = 3.42$ mV

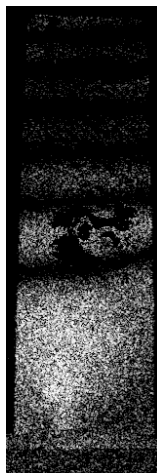


Fig. 3.16 Holographic interferograms obtained for the PZT composite material specimens with PVB binding material

During the poling process each specimen was subjected to a high electric field (5kV) which effects the PZT composite material and orientates dipoles in the direction of the electric field. After pole alignment which takes 30 minutes, electrical field is switched off and dipoles of PZT composite material do not return to their initial orientation. As a result, microscopic defects in the crystalline grating arise which give the PZT composite material abundant microscopic dipoles and they are orientated in same direction.

Reverse piezoelectric method was applied to analyse resonant frequencies of specimens with 20% PVB of binding materials **Fig. 3.16**. The PRISM system was chosen for experimental analysis. To discover the resonant frequency, voltage was set to 100V and the amplitude of vibration was measured applying different frequencies. A vibration amplitude of 100 nm was detected at a resonant frequency of 186 Hz.

A comparison of properties of different piezoelectric materials is presented in **Table 13**, where PVDF, PZT ceramic and the novel PZT composite materials are compared. The piezoelectric constant for the novel material decreases in comparison to PZT ceramics; however, it is still much higher comparing to PVDF.

Table 13 PZT composite properties compared to other piezoelectric materials

Material property	PVDF	PZT	PZT composite
Density, g/cm ³	1.78	7.6	6.3
Piezoelectric constant d_{33} , pC/N	23	400	35
Voltage constant g_{33} , V•m/N	340	25	35
Young's modulus, GPa	8.3	63	3.9

3.4 Conclusion

The first part of the chapter discusses the PZT synthesis, mixing with polymer obtaining PZT composite material of different concentrations. Chemical, mechanical and piezoelectric properties were analyzed to compare the specimens with different concentrations, which have showed that the sample with 80% of PZT concentration presents the best results. It generated up to 80 μ V of electric potential.

Moreover, the chapter describes the improvement of piezoelectric properties of PZT composite material. For that purpose, different thicknesses of the PZT composite were analyzed and the polarization process was performed. Polarization improved the piezoelectric properties of the material and as the experimental analysis shows, the greatest achievement is for the thinnest polarized specimen with a thickness of 25 μ m, which generated up to 3.4 mV. Furthermore, the influence of binding material influence on PZT composite was analyzed. FTIR spectroscopy showed that mixing the nanoparticles of PZT ceramics with PVB, no chemical reactions occurred and the piezoelectric properties remained the same. Finally, natural frequency was calculated and compared to the first resonant frequency of regular PZT materials, which shows that the frequency of the novel material decreases by 2.3 times.

Thus, results prove that the novel PZT composite was created with piezoelectric properties on the micrometric level. Results are substantive because the surface morphology, mechanical and piezoelectric properties become important when micro composite material is used to construct smaller, cheaper, more sensitive and effective biosensors for medical application.

4 PERSPECTIVE BIOMEDICAL APPLICATION

4.1 Biomedical application of periodical microstructures based on Surface plasmon resonance

As experimental results show, a novel cantilever-type element with a PZT composite material works in both, direct and reverse piezoelectric effects. The designed novel piezoelectric PZT composite material is a perspective material for future experimentations. This unique material allows direct observation of attraction interactions in real time. Sensing elements with piezoelectric effect use an active method for measurements in medical or pharmaceutical fields. Embossing of periodical microstructure in PZT composite material allows to use such a platform for analyzing the chemical composition, interactions of bio-molecules, to analyze functional data that is related to the physiological effect of a living system. Such a platform is potentially appropriate in many application fields: pharmacy, biology, medicine, environmental measurements in specific areas, etc.

For this experiment, PZT composite material was screen-printed on copper foil and then a periodical micro structure was embossed with a period of forty microns. The cantilever-type piezoelectric sensing platform consists of a thin layer PZT composite material film coated on copper foil. On the top of PZT composite material film applied opposite electrode. A periodical microstructure was formed in the piezoelectric material using the hot-embossing technique. A schematic view of designed sensor is presented in **Fig. 4.1**.

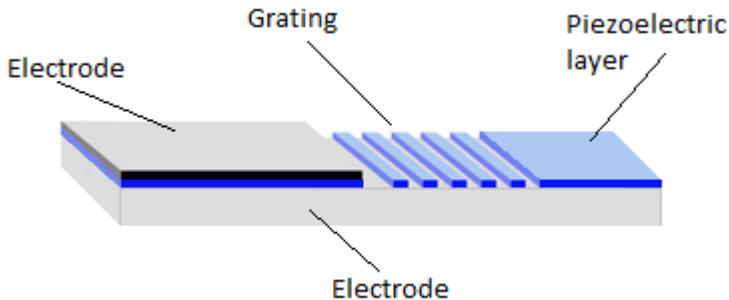


Fig. 4.1 A principal scheme of a cantilever-type piezoelectric sensing platform

AFM was used for surface morphology measurements of the imprinted structure. Due to the brittleness and inelasticity of PZT ceramics, it is rather hard to imprint a periodical microstructure, but the novel PZT composite material improves these properties by including poly methyl methacrylate. A well-defined periodical grating was formed from the novel PZT composite material **Fig. 4.2**. Average grating period of 40 μm with an average depth of 380 nm and a rather smooth surface with the roughness of $R_q = 129.8$ nm.

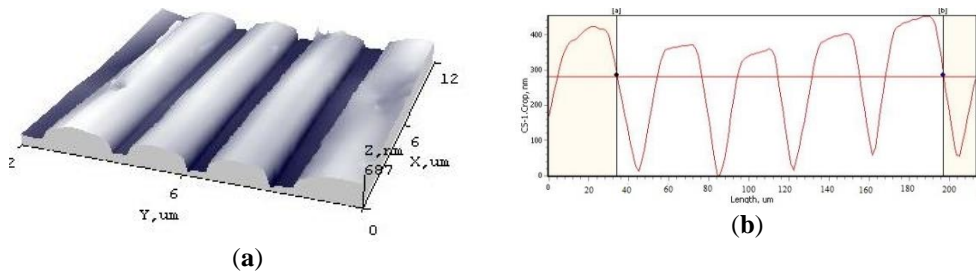
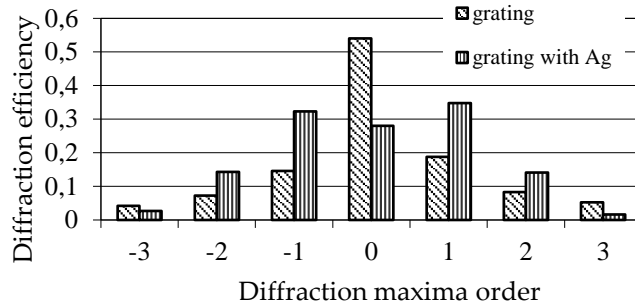


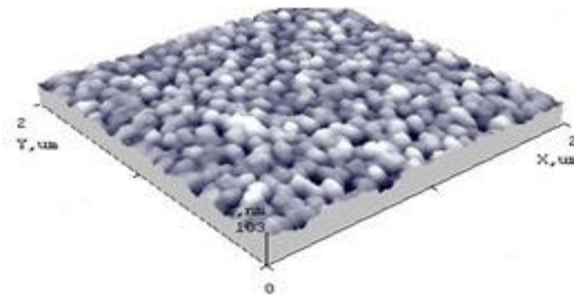
Fig. 4.2 AFM view of 40 microns imprinted microstructure on a PZT composite material (a) 3D imprinted view; (b) cross section of imprinted structure

To use such a sensing platform for biomaterial investigation it is advisable to cover the surface with silver nanoparticles. A silver coating helps to avoid direct contact of the PZT coating with the analyte. Moreover, surface plasmon resonance ensures the optical signal (absorption) and nanoparticles are used as biological marks for quantitative detection of bio molecules in an analyte. Besides, a combination of piezoelectric PZT composite material and SPR properties in one element is a very effective way to expand the working range of the element. Measurements were taken to prove the designed sensing platform with Ag nanoparticles **Fig.4.3**.

The surface view of grating with silver nanoparticles performed with AFM showed that the size of Ag was ~ 17 nm in diameter **Fig. 4.3b**. A laser diffractometer was used to measure diffraction efficiency **Fig. 4.3a**. A helium-neon red light laser was directed at the designed element with an embossed grating with and without Ag nanoparticles. The zero-order diffraction energy of the element without Ag nanoparticles was about 54% and decreased on its first orders to around 17%. Basically, it was concentrated on its zero order. However, diffracted energy of the element with silver nanoparticle coating reaches only 28% on its zero order, but increases to 33% in its first orders, and reaches up to 15% in second orders, while the element without Ag nanoparticles shows a result of order up to 8%. The most sought after parameter is the strength diffraction efficiency in first orders. Higher diffraction efficiency of these maxima is highly desirable in various applications. In ideal conditions, an element would have symmetrical diffraction maxima in negative and positive orders. Diffraction efficiency with Ag at -1 order is 32% and at 1 order is 34%; the maxima improve the optical response of a novel sensing element. Piezoelectric material with imprinted periodic microstructure has a unique property to change its optical parameters considering the deformation of the piezoelectric layer caused by electrical signal.



a)



b)

Fig.4.3 (a) Diffraction efficiency measurement results, (b) AFM view of a grating top coated with Ag nanoparticles

A future perspective allows to create a specific micro sensor with controllable mechanical and optical parameters which could ensure higher functionality of MEMS. The designed cantilever-type piezoelectric platform can be integrated in MEMS for the analysis of functional data as physiological effects of an analyte, type and concentration of molecules, etc. For example, blood cells hematopoiesis analysis could be performed by applying a novel piezoelectric platform with the SPR effect **Fig. 4.4**. A blood stem cell and the stages of its differentiation are presented at the top. In peripheral blood flow we can find final stage blood cells which are very well known for medical science, such as erythrocytes, platelets and lymphocytes. Normally blood completely renews in the human body in 100 days. When particularly differentiated or not differentiated cells, such as monoblast, myeloblast, lymphoblast are detected in the blood, a pathology is stated. The main task is to detect the not differentiated cells in blood in an early stage before they lead to a disease.

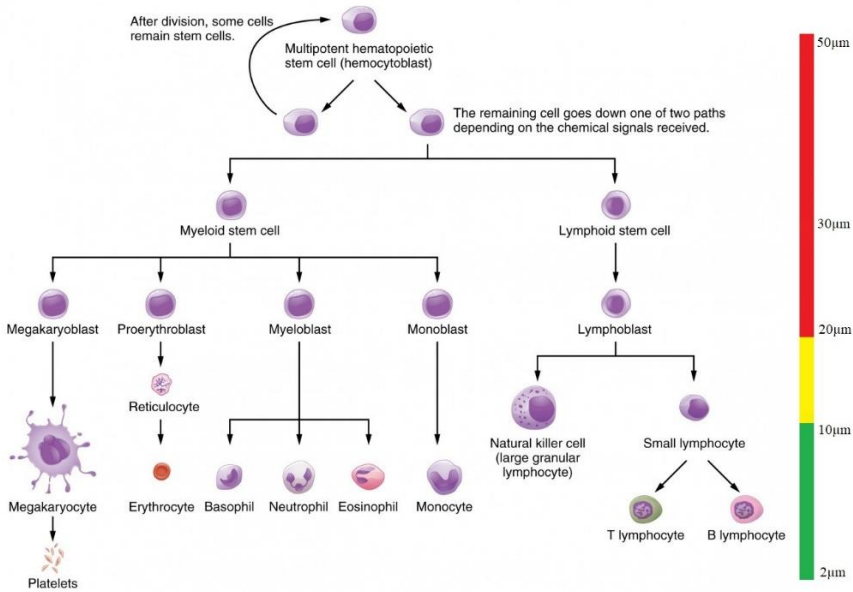


Fig. 4.4 Blood cells hematopoiesis evolution scheme (Calvi, Link, 2015)

PZT composite material allows to create a simple design sensor, when PZT composite material periodic microstructure with Ag coating is placed in a flow tube **Fig. 4.5**. Periodical grating with a period of 40 μm attracts not differentiated blasts with the size of about 20 μm , while differentiated blasts in smaller size easily flow through the tube. The SPR signal is reflected light intensity measured with a light detector. When the SPR effect appears, evident intensity of reflected light is detected. The interaction of blood particles is analyzed and the SPR signal is detected when blood flows through the tube and interacts with the surface of the sensor. When analyzing most biologically active materials, one interactive material is covalently attracted to the surface of the sensor **Fig.4.5**. A laser light is pointed at surface of the sensor and an uninterrupted SPR signal is detected. The signal changes are registered in a graph which is called a sensogram **Fig.4.6**. Using a sensogram data concentration of analyst can be described.

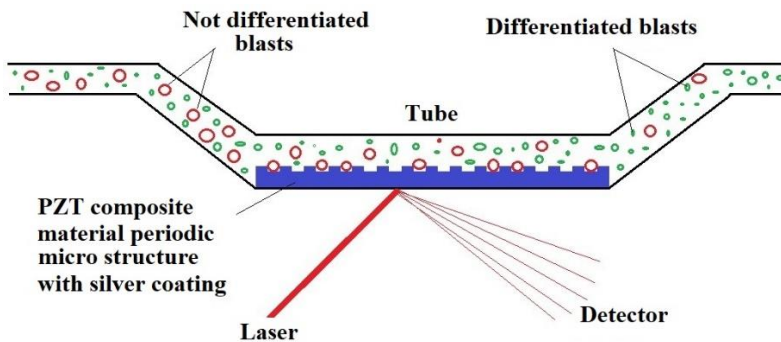


Fig. 4.5 Sensor principle scheme

After measurement, the regeneration process is applied, which requires an electric impulse to be applied to the sensor, makes the grating period change and releases attracted blasts. This option allows to prepare the sensor for further analyses in just a few seconds. Since the sensor is micro-sized only a drop of blood is required for analysis. A simple and low-cost sensor production allows to perform periodical analysis even at home.

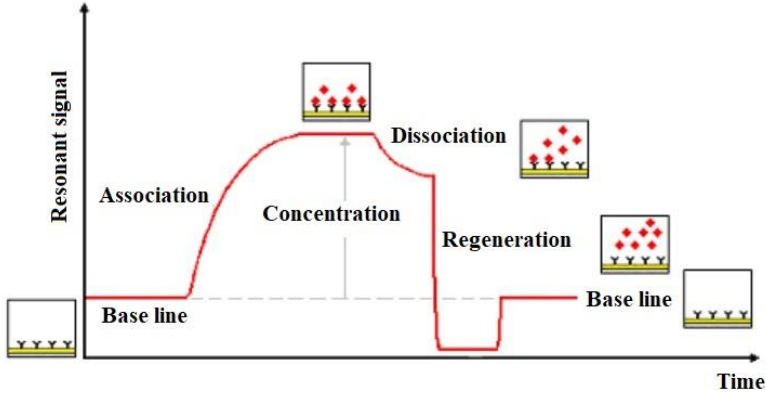


Fig.4.6 A typical SPR sensogram

Novel composite material provides new solutions for developing various sensing platforms including SPR sensors for biomedical analysis and monitoring. Also, it is a great base for further SPR sensing platform investigation and development.

4.2 Cantilever-type viscometric sensor

A micro-cantilever was designed with a novel PZT composite piezoelectric material based on PZT powder mixed with polyvinyl butyral and electrical contacts attached on two sides of the cantilever **Fig. 4.7**. For numerical analysis, PZT composite material with 80% of PZT concentration was selected. This PZT composite material has lower stiffness than PZT ceramics and ensures higher sensitivity at lower resonant frequency. It was screen-printed using a 140/34 mesh screen and poled using an electrical field of 5 kV. Moreover, to improve the features of electro-optic functionality a microstructure can be embedded within the periodical grating.

The principle design of the sensing element for glucose detection is schematically presented in **Fig. 4.7**. The structure consists of an aluminum beam as a base and PZT composite material at the end covered by Al electric contacts. It is placed in liquid and due to the voltage applied to the designed platform contacts, the PZT composite material excites the end of cantilever due to its piezoelectric properties. If the glucose concentration in liquid changes, feedback in the form of frequency shift of the micro-cantilever response is obtained. Analytical, numerical and experimental investigations have to be performed for effective usage of such type of sensing platform. Analytical equation of motion and finite element analysis are presented in next section.

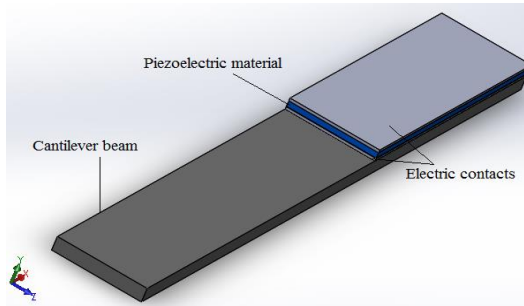


Fig. 4.7 Cantilever beam design with electrical elements

A computer-automated analysis of complex structural models is particularly suitable mathematical modelling as a method of structural analysis. The cantilever-type platform was analyzed where one of the ends is fixed and the other is free to oscillate under the effect of force. Such a piezoelectric platform with all functional layers can be represented as single two-dimensional finite element beam element in horizontal orientation with concentrated mass on the free end as presented in **Fig.4.8**. PZT composite material is presented as a panel of mass m and length a , attached to an elastic beam which deviates by d_y from the center of mass along y axis and deviates by angle θ in plane $x y$ under the piezoelectric effect.

As a base element of the sensor, elastic metal console was chosen. Under the effect of transversal loads bending, axial deformations and twisting can be traced. Bending deformation characteristics are rotational and transversal displacements. Therefore, rotation and transversal displacement can be an expression of beam element mobility at a node. Using the same marking reference system for each node a stiffness matrix is formed:

Counter-clockwise direction is assumed to be positive for Moments and rotations.

Positive direction of Y axis is assumed as positive for Displacements and Forces.

4.2.1 Phenomenological mathematical model for cantilever

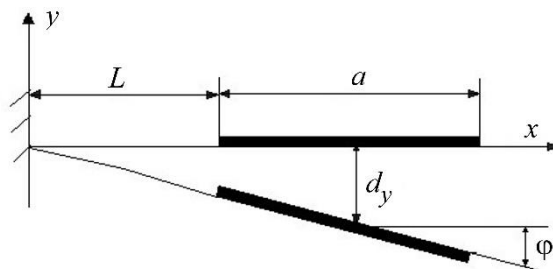


Fig.4.8 A schematic representation of the cantilever with piezoelectric material and its essential geometrical parameters

To determine the vibration frequency, mass and stiffness matrices expressions have to be expressed. Considering that the plate has 2 depth of field (DOF), its

displacement vector is $u = [d_y, \varphi]^T$, where L is length of the beam not covered by the piezoelectric material plate.

The mass of the cantilever in presented platform is insignificant comparing to piezoelectric panel mass m , therefore it is modelled as the ideal elastic element. Beams elasticity force is:

$$F_{el} = \left[12 \left[d_y - \frac{1}{2} a \varphi \right] - 6 \varphi \right] k, \quad (4.1)$$

and torque

$$T_{el} = \left[-6 \left[d_y - \frac{1}{2} a \varphi \right] + 4 \varphi \right] k, \quad (4.2)$$

$\left(d_y - \frac{1}{2} a \varphi \right)$ which is the displacement of the free end of the cantilever. Spring vector of Elasticity force is:

$$R_{el} = [F_{el}, T_{el}]^T, \quad (4.3)$$

Using beam theory, the shear force of the beam is calculated as

$$\hat{F}_{el} = -EI \frac{\partial^3 v}{\partial x^3} = \frac{EI}{L^3} \left[12 d_y - 6L \left(1 + \frac{a}{L} \right) \varphi \right], \quad (4.4)$$

Similarly, the bending moment is obtained using

$$\hat{T}_{el} = EI \frac{d^2 v}{dx^2} = \frac{EI}{L^3} \left[-6L d_y + \left(4 + \frac{3a}{L} \right) L^2 \varphi \right], \quad (4.5)$$

v is transverse displacement function:

$$v = \left[-\frac{2}{L^3} d_y + \frac{1}{L^2} \left(1 + \frac{a}{L} \right) \varphi \right] x^3 + \left[\frac{3}{L^2} d_y - \frac{1}{L^2} \left(1 + \frac{3a}{2L} \right) \varphi \right] x^2 \quad (4.6)$$

Writing the above in matrix form we get,

$$\begin{bmatrix} \hat{F}_{el} \\ \hat{T}_{el} \end{bmatrix} = \frac{EI}{L^3} \begin{bmatrix} 12 & -6L \left(1 + \frac{a}{L} \right) \\ -6L & \left(4 + \frac{3a}{L} \right) L^2 \end{bmatrix} \begin{bmatrix} d_y \\ \varphi \end{bmatrix}, \quad (4.7)$$

$$K = k \begin{bmatrix} 12 & -6L \left(1 + \frac{a}{L} \right) \\ -6L & \left(4 + \frac{3a}{L} \right) L^2 \end{bmatrix} \text{ is the stiffness matrix of the beam and } k = \frac{EI}{L^3}.$$

Here E is Young's modulus of the beam material. We know that $R_{elect} = Ku$, where K is the stiffness matrix of the cantilever. Here F_f and torque M_f are the forces acting on the piezoelectric panel due to fluid-panel interaction and can be obtained from the solution of adequately formulated problem in fluid dynamics. Due to viscous and inertia properties of the fluid, they can be considered as dependent on motion parameters (velocity and acceleration) of the panel. Applying vector notation, the fluid force can be expressed as follows:

$$R_F = [F_f, T_f]^T. \quad (4.8)$$

Or the force is

$$R_F = T_f \ddot{u} + D_f \dot{u}, \quad (4.9)$$

where M_f and D_f is the mass and fluid damping matrices accordingly. Then the oscillatory motion of the plate can be expressed:

$$\begin{aligned} M \ddot{d}_y + F_{el} + F_f &= 0 \\ \frac{1}{2} M a^2 \ddot{\varphi} + T_{el} &= F_{el} \left(\frac{1}{2} a \right) - T_f - T_{elect} \end{aligned} \quad (4.10)$$

According to Newton's second law, the equation of motion of the damped system damping is given as

$$M \ddot{u} + C \dot{u} + K u = F. \quad (4.11)$$

For this case, the acceleration is in direction and the damping, as well as the spring force is zero. In matrix form, it is given as:

$$(M + M_f) \ddot{u} + D_f \dot{u} + K u = R_{elect}, \quad (4.12)$$

where the mass matrix, stiffness matrix, and electric force vector are as follows:

$$M = \begin{bmatrix} m & 0 \\ 0 & \frac{1}{12} m (a/L)^2 \end{bmatrix}, \quad (4.13)$$

$$K = k \begin{bmatrix} 12 & -6L \left(1 + \frac{a}{L} \right) \\ -6L \left(1 + \frac{a}{L} \right) & 4L^2 + 6aL + 27a^2 \end{bmatrix}, \quad (4.14)$$

$$R_{elect} = \begin{bmatrix} 0 \\ \frac{T_{elect}}{L} \end{bmatrix}. \quad (4.15)$$

4.2.2 Numerical analysis

In order to analyze the modes of vibration, micro-cantilever finite element method (FEM) model was build **Fig. 4.11**. The designed model also analyzed transient processes **Fig.4.9** and **Fig.4.10**. Comsol Multiphysics software has been used to model a vibrating micro-cantilever. To improve the design and manufacture of micro-cantilever FEM results of calculation are useful and mesh analysis model and simulation parameters are presented in **Fig.4.11**.

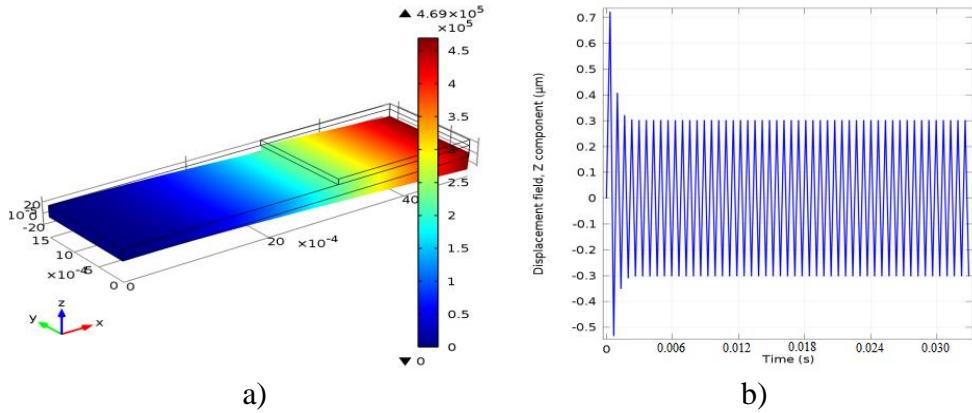


Fig. 4.9 a) A transient analysis model without damping, b) a graph for transient analysis model without damping

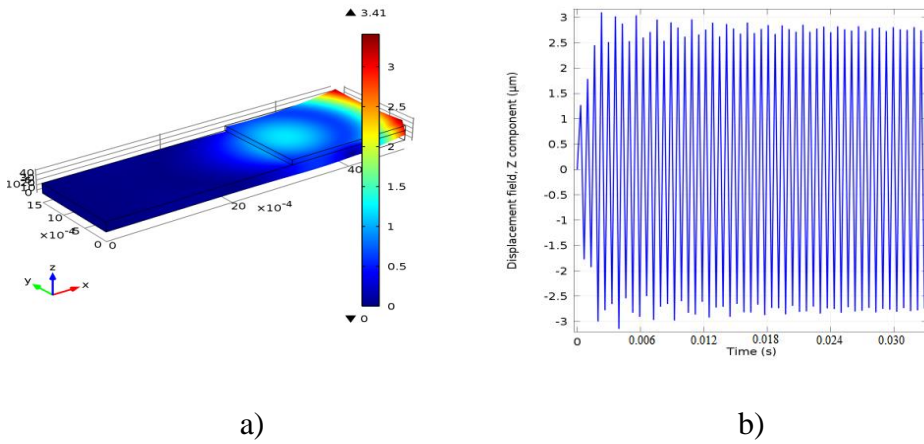


Fig.4.10 a) A transient analysis model with damping, b) a graph for Transient analysis model with damping

The main geometric parameters of a viscometric micro-sensor and optimal regimes of the cantilever were established with a Comsol Multiphysics simulation. The analyzed dimensions of the cantilever were: length – 5mm, width – 1.5 mm, thickness 0.075 mm and the dimensions of the piezoelectric material were: length – 2mm, width 1.5 mm, thickness – 0.025 mm. The determined theoretical frequency of investigated cantilever platform was 1.6 kHz.

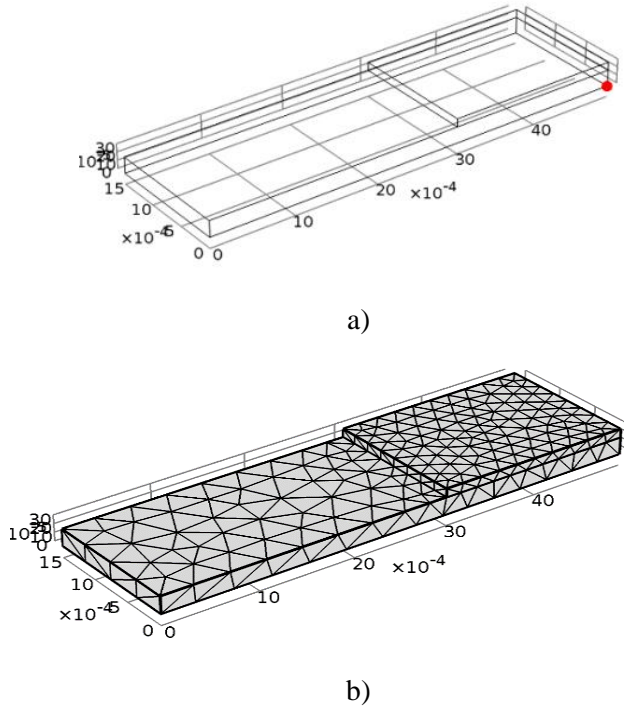


Fig.4.11 (a) Transient analysis point location, (b) Meshed analysis model

4.2.3 Experimental application

For this experimental setup one of the ends of cantilever was fixed in a bracket and the other end, with screen-printed PZT composite material panel with electrical contacts on both sides, is suspended to the gravity. Electrical contacts are connected to a PicoScope oscilloscope measurement system and data from the oscilloscope is transferred to a computer **Fig.4.12** where it is converted into a graphic form (variation of amplitude in time are presented in a graphic).

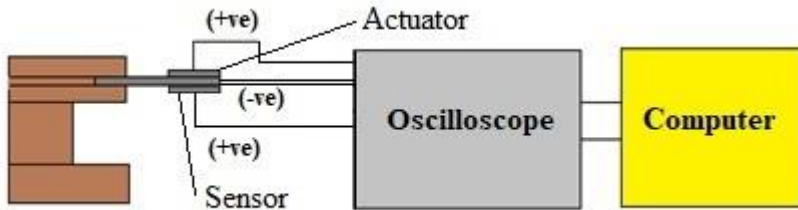


Fig. 4.12 Experimental setup of cantilever vibration analysis

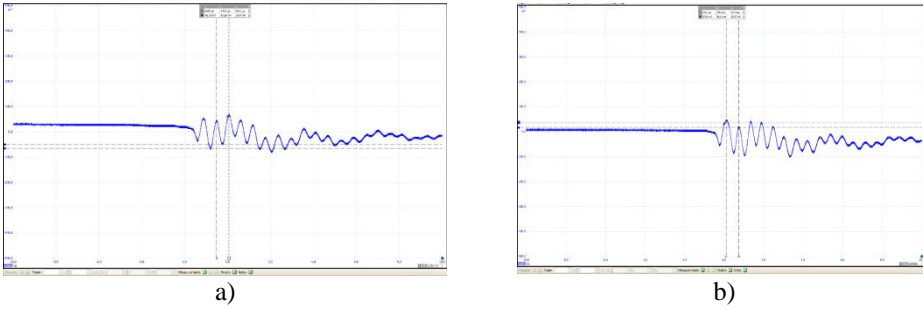


Fig.4.13 Bump-test results: a-test 1; b- test 2

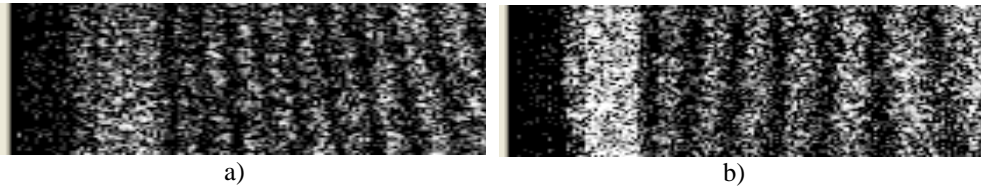


Fig.4.14 A holographic interferogram of vibrating cantilever-type platform in liquid: a-liquid without glucose; b-liquid with glucose

For experimental setup frequency interval was from 1.5 kHz to 1.7 kHz detected with a bump test and was comparatively equal to the theoretical resonant frequency value. To verify the created finite element method, model a holographic interferometry visualization of the vibrating cantilever platform was performed. Holographic interferograms of a working viscometric sensor in two different liquids, without glucose and with glucose are presented in **Fig.4.14**. In both cases, the cantilever platform was excited at 1.6 kHz and the amplitude of vibrating platform in liquid with glucose was about 30% smaller in comparison to the vibrating platform in liquid without glucose. These experiments allow to create a non-invasive sensor with PZT composite material for glucose level detection in various physiological liquids.

4.3 Conclusion

The novelty is in the designed material PZT; i.e., the obtained material is not classic PZT, it has wider application areas. The designed cantilever-type sensing platform was covered with silver nanoparticles. Experimental results showed that it did not affect any piezoelectric properties, but increased the usage not only in MEMS fabrication, but it can also be used for MOEMS. The designed micro sensor is suitable for a system with indicated resonant frequency by changing the active layer dimensions or geometrical parameters of the sensing element. The aim of this research was to create a micro-sensor with controllable parameters on the micrometric level which ensures higher functionality of MEMS. The creation of this novel universal functional element allows to integrate it in multifarious micro-electro-mechanical-systems. This material is suitable for various systems and can be used: in energy harvesting, for electric filters, high stability electric oscillation sources (as generators), sensors for testing proteins, viruses, chemical species, etc.

GENERAL CONCLUSION

1. Scientific literature presents many smart materials and nano composite materials with various exclusive optic, mechanic, electric and other options. However, there is not enough information about elastic ceramics with the piezoelectric effect, especially on the micro-metric level. Piezoelectric materials can be used in a wide range of sensing by adapting them to specific conditions. Piezoelectric ceramic is a very promising material, but it has some disadvantages, such as cracking, complicated production on micro-level, longevity. It is expedient to create novel piezoelectric composite material with piezoelectric effect on the micro-metric level and to solve the problems of cracking, complicated production and longevity.
2. PZT 52/48 ceramic and PVB polymer were chosen to create novel composite material. PZT ceramic was synthesized in a laboratory and its authenticity was confirmed with X-ray diffraction analysis. Therefore, the synthesized PZT nanoparticles were mixed with PVB under specific conditions in various proportions of PZT with PVB and screen-printed on a substrate. The screen-printing technique allows for easy application and makes the production inexpensive. Results showed that 80% of PZT concentration lead to improved surface morphology, mechanical and piezoelectric properties. The properties of the new material allow to imprint a periodical microstructure with a symmetric replicated shape, the period of 2 μm and depth average to 350 nm. Polymer analysis in composite material showed that there was no chemical reaction in composite material which indicates that PVB did not affect any chemical properties of the PZT.
3. PZT composite material with 80% concentration of PZT nano particles achieved the highest results and generated up to 80 μV of electrical potential. Different thicknesses of the novel material were achieved by using various screens for the screen-printing technique. Morphology analysis showed the layer of 25 μm thickness has an even and solid surface. The polarization process allowed to generate electrical potential of up to 3.42 mV. 80% PZT concentration, 25 μm layer thickness and polarization improves the electrical potential of the PZT composite material and makes it 42 times more effective comparing to the results received at the very beginning of novel PZT composite material investigation.
4. Perspective application of novel PZT composite material in biomedical application reveals that the material is suitable for creating micro-opto-electro-mechanical systems, micro sensing systems, micro actuators or at least improve and miniaturize the existing systems. The periodical micro structure imprinted in to PZT composite material and covered with silver nanoparticles can be used to create a micro-opto-electro-mechanical sensor with surface plasmon resonant effect where the efficiency can be controlled using the piezoelectric properties of materials. Also, this novel material demonstrates a unique possibility to sense and generate material in one system. The cantilever platform was excited at 1.6 kHz and the amplitude of vibrating platform in liquid with glucose decreased by about 30% comparing to vibrating the platform in liquid without glucose.

BIBLIOGRAPHY

Publications in journals listed in the ISI Web of Science database with citation index

1. Janušas, Giedrius; Ponelytė, Sigita; Brunius, Alfredas; Guobienė, Asta; Prosyčevas, Igoris; Vilkauskas, Andrius; Palevičius, Arvydas. Periodical microstructures based on novel piezoelectric material for biomedical applications // *Sensors*. Basel: MDPI AG. ISSN 1424-8220. 2015, vol. 15 (12), p. 31699-31708. [Academic Search Research & Development; Academic Search Complete; Academic Search Elite; Directory of Open Access Journals; Academic Search Alumni Edition; MEDLINE; Science Citation Index Expanded (Web of Science); Academic Search Premier] [Cite index: 2,033 (2015, In Cites JCR SCIE)] [Cite Score: 2,21, SNIP: 1,643, SJR: 0,647 (2015, Scopus JM)].
2. Janušas, Giedrius; Ponelytė, Sigita; Brunius, Alfredas; Guobienė, Asta; Vilkauskas, Andrius; Palevičius, Arvydas. Influence of PZT coating thickness and electrical pole alignment on micro-resonator properties // *Sensors*. Basel: MDPI AG. ISSN 1424-8220. eISSN 1424-8220. 2016, vol. 16, (11), article 1893, p. 1-9. [Academic Search Complete; Scopus; MEDLINE; Science Citation Index Expanded (Web of Science)] [Cite index: 2,677 (2016, In Cites JCR SCIE)] [Cite Score: 2,78, SNIP: 1,614, SJR: 0,623 (2016, Scopus JM)].
3. Brunius, Alfredas; Rayappan, Christopher; Palevičius, Arvydas; Janušas, Giedrius; Pilkauskas, Kęstutis; Janušas, Tomas. Design and analysis of viscometric sensor with embedded microstructure for biomedical applications // *Mechanika*. Kaunas: KTU. ISSN 1392-1207. eISSN 2029-6983. 2018, Vol. 24 (1), p. 115-120. [Academic Search Complete; Scopus; INSPEC; Science Citation Index Expanded (Web of Science)] [Cite index: 0,529 (2017, In Cites JCR SCIE)] [Cite Score: 0,51, SNIP: 0,594, SJR: 0,186 (2017, Scopus JM)].
4. Janušas, Giedrius; Palevičius, Arvydas; Čekas, Elingas; Brunius, Alfredas. Development and analysis of electro-optical microresonator with low range natural frequency // *Microsystem Technologies*. Berlin: Springer. ISSN 0946-7076. eISSN 1432-1858. 2017, Vol. 23, iss. 10, p. 4487-4493. DOI: 10.1007/s00542-016-3233-4. [Scopus; SpringerLink; Science Citation Index Expanded (Web of Science)] [Cite. index: 1,581 (2017, In Cites JCR SCIE)] [Cite Score: 1,34, SNIP: 0,803, SJR: 0,346 (2017, Scopus JM)].

Conference articles and proceedings

1. Brunius, Alfredas; Palevičius, Arvydas; Janušas, Giedrius; Guobienė, Asta; Prosyčevas, Igoris. Novel piezoelectric effect based material for periodical microstructure formation // *Mechanika 2015: proceedings of the 20th international scientific conference*, 23, 24 April 2015, Kaunas University of Technology, Lithuania / Kaunas University of Technology, Lithuanian Academy of Science, IFTOMM National Committee of Lithuania, Baltic Association of Mechanical Engineering. Kaunas: ISSN 1822-2951. 2015, p. 67-71.
2. Janušas, Giedrius; Palevičius, Arvydas; Čekas, Elingas; Brunius, Alfredas; Baucė, Jokūbas. Development and analysis of new type microresonator with electro-optic

feedback // Proceedings of SPIE: Optical modelling and design IV: Brussels, Belgium, April 03, 2016. Bellingham, WA: SPIE. ISSN 0277-786X. 2016, vol. 9889, article 98891N, p. 1-8.

3. Janušas, Giedrius; Guobienė, Asta; Palevičius, Arvydas; Brunius, Alfredas; Čekas, Elingas; Baltrušaitis, Valentinas; Šakalys, Rokas. Influence of binding material of PZT coating on microresonator's electrical and mechanical properties // Proceedings of SPIE: Smart sensors, actuators and MEMS VIII. Bellingham, WA: SPIE. ISSN 0277-786X. 2017, Vol. 10246, Article 102461E, p. 1-7.

REFERENCES

1. Akyilmaz E., Yorganci E., Asav E. Do copper ions activate tyrosinase enzyme? A biosensor model for the solution. *Bio electrochemistry*. (2010); 78:155–160.
2. Alply S., Mantese J., Troilier- McKinstry S., Zhang Q., Whatmore R., “Next generation electrocaloric and pyroelectric materials for solid-state electrothermal energy interconversion” *MRS Bulletin*, Vol. 39(12), p. 1099-1111, (2014)
3. Ando T. High-speed atomic force microscopy and its future prospects. *Biophysical Reviews*. (2018) Vol. 10(2) p. 285-292.
4. Anjanappa M., Datta K., and Song T. “Introduction to Sensors and Actuators” *Mechatronic systems, sensors and actuators*, Section 3, p. 17-1 (2007).
5. Auricchio F., Sacco E., A one-dimensional model for super-elastic shape-memory alloys with different elastic properties between austenite and martensite, *International Journal of Non-Linear Mechanics*, 32 (1997), p. 1101-1114.
6. Backer D., Rakowski M., Poghossiana A., Biselli M., Wagner P., Schoning M.J. Chip-based ampere-metric enzyme sensor system for monitoring of bioprocesses by flow-injection analysis. *Journal of Biotechnology* (2013) Vol. 163, p. 371–376.
7. Bader S.D., Erskine J.L.,” Magneto-Optical Effects in Ultrathin Magnetic Structures”. *Springer* (1994)
8. Becker K., Beer C., Freitag M., Kuck U. Genome-wide identification of target genes of a mating-type a-domain transcription factor reveals functions beyond sexual development. *Molecular Microbiology*. (2015) Vol. 96(5), p. 1002–1022).
9. Bedford, E.E.; Spadavecchia, J.; Pradier, C.M.; Gu, F.X. Surface plasmon resonance biosensors incorporating gold nanoparticles. *Macromolecular Bioscience*, Vol. 12, p, 724–739. (2012)
10. Berens C., Suess B. Riboswitch engineering – making the all-important second and third steps. *Current Opinion Biotechnology*. (2015) Vol. 31, p. 10–15.
11. Bermejo C., Haerizadeh F., Takanaga H., Chermak D., Frommer W.B. Optical sensors for measuring dynamic changes of cytosolic metabolite levels in yeast. *Journal of Nature Protocols*. (2011) Vol. 6, p. 1806–1817).
12. Bhushan, B. Sundararajan S., Zorman, X. Li, C.A., Mehregany, M., Micro/nanotribological studies of single-crystal silicon and polysilicon and Si C films for use in MEMS devices, *Tribology Issues and Opportunities in MEMS*, Kluwer Academic Publishers, Dordrecht, The Netherlands (1998), pp. 407-430
13. Bhushan, B., Nanotribology and nano-mechanics of MEMS/NEMS and BIOMEMS/BIONEMS materials and devices. *Microelectronic engineering Vol 84* (3), (2007), p. 387-412.
14. Boggs, R. N. How Memory Metals Shape Product Designs, *Des. News*, vol. 49, p. 72–74, June 1993.
15. Bogue, R (2012) "Smart materials: a review of recent developments", *Assembly Automation*, Vol. 32 Issue: 1, pp.3-7.
16. Bossis G., Laci S., Meunier A., Volkova O., “Magneto-rheological fluids” *Journal of Magnetism and Magnetic Materials* Volume 252, (2002), p. 224-228.
17. Bowen C., Taylor J., LeBoulbar E., Zabek D., Chauhan A., Vaish R., Pyroelectric Materials and Devices for Energy Harvesting Applications. *Energy Environ.* (2014).
18. Bunaciu A. A., Udriștioiu E. G., Aboul-Enein H. Y., “X-Ray Diffraction: Instrumentation and Applications” *Critical Reviews in Analytical Chemistry*, Vol. 45 (4), p. 289-299, (2015), PMID: 25831472
19. Buschow K.H.J., Boer F.R. (2003) Magnetostrictive Materials. In: *Physics of Magnetism and Magnetic Materials*. Springer, Boston, MA

20. Calvi L.M., Link D.C., The hematopoietic stem cell niche in homeostasis and disease. *Blood*, Vol. 126(22), p. 2443-2451, (2015).
21. Chen Y.W., Liu M., Kaneko T., McIntyre P.C., Atomic layer deposited hafnium oxide gate dielectrics for charge-based biosensors. *Electrochemical and Solid-State Letters* (2010) Vol. 13 p. 29–32.
22. Cote G.L.; Lec R.M.; Pishko M.V. “Emerging biomedical sensing technologies and their applications” *Sensors Journal* Vol. 3(3), p. 251 - 266 (2003), ISSN: 1558-1748
23. Duan W.H.; Wang Q.; Quek S.T. Applications of Piezoelectric Materials in Structural Health Monitoring and Repair: Selected Research Examples. *Materials* (2010), Vol. 3, p. 5169-5194.
24. Dufrene, Y. F., Ando T., Garcia R., Alsteens D., Martinez-Martin D., Engel A., Gerber C., Muller D. J., Imaging modes of atomic force microscopy for application in molecular and cell biology. *Nature nanotechnology* Vol. 12 (2017), p 295-307.
25. Dziąbowska Karolina, Czaczyk Elżbieta and Nidzworski Dawid “Application of Electrochemical Methods in Biosensing Technologies”, *Biosensing Technologies for the Detection of Pathogens* p. 151-171, (2017).
26. Edelstein R., The BARC biosensor applied to the detection of biological warfare agents. *Biosensors and Bioelectronics* Vol. 14, (2000) p. 805-813.
27. Fukada, E. History and recent progress in piezoelectric polymers. *IEEE transactions on ultrasonics, ferroelectrics, and frequency control*. vol. 47(6). p. 1277-1290, (2000).
28. Furlong C., Pryputniewicz R.J., “Optoelectronic characterization of shape and deformation of MEMS accelerometers used in transportation applications” *Optical engineering* Vol. 42(5), (2003).
29. Gabbert U. and H. S. Tzou (eds.), *Smart Structures and Structronic Systems, IUTAM Symposium on Smart Structures and Structronic Systems, London, (2001)*.
30. Galassi C., Roncari E., Capiani C., Costa A. (2000) Influence of Processing Parameters on the Properties of PZT Materials. *Piezoelectric Materials: Advances in Science, Technology and Applications. NATO Science Series (Series 3. High Technology), vol 76. Springer, Dordrecht, ISBN978-0-7923-6213-5*.
31. German N., Ramanaviciene A., Voronovic J., Ramanavicius A. Glucose biosensor based on graphite electrodes modified with glucose oxidase and colloidal gold nanoparticles. *Mikrochim Acta*. (2010) Vol. 168, p. 221–229.
32. Ghasemi-Varnamkhasti M., Rodriguez-Mendez M.L., Mohtasebi S.S. Monitoring the aging of beers using a bioelectronic tongue. *Food Control*. (2012) Vol. 25 p. 216–224.
33. Goldsmith, C. S., Miller, S. E. Modern uses of electron microscopy for detection of viruses. *Clinical Microbiology Reviews* (2009). Vol. 22, p. 552–563.
34. Goldstein J., Newbury D.E., Joy D.C., Lyman C.E., Echlin P., Lifshin E., Sawyer L., Michael J.R., *Scanning Electron Microscopy and X-Ray Microanalysis, Springer* (2003) Vol. 3.
35. Guegan Q. and Foulc J., "Dielectric response of electrorheological fluids: Application to the electrical characterization of particles suspended in liquid medium," *IEEE International Conference on Dielectric Liquids*, (2008), p. 1-4. ICDL.2008.4622494
36. Guo Y., Langlois J. M., Goddard W. A., *Electronic Structure and Valence-Bond, Band Structure of Cuprate Superconducting Materials* Vol. 239 (4842), p. 896-899, (1988), ISSN 0036-8075.

37. Haertling G. H., *Ferroelectric Ceramics: History and Technology*, *Centennial Symposium on Perspectives on Ceramic and Glass Science and Technology*, Paper No. SXVIII-007-98, (1998).
38. Haertling G. H., PLZT electrooptic materials and applications—a review, *Ferroelectrics* vol 75 (1) p. 25-55, (1987).
39. Hinze S., Bibliographical cartography of an emerging interdisciplinary discipline: The case of bioelectronics. *Scientometrics* Vol. 29: (1994) p. 353-376.
40. Hnatushenko, V. Vasyliiev, V. Remote sensing image fusion using ICA and optimized wavelet transform. *ISPRS - International Archives of the Photogrammetry, Remote Sensing and Spatial Information Sciences*. (2016). XLI-B7. 653-659. 10.5194
41. Hodgson, D. E. *Proceedings of Engineering Aspects of Shape Memory Alloys*, Lansing, MI (Butterworth Scientific, 1988).
42. Hong W., Zhao X., Suo, Z., „ Large deformation and electrochemistry of polyelectrolyte gels “, *Journal of the Mechanics and Physics of Solids*, V. 58 (4), (2010), p. 558-577, ISSN 0022-5096.
43. Horvath Eszter, Torok Adam, Ficzer Peter, Zador Istvan, Racz Pal, “Optimization of Computer-aided Screen-Printing Design” *Acta Polytechnica Hungarica*, Vol. 11(8), p. 29-44, (2014).
44. Hott Roland, Kleiner Reinhold, Wolf Thomas, Zwicknagl Gertrud, “Superconducting materials –a topical overview” *Springer*, (2004).
45. Hyo Seung Han., Junwoo Park., Tien Dat Nguyen "A highly sensitive dual mode tactile and proximity sensor using Carbon Micro coils for robotic applications," *IEEE International Conference on Robotics and Automation (ICRA)*, Stockholm, (2016), p. 97-102. ICRA.2016.7487121
46. Ibraheem A., Campbell RE (2010) Designs and applications of fluorescent protein-based biosensors. *Current Opinion in Chemical Biology* 14: 30-36.
47. Jianqiao He, Xian Z. Chong Z., Fuqiang H., Synthesis, structure, magnetic and optoelectric properties of layered Na M 0.5 Sn 0.5 S 2 (M= Mn, Fe). *Journal of Alloys and Compounds*. (2018).
48. Jones A.M., Grossmann G., Danielson J.A.H. In vivo biochemistry: applications for small molecule biosensors in plant biology. *Journal of Current Opinion about Plant Biology*. (2013) Vol. 16, p. 389–395.
49. Khan W.A., Raouf A., Cheng K., Augmented Reality for Sensors, Transducers and Actuators. *Virtual Manufacturing*. *Springer*, p 97-126. (2011).
50. Kikuchi Y., "Magnetostrictive materials and applications," in *IEEE Transactions on Magnetism*, vol. 4, no. 2, p. 107-117, (1968).
51. Kimel A.V. Kirilyuk A. Rasing T., “Femtosecond opto-magnetism: ultrafast laser manipulation of magnetic materials”, *Laser and Photon*, No. 3, 275–287 (2007).
52. Kong, D. and Xiao, X. “High Cycle-life Shape Memory Polymer at High Temperature” *Nature*, Scientific Reports Vol. 6, Article number 33610 (2016)
53. Kwon H. J., Osada Y., Gong J. P., “Polyelectrolyte Gels-Fundamentals and Applications” *Polymer Journal*, Vol. 38, No. 12, p. 1211–1219 (2006)
54. Lammerink, T. S. J., Tas, N. R., Elwenspoek, M. C., & Fluitman, J. H. J. (1993). Micro-liquid flow sensor. *Sensors and actuators. A: Physical*, Vol. 37, p. 45-50.
55. Larbalestier D., Gurevich A. D., Feldmann M., Polyanskii A., High- T_c superconducting materials for electric power applications, *Nature* vol. 414, p. 368–377, (2001).
56. Leatherbarrow R.J., Edwards P.R., Analysis of molecular recognition using optical biosensors. *Current Opinion in Chemical Biology*, (1999) vol. 3 p. 544–547.

57. Lee M., Zine N., Baraket A., A novel biosensor based on hafnium oxide: application for early stage detection of human interleukin-10. *Sensors and Actuators B*. (2012) Vol. 175, p. 201–207.
58. Li X., Bhushan B., Takashima K., Baek C., Kim Y., Mechanical characterization of micro/nanoscale structures for MEMS/NEMS applications using nanoindentation techniques. *Ultramicroscopy* (2003), P 481–494
59. Li, Y. F. and Chen, X. B. "On the dynamic behavior of a force/torque sensor for robots," in *IEEE Transactions on Instrumentation and Measurement*, vol. 47, no. 1, pp. 304–308, (1998).
60. Lin G., Makarov D., Schmidt O. G., "Magnetic sensing platform technologies for biomedical applications", *Lab Chip*" (2017), Vol. 17 (11), p. 1884–1912
61. Lippincott-Schwartz J., Patterson G.H., Development and use of fluorescent protein markers in living cells. *Science*. (2003) vol. 300 p. 87–91.
62. Lixia Li, Yuzhang Liang, Jianye Guang, Wenli Cui, Xinpu Zhang, Jean-Francois Masson, and Wei Peng, "Dual Kretschmann and Otto configuration fiber surface plasmon resonance biosensor," *Optics Express* 25, 26950–26957 (2017)
63. Losego M. D., Maria J-P., "Reproducibility and ferroelectric fatigue of lead zirconate titanate (PZT) thin films deposited directly on copper via a composite gel architecture" *Journal of the American Ceramic Society* Vol. 93, p 3983–3985, (2010).
64. Lynch Kevin M., Marchuk Nicholas, Elwin Matthew L., "Sensors" *Embedded Computing and Mechatronics with the PIC32 microcontroller*, (2016), Pages 317–340, ISBN 9780124201651
65. Maetani T., Nakamitsu Y., Sakurai J., Nakagawa S., Hata S., "Combinatorial Search of Magnetostrictive Materials for Sensors" *Electrical Engineering in Japan* Vol. 97 (9) (2014), p. 12–19
66. Maiwa H., Piezoelectric Energy Harvesting, Piezoelectric Materials Toshio Ogawa, Intech (2016). P. 130–142.
67. Mantyjarvi, J. Himberg J. and Seppanen, T. "Recognizing human motion with multiple acceleration sensors," *IEEE International Conference on Systems, Man and Cybernetics. E-Systems and e-Man for Cybernetics in Cyberspace* Tucson, AZ, USA, (2001), p. 747–752 vol.2. ICSMC.2001.973004
68. McKinstry S. T., Muralt P., Thin Film Piezoelectrics for MEMS, *Journal of Electroceramics* (2004) Vol. 12, p 7–17. ISSN1385-3449.
69. Mehrotra P., Biosensors and their applications - A review. *Journal of oral biology and craniofacial research*, Vol. 6(2), p. 153–159. (2016).
70. Mishra R., Dominguez R., Bhand S., Munoz R., Marty J., A novel automated flow-based biosensor for the determination of organophosphate pesticides in milk. *Biosens Bioelectron*. (2012) Vol. 32 p. 56–61.
71. Mizutani T., Kondo T., Darmanin S., Tsuda M., Tanaka S., Tobiume M., A novel FRET-based biosensor for the measurement of BCR-ABL activity and its response to drugs in living cells. *Journal of Clinical Cancer Research*. 2010 Vol. 16. P. 3964–3975.
72. Nadarajah A. and Sheldon M. T., Optoelectronic phenomena in gold metal nanostructures due to the inverse Faraday effect, *Optics Express* Vol. 25 (11), p. 12753–12764, (2017)
73. Nathanson, H. C., W. E. Newell, R. A. Wickstrom and J. R. Davis. The resonant gate transistor. *IEEE Transactions on Electron Devices*. 1967, 14(3): p. 117–133.
74. Okumoto S. Quantitative imaging using genetically encoded sensors for small molecules in plants. *The Plant Journal*. (2012) Vol. 70, p. 108–117.

75. Ooi K.G.J., Galatowicz G., Towler H.M.A., Lightman S.L., Calder V.L. Multiplex cytokine detection versus ELISA for aqueous humor: IL-5, IL-10, and IFN profiles in uveitis. *Journal of Investigative ophthalmology and visual science*. (2006) Vol. 47, p. 272–277.
76. Palmer A.E., Design and application of genetically encoded biosensors. *Trends in Biotechnology* Vol. 29, (2011) p. 144-152.
77. Pan, M. J., Rehrig P. W., Kucera J. P., Park E. E., Hackenberger W. S., “Comparison of actuator properties for piezoelectric and electrostrictive materials”, Proceeding SPIE 3992, Smart structures and materials, (2000).
78. Pawlak, A Sensors and Actuators in Mechatronics: Design and Applications (2006) p. 153-168 ISBN 9780849390135
79. Radmacher, M., Tillmann, R. W., Fritz, M., Gaub, H. E., *From molecules to cells: imaging soft samples with the atomic force microscope*. *Science* Vol. 257, (1992) p. 1900–1905.
80. Ragulskis M., Ostasevicius V., Palevicius A. Numerical Investigation of Microstructures Using Principles of Holographic Interferometry. SPIE Proceedings, Vol.4827, (2002), 103-111.
81. Rahalkar, A. and Muthukumar, M., “Diffusion of Polyelectrolytes in Polyelectrolyte Gels”, *Macromolecules* v. 50 (20) p. 158-168, (2017).
82. Rahman A., Rahaman Z., Samsuddoha N., A Review on Cuprate Based Superconducting Materials Including Characteristics and Applications, *American Journal of Physics and Applications*. Vol. 3, No. 2, p. 39-56. (2015)
83. Rea G., Polticelli F., Antonacci A., Structure based design of novel *Chlamydomonas reinhardtii* D1-D2 photosynthetic proteins for herbicide monitoring. *Journal of Protein Science*. (2009) Vol. 18, p. 2139–2151.
84. Rechnitz G.A., Biochemical electrodes uses tissues slice. *Chemical engineering news*. 1978; 56:16–21.
85. Reimer L., Scanning electron microscopy, Springer series in optical sciences, Vol. 2, (1998).
86. Reyes-Vera E., Cristiano M. B. Cordeiro, and Pedro Torres, "Highly sensitive temperature sensor using a Sagnac loop interferometer based on a side-hole photonic crystal fiber filled with metal," *Appl. Opt.*56, p. 156-162 (2017)
87. Rhind A.W. Anjanappa M. Microcontroller based sensor to measure serum column height. *Mechatronics* 9 (1999) p. 329-348.
88. Safari A, Akdogan EK (2008) Piezoelectric and acoustic materials for transducer applications. *Springer, New York*. ISBN978-0-387-76538-9.
89. Scanlan R. M., Malozemoff A. P., and Larbalestier D. C., "Superconducting materials for large scale applications," in *Proceedings of the IEEE*, vol. 92 (10), p. 1639-1654, (2004).
90. Schembri R, Spong J, Peters A, Rochford P, Wilksch P, O'Donoghue FJ, Greenwood K., Light sensors for objective light measurement in ambulatory polysomnography. *Plos ONE* 12(11) Italy, (2017).
91. Scognamiglio V., Arduini F., Palleschi G., Rea G. Bio sensing technology for sustainable food safety. *Trends analytical chemistry*. (2014); Vol. 62 p. 1–10.
92. Scognamiglio V., Arduini F., Palleschi G., Rea G. Biosensing technology for sustainable food safety. *Trends in Analytical Chemistry* (2014) 62 p. 1–10.
93. Sharma A., Olszewski O.Z., Torres J., Mathewson A., Houlihan R., Fabrication, Simulation and Characterization of MEMS Piezoelectric Vibration Energy Harvester for Low Frequency, *Procedia Engineering*, Vol. 120, (2015), p. 645-650, ISSN 1877-7058.

94. Singh, P. "SPR Biosensors: Historical Perspectives and Current Challenges" *Sensors and Actuators B Chemical*. Vol. 229, p. 110–130. (2016)
95. Situ C., Advances in surface plasmon resonance biosensor technology towards high-throughput, food-safety analysis. *TRAC* Vol. 29 (2010) p. 1305-1315.
96. Smith G. S., Pulskamp J. Sanchez L., Potrepka D., Proie R. M., Ivanov T., Rudy Q. R. Nothwang W., Bedair S. S., Meyer D. C., G. Polcawich, R., PZT-based piezoelectric MEMS technology. *Journal of the American Ceramic Society*. Vol. 95(6), (2012).
97. Srinivasan, R. M. Pyroelectric Materials. *Bulletin of Materials Science*. Vol. 6. P. 317-325. (1984).
98. Suikkola, J., Bjorninen T., Mosallaei M., Kankkunen T., Iso-Ketola P., Ukkonen L., Vanhala J., Mantysalo M., "Screen-Printing Fabrication and Characterization of Stretchable Electronics" *Scientific Reports* Vol. 6, (2016).
99. Sun L., Huang W. M., Wang C.C., Ding Z., Zhao Y., Tang C., Gao X. Y., "Polymeric shape memory materials and actuators", *Liquid Crystals* Vol. 41 (3), p. 277-289, (2014)
100. Suprun E., Evtugyn G., Budnikov H., Ricci F., Moscone D., Palleschi G. Acetylcholinesterase sensor based on screen-printed carbon electrode modified with Prussian blue. *Journal of Analytical and Bioanalytical Chemistry*. (2005) Vol. 383, p. 597–604.
101. Tamayo J., Chemical sensors and biosensors in liquid environment based on microcantilevers with amplified quality factor. *Ultramicroscopy* Vol. 86 (2001) p. 167-173.
102. Torun O., Boyaci I., Temur E., Tamer U. Comparison of sensing strategies in SPR biosensor for rapid and sensitive enumeration of bacteria. *Biosens Bioelectron*. (2012); Vol. 37 p. 53–60.
103. Tzou H. S. and M. C. Natori, Piezoelectric Materials and Continua, *Encyclopedia of Vibration*, (2001) p. 1011–1018, Academic Press, London, UK.
104. Tzou H. S., Lee H.-J., Arnold S. M., (2004) Smart Materials, Precision Sensors/Actuators, Smart Structures, and Structronic Systems, *Mechanics of Advanced Materials and Structures*, 11:4-5, p. 367-393.
105. Uchino K. "The Development of Piezoelectric Materials and the New Perspective" *Advanced Piezoelectric Materials* p. 1-92. (2017).
106. Ugwu E.I., Limbi L. W., Onyekachi K., Sambo J. E., Analysis of the Influence of Dielectric Polarization on the Study of Electronic Orientation of Electromagnetic Field Propagating Through Oxide Based Thin Film. *Advances in Materials*. Vol. 5(3), (2016), p. 13-17.
107. Wang H., Nakata E., Hamachi I., Recent progress in strategies for the creation of protein-based fluorescent biosensors. *Journal of Chem BioChem*. (2009) Vol. 10, p. 2560–2577.
108. Wang J., (2006) Zinc oxide nano comb biosensor for glucose detection. *Applied Physics Letters* Vol. 88.
109. Wang J., DNA biosensors based on peptide nucleic acid (PNA) recognition layers. *A review. Biosens Bioelectron*. (1998); 13, p. 757–762.
110. Wang Q, He H, Li B, Lin H, Zhang Y, UV–Vis and ATR–FTIR spectroscopic investigations of postmortem interval based on the changes in rabbit plasma. *Plos one* 12(7): (2017).
111. Wang, Xu-dong, Wolfbeis, Otto S., "Fiber-Optic Chemical Sensors and Biosensors" *Analytical Chemistry*, Vol. 88 (1), p. 203-227, (2016)

112. Wei, Z.G., Sandström, R., Miyazaki, S. “Shape-memory materials and hybrid composites for smart systems: Part I Shape-memory materials” *Journal of Materials Science* p. 3743-3744. (1998)
113. Wereley N. M. and Pang L. “Nondimensional analysis of semi-active electrorheological and magnetorheological dampers using approximate parallel plate models”, *Smart Materials and Structures*, v 7(5), (1998).
114. Woolston B.M., Edgar S., Stephanopoulos G. Metabolic engineering: past and future. *Annual Review of Chemical and Biomolecular Engineering*. (2013) Vol. 4, p. 259–288.
115. Worgull, M., “Hot Embossing Technique” *Hot embossing* p. 227-245. (2009).
116. Wu B., Piatkevich K.D., Lionnet T., Singer R.H., Verkhusha V.V., Modern fluorescent proteins and imaging technologies to study gene expression, nuclear localization, and dynamics. *Current Opinion in Chemical Biology*. (2011) Vol. 23 p. 310–317.
117. Xie X.D., Wang Q., A study on a high efficient cylinder composite piezoelectric energy harvester, *Composite Structures*, Vol. 161, (2017), p. 237-245, ISSN 0263-8223.
118. Yan C., Dong F., Chun-yuan B., Si-rong Z., Jian-guo S., Recent progress of commercially available biosensors in china and their applications in fermentation processes. *Journal of Northeast Agricultural University* Vol. 21(4) 2014, p. 73-85.
119. Ying-Qing Guo, Zhao-Dong Xu, Bing-Bing Chen, Cheng-Song Ran, Wei-Yang Guo, “Preparation and Experimental Study of Magnetorheological Fluids for Vibration Control” *International Journal of Acoustics and Vibration*, Vol. 22, No. 2, p. 194-200, (2017)
120. Young, D.T., L. Chapman, C.L. Muller, X. Cai, and C.S. Grimmond, A Low-Cost Wireless Temperature Sensor: Evaluation for Use in Environmental Monitoring Applications. *Oceanic Technol.*, Vol. 31, p. 938–944, (2014).
121. Zhang Da-Guang, Li Meng-Han, Zhou Hao-Miao, “A general one-dimension nonlinear magneto-elastic coupled constitutive model for magnetostrictive materials” *AIP Advances* Vol. 5, (2017).
122. Zhang Fuzhong, Keasling Jay, “Biosensors and their applications in microbial metabolic engineering”, *Trends in Microbiology* Vol. 19(7) p. 323-329, (2011).
123. Zhao Y., Li S., Davidson A., Yang B., Wang Q., Lin Q., “A MEMS viscometric sensor for continuous glucose monitoring” *Journal of Micromechanics and Microengineering* Vol. 17(12), p. 25-28, (2007).

SL344. 2019-04-23, 11,25 leidyb. apsk. I. Tiražas 15 egz. Užsakymas 97 .
Išleido Kauno technologijos universitetas, K. Donelaičio g. 73, 44249 Kaunas
Spausdino leidyklos „Technologija“ spaustuvė, Studentų g. 54, 51424 Kaunas